IODP
INTERNATIONAL OCEAN DISCOVERY PROGRAM

International Ocean Discovery Program Expedition 393 Preliminary Report

South Atlantic Transect 2

7 June–7 August 2022

Damon A.H. Teagle, Julia Reece, Rosalind M. Coggon, Jason B. Sylvan, Gail L. Christeson, Trevor J. Williams, Emily R. Estes, and the Expedition 393 Scientists

Publisher's notes

Core samples and the wider set of data from the science program covered in this report are under moratorium and accessible only to Science Party members until 23 January 2024.

This publication was prepared by the *JOIDES Resolution* Science Operator (JRSO) at Texas A&M University (TAMU) as an account of work performed under the International Ocean Discovery Program (IODP). This material is based upon work supported by the JRSO, which is a major facility funded by the National Science Foundation Cooperative Agreement Number OCE1326927. Funding for IODP is provided by the following international partners:

National Science Foundation (NSF), United States
Ministry of Education, Culture, Sports, Science and Technology (MEXT), Japan
European Consortium for Ocean Research Drilling (ECORD)
Ministry of Science and Technology (MOST), People's Republic of China
Australia-New Zealand IODP Consortium (ANZIC)
Ministry of Earth Sciences (MoES), India

Portions of this work may have been published in whole or in part in other IODP documents or publications.

Disclaimer

Copyright

Citation

Teagle, D.A.H., Reece, J., Coggon, R.M., Sylvan, J.B., Christeson, G.L., Williams, T.J., Estes, E.R., and the Expedition 393 Scientists, 2023. Expedition 393 Preliminary Report: South Atlantic Transect 2. International Ocean Discovery Program. https://doi.org/10.14379/iodp.pr.393.2023

ISSN

World Wide Web: 2372-9562

January 2023

Expedition 393 participants

Expedition 393 scientists

Damon A.H. Teagle
Co-Chief Scientist Expedition 393
School of Ocean and Earth Science
University of Southampton
United Kingdom
Damon.Teagle@southampton.ac.uk

Julia Reece
Co-Chief Scientist Expedition 393
Department of Geology and Geophysics
Texas A&M University
USA
jreece@geos.tamu.edu

Rosalind M. Coggon*
Co-Chief Scientist Expedition 390
School of Ocean and Earth Science
University of Southampton
United Kingdom
R.M.Coggon@soton.ac.uk

Jason B. Sylvan*
Co-Chief Scientist Expedition 390
Department of Oceanography
Texas A&M University
USA
jasonsylvan@tamu.edu

Gail L. Christeson*
Site Survey Data Lead
Marine Geology and Geophysics
National Science Foundation
USA
gchriste@nsf.gov

Also at
University of Texas Institute for Geophysics
USA
glchristeson@utexas.edu

Trevor J. Williams
Expedition Project Manager/Staff Scientist Expedition 393
International Ocean Discovery Program
Texas A&M University
USA
williams@iodp.tamu.edu

Emily R. Estes*
Expedition Project Manager/Staff Scientist Expedition 390
International Ocean Discovery Program
Texas A&M University
USA
estes@iodp.tamu.edu

Elmar Albers
Petrologist
Department of Geosciences
University of Bremen
Germany
e.albers@uni-bremen.de

Chiara Amadori
Physical Properties Specialist/Stratigraphic Correlator
Department of Earth and Environmental Sciences
University of Pavia
Italy
chiara.amadori@unipv.it

Thomas M. Belgrano
Petrologist
School of Ocean and Earth Science
University of Southampton
United Kingdom
T.Belgrano@soton.ac.uk

Chiara Borrelli*
Paleontologist (benthic foraminifera)
Department of Earth and Environmental Sciences
University of Rochester
USA
cborrelli@ur.rochester.edu

Timothy D'Angelo
Microbiologist/Organic Geochemist
Bigelow Laboratory for Ocean Sciences
USA
tdangelo@bigelow.org

Nobuhiro Doi
Micropaleontologist (nannofossils)
Division of Earth and Environmental Sciences
Chiba University
Japan
afna1872@chiba-u.jp

Aled Evans
Petrologist
School of Ocean and Earth Science
University of Southampton
United Kingdom
a.evans@southampton.ac.uk

Gilles M. Guerin
Physical Properties/Downhole Measurements Specialist
Lamont-Doherty Earth Observatory
Columbia University
USA
guerin@ldeo.columbia.edu

Michelle Harris
Petrologist
School of Geography, Earth and Environmental Sciences
University of Plymouth
United Kingdom
michelle.harris@plymouth.ac.uk

Victoria M. Hojnacki*
Sedimentologist
Earth and Environmental Sciences
Montclair State University
USA
hojnackiv1@montclair.edu

*Shore-based participant

Gilbert Hong
Paleomagnetist
School of Earth and Environmental Sciences
Seoul National University
Republic of Korea
hongfellow@snu.ac.kr

Xiaobo Jin*
Micropaleontologist (nannofossils)
School of Ocean and Earth Science
Tongji University
China
386jinxiaobo@tongji.edu.cn

Mallika Jonnalagadda
Petrologist
Interdisciplinary School of Science
Savitribai Phule Pune University
India
jmallika@gmail.com

Daisuke Kuwano
Paleontologist (nannofossils)
Division of Earth and Environmental Sciences
Chiba University
Japan
dkuwano@chiba-u.jp

Jessica M. Labonte
Microbiologist
Department of Marine Biology
Texas A&M University at Galveston
USA
labontej@tamug.edu

Adriane R. Lam*
Micropaleontologist (planktic foraminifera)
Department of Geological Sciences and Environmental Studies
Binghamton University
USA
alam@binghamton.edu

Marcin Latas
Paleontologist (planktic foraminifera)
Earth Sciences
University College London
United Kingdom
marcin.latas@ucl.ac.uk

Wanyi Lu
Physical Properties Specialist/Stratigraphic Correlator
Department of Geology and Geophysics
Woods Hole Oceanographic Institution
USA
wlu@whoi.edu

Paul Moal-Darrigade
Sedimentologist
UMR EPOC Oceanic and Continental Environments and Paleoenvironments
University of Bordeaux
France
paul.moal@u-bordeaux.fr

Stephen F. Pekar
Sedimentologist
School of Earth and Environmental Sciences
Queens College (CUNY)
USA
stephen.pekar@qc.cuny.edu

Claudio Robustelli Test
Paleomagnetist
Department of Earth Sciences
University of Torino
Italy
claudio.robustellite@edu.unito.it

Jeffrey G. Ryan
Inorganic Geochemist
School of Geosciences
University of South Florida, Tampa
USA
ryan@mail.usf.edu

Danielle Santiago Ramos
Inorganic Geochemist
Department of Marine and Coastal Sciences
Rutgers University, New Brunswick
USA
santiagoramos@marine.rutgers.edu

Alina Shchepetkina
Sedimentologist
Instituto Dom Luiz
University of Lisbon
Portugal
ashchepetkina@fc.ul.pt

Alexandra Villa
Inorganic/Organic Geochemist
Department of Geoscience
University of Wisconsin-Madison
USA
avilla2@wisc.edu

Shu Ying Wee
Microbiologist/Organic Geochemist
Department of Oceanography
Texas A&M University
USA
s66z977@tamu.edu

Sarah J. Widlansky
Physical Properties Specialist
Department of Earth Sciences
University of New Hampshire
USA
sarah.widlansky@unh.edu

GuoLiang Zhang*
Petrologist
Institute of Oceanology
Chinese Academy of Sciences
China
zhangguoliang@qdio.ac.cn

Expedition 393 outreach

Tessa Lund Peixoto
Outreach Officer
JVS Boston
USA
tessa.peixoto@gmail.com

Operational and technical staff

Siem Offshore AS officials

Expedition 393

Thomas Hartt
Master of the Drilling Vessel

Wayne Lambert
Drilling Supervisor

JRSO shipboard personnel and technical representatives

Expedition 393

Heather Barnes
Assistant Laboratory Officer

Erick Bravo
Marine Laboratory Specialist

Michael Cannon
Marine Computer Specialist

Oscar Cavazos
Marine Laboratory Specialist

Bridgette Cervera
Marine Laboratory Specialist

Etienne Claassen
Marine Instrumentation Specialist

Lisa Crowder
Laboratory Officer

Douglas Cummings
Publications Specialist

Kirby Garrett
Logging Engineer (Schlumberger)

Kevin Grigar
Operations Superintendent

Luan Heywood
Marine Laboratory Specialist

Jan Kotze
Marine Instrumentation Specialist

Nick Logan
Marine Computer Specialist

Zenon Mateo
Marine Laboratory Specialist

Mallory Mintz
Marine Laboratory Specialist

Eric Moortgat
Laboratory Officer

Michelle Penkrot
Curatorial Specialist

Doris Lajas
Assistant Laboratory Officer

Alexander Roth
Marine Laboratory Specialist

Johanna Suhonen
Marine Laboratory Specialist

Kara Vadman
Marine Laboratory Specialist

Hai Zhao
Applications Developer

Abstract

The South Atlantic Transect (SAT) is a multidisciplinary scientific ocean drilling experiment designed to investigate the evolution of the oceanic crust and overlying sediments across the western flank of the Mid-Atlantic Ridge. This project comprises four International Ocean Discovery Program expeditions: fully staffed Expeditions 390 and 393 (April–August 2022) built on engineering preparations during Expeditions 390C and 395E that took place without science parties during the height of the Coronavirus Disease 2019 (COVID-19) pandemic. Through operations along a crustal flow line at ~31°S, the SAT recovered complete sedimentary sections and the upper ~40–340 m of the underlying ocean crust formed at a slow to intermediate spreading rate at the Mid-Atlantic Ridge over the past ~61 My. The sediments along this transect were originally spot cored more than 50 y ago during Deep Sea Drilling Project Leg 3 (December 1968–January 1969) to help verify the theories of seafloor spreading and plate tectonics.

The SAT expeditions targeted six primary sites on 7, 15, 31, 49, and 61 Ma ocean crust that fill critical gaps in our sampling of intact in situ ocean crust with regards to crustal age, spreading rate, and sediment thickness. Drilling these sites was required to investigate the history, duration, and intensity of the low-temperature hydrothermal interactions between the aging ocean crust and the evolving South Atlantic Ocean. This knowledge will improve the quantification of past hydrothermal contributions to global biogeochemical cycles and help develop a predictive understanding of the impacts of variable hydrothermal processes and exchanges. Samples from the transect of the previously unexplored sediment- and basalt-hosted deep biosphere beneath the South Atlantic Gyre are essential to refine global biomass estimates and examine microbial ecosystems' responses to variable conditions in a low-energy gyre and aging ocean crust.

The transect is located near World Ocean Circulation Experiment Line A10, which provides a baseline for records of carbonate chemistry and deepwater mass properties across the western South Atlantic through key Cenozoic intervals of elevated atmospheric CO_2 and rapid climate change. Reconstruction of the history of the deep western boundary current and deepwater formation in the Atlantic basins will yield crucial data to test hypotheses regarding the role of evolving thermohaline circulation patterns in climate change and the effects of tectonic gateways and climate on ocean acidification.

During engineering Expeditions 390C and 395E, a single hole was cored through the sediment cover and into the uppermost rocks of the ocean crust with the advanced piston corer (APC) and extended core barrel (XCB) systems at five of the six primary proposed SAT sites. Reentry systems with casing were then installed either into basement or within 10 m of basement at each of those five sites. Expedition 390 (7 April–7 June 2022) conducted operations at three of the SAT sites, recovering 700 m of core (77%) over 30.3 days of on-site operations. Sediment coring, basement coring, and wireline logging were conducted at two sites on 61 Ma crust (Sites U1556 and U1557), and sediment coring was completed at the 7 Ma Site U1559.

Expedition 393 operated at four sites, drilling in 12 holes to complete this initial phase of the SAT. Complete sedimentary sections were collected at Sites U1558, U1583, and U1560 on 49, 31, and 15 Ma crust, respectively, and together with 257.7 m of sediments cored during earlier operations, more than 600 m of sediments was characterized. The uppermost ocean crust was drilled at Sites U1558, U1560, and U1583 with good penetration (~130 to ~204 meters subbasement), but at the youngest ~7 Ma Site U1559, only ~43 m of basement penetration was achieved in this initial attempt. Geophysical wireline logs were aquired at Sites U1583 and U1560. Expeditions 390 and 393 established legacy sites available for future deepening and downhole basement hydrothermal and microbiological experiments at Sites U1557, U1560, and U1559 on 61, 15, and 7 Ma crust, respectively.

1. Introduction

During the multidisciplinary South Atlantic Transect (SAT) experiment, comprising International Ocean Discovery Program (IODP) Expeditions 390 and 393, supported by preparatory engineer-

ing Expeditions 390C and 395E, a transect was drilled along a crustal flow line at ~31°S across the western flank of the southern Mid-Atlantic Ridge. The principal aims of the SAT expeditions are to investigate the hydrothermal evolution of the aging ocean crust, characterize the nature and variation of sediment- and basement-hosted microbial communities with increasing substrate age, and investigate the paleoceanographic evolution of the South Atlantic Ocean, including the responses of the deep-ocean and subtropical gyre to changing global climate. The SAT expeditions revisited an area first cored in 1968, when coring during Deep Sea Drilling Project (DSDP) Leg 3 accomplished one of the great achievements of scientific ocean drilling by recovering sediments from a transect of spot cored holes across the South Atlantic between ~28° and 30°S (Figure **F1**). This coring demonstrated that basal sediment age increases with distance from the ridge axis, which provided definitive proof for the theory of seafloor spreading (The Shipboard Scientific Party, 1970). By revisiting the Leg 3 transect region, the SAT expeditions have been designed to take advantage of dramatic advances in drilling technology and analytical capabilities since the earliest days of scientific ocean drilling to address many high-priority scientific objectives. Although the great majority of Expedition 393 operations were successful, some of our drilling challenges will be familiar to the earliest seafloor explorers aboard *Glomar Challenger*.

Despite more than 50 y of scientific ocean drilling since Leg 3, major gaps remain in our observations of the evolving Earth system. These gaps include drill cores of ocean crust of different ages formed across a representative range of spreading rates, virtually unexplored biogeographic microbial provinces, and continuous samples of key intervals in Earth's climate, changing ocean chemistry, or magnetic field. Transects of drill holes that sample both the sediment cover and the uppermost oceanic crust in a particular ocean basin can provide essential knowledge of how interconnected processes have evolved over Earth's history and responded to changes in external drivers such as atmospheric CO_2 concentrations, evolving marine life, oceanic gateways, or major ocean currents. Transects that sample tens of millions of years of ocean crust formed at the same

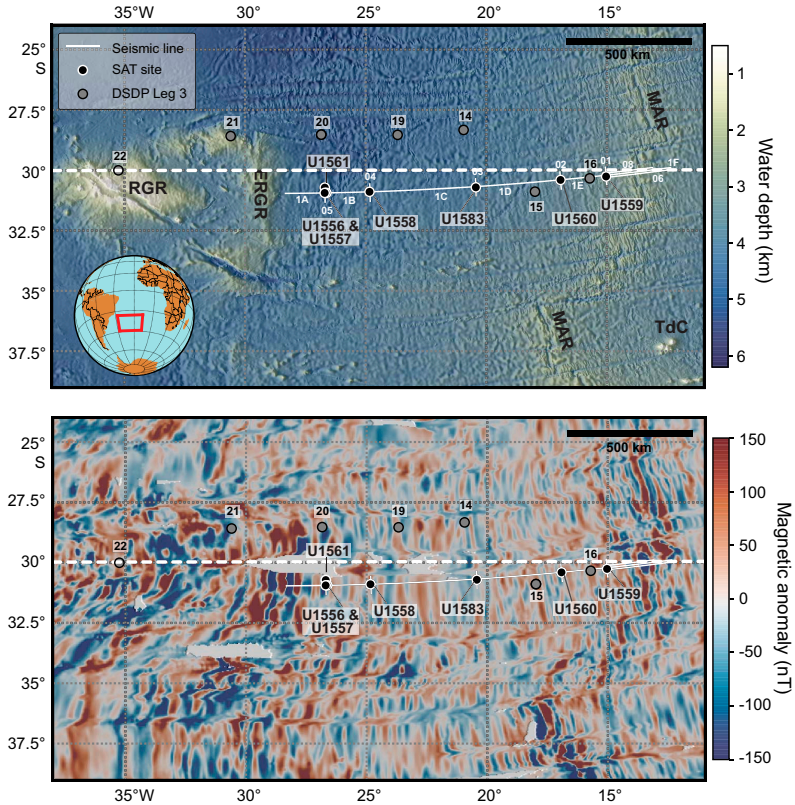

Figure F1. SAT study region. Top: bathymetry (Ryan et al., 2009) of South Atlantic Ocean. Inset shows regional setting. Bottom: magnetic anomalies (Meyer et al., 2017). Solid lines = CREST seismic reflection profiles (Reece et al., 2019), dashed line = WOCE Line A10. MAR = Mid-Atlantic Ridge, RGR = Rio Grande Rise, ERGR = eastern Rio Grande Rise, TdC = Tristan de Cunha.

mid-ocean ridge (MOR) segment can provide important information about the timing, duration, and intensity of hydrothermal exchange. However, sampling both the sediment and the underlying basaltic basement in a specific ocean region has rarely been undertaken in a systematic manner, and the few transects previously accomplished cover relatively short intervals of recent Earth history (e.g., Juan de Fuca Ridge, 0–3.5 Ma [Shipboard Scientific Party, 1997; Expedition 301 Scientists, 2005; Expedition 327 Scientists, 2011], and Costa Rica Rift, 0–7 Ma [Shipboard Scientific Party, 1983, 1985]).

On average, a discernible conductive heat flow deficit exists out to 65 Ma in ocean crust formed at the full range of spreading rates (e.g., Von Herzen, 1959; Lister, 1972; Stein and Stein, 1994) (Figure **F2**). This requires that out to this age, there is significant advection by seawater-derived hydrothermal fluids from the cooling of the oceanic lithosphere. However, seafloor heat flow measurements are sparse and show large ranges even within small regions (e.g., Hole 504B region, Langseth et al., 1988; Mottl et al., 1983, 1985; Mottl and Gieskes, 1990; Shipboard Scientific Party, 1993b). Basement hydrologic flow can occur in crust of all ages if sufficient hydrologic heads can be established because crustal age is only one of a suite of interlinked parameters that influence the duration, depth, and intensity of off-axis hydrothermal fluid flow, including basement topography; volcanic stratigraphy and flow morphology; and sediment type, thickness, and completeness of basement blanketing (e.g., Fisher and Harris, 2010). Although simple relationships may not exist between crustal age, fluid flow, crustal properties, thermal and chemical exchange, and biological activity (cf. Kardell et al., 2019, 2021; Christeson et al., 2020), the potential for such relationships has not yet been investigated in a systematic aging transect of tens of millions of years duration.

Consequently, the SAT expeditions were designed to recover complete sediment sections and the uppermost ~250 m of basaltic ocean crust produced between ~7 and 61 Ma at the slow/intermediate-spreading Mid-Atlantic Ridge, returning to the Leg 3 transect region to achieve the following objectives:

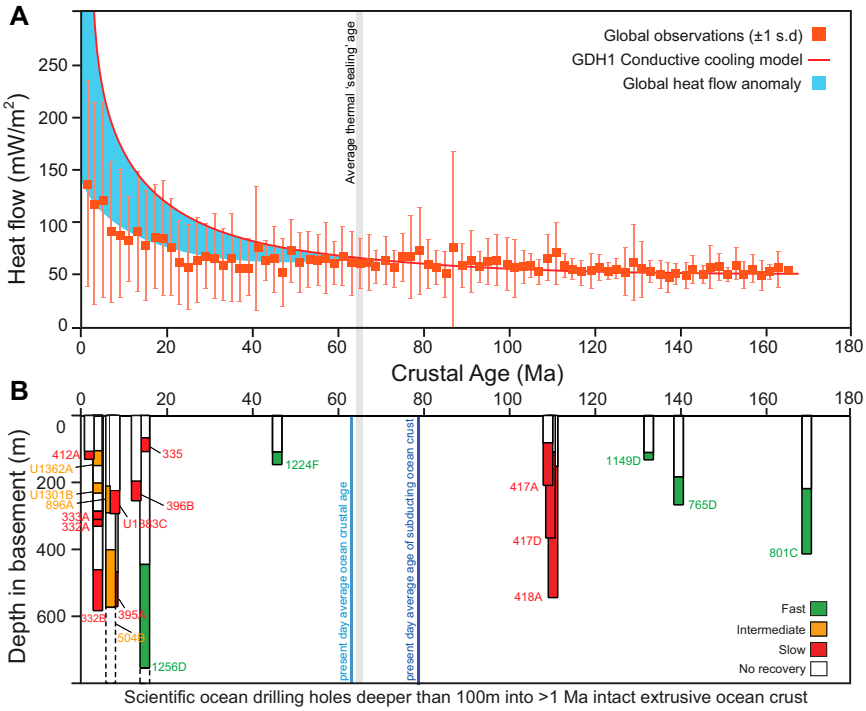

Figure F2. A. Discrepancy between observed and predicted conductive heat flow. Global heat flow anomaly indicates hydrothermal circulation persists across ridge flanks for ~65 My on average (modified from Stein and Stein, 1994). B. Compilation of all scientific ocean drilling holes that penetrate >100 m into intact upper (basaltic) ocean crust vs. crustal age, excluding drill holes that penetrated seamounts, oceanic plateaus, back-arc basement, hydrothermal mounds, or passive continental margins (after Michibayashi et al., 2019). Colors show spreading rate each crustal section formed at, and proportion of cored interval that is colored indicates average core recovery. Dashed lines = two holes that penetrated through entire upper ocean crust into underlying sheeted dikes.

1. Quantify the timing, duration, and extent of ridge flank hydrothermal fluid-rock exchange;
2. Investigate sediment- and basement-hosted microbial community variation with substrate composition and age; and
3. Investigate the responses of Atlantic Ocean circulation patterns and the Earth's climate system to rapid climate change, including elevated atmospheric CO_2 during the Cenozoic.

The initial target depth of the SAT expeditions of 250 m of ocean crust penetration is not sufficient to constrain the full depth extent of low-temperature hydrothermal seawater-basalt exchange (e.g., Shipboard Scientists, 2003b; Alt, 2004), but deeper coring will require longer operational time. Consequently, basement drilling at the SAT sites was planned as scientific ocean drilling legacy holes with reentry cones and deep casing into or near to the oceanic volcanic rocks.

Expeditions 390 and 393 were delayed because of the Coronavirus Disease 2019 (COVID-19) pandemic. However, engineering and sediment coring operations during Expeditions 390C and 395E (Estes et al., 2021; Williams et al., 2021), which sailed without science parties, cored initial sediment sections and installed reentry cones and casing systems at most sites to maximize science operations during the fully staffed expeditions. The SAT expeditions targeted six primary sites on 7, 15, 31, 49, and 61 Ma ocean crust (Figure **F1**) to fill critical gaps in our sampling of intact in situ ocean crust with regards to crustal age, spreading rate, and sediment thickness (Figures **F2**, **F3**; Table **T1**).

These sections of upper ocean crust will enable us to quantify the magnitude and duration of low-temperature chemical exchange with the overlying oceans; investigate the impact of changing ocean conditions on hydrothermal exchange; determine the critical thermal, hydrogeologic, chemical, and microbial transitions across the ridge flank; and evaluate hydrothermal contributions to global biogeochemical cycles. Coring during Expeditions 390 and 393 also sampled the sedimentary and upper crustal deep biosphere along the transect, allowing exploration of the microbial ecosystems' responses to variations in habitat conditions in a low-energy gyre and aging ocean crust. Sediments recovered during the SAT expeditions include Cenozoic stratigraphic sections required to investigate the Earth system's past responses to high atmospheric CO_2 and temperatures and better predict the impacts of projected future anthropogenic increases in atmospheric CO_2. The transect also provides a paleoceanographic record near World Ocean Circulation Experiment (WOCE) Line A10, enabling reconstruction of the history of the deep western boundary current and the sources of deepwater formation in the Atlantic basins.

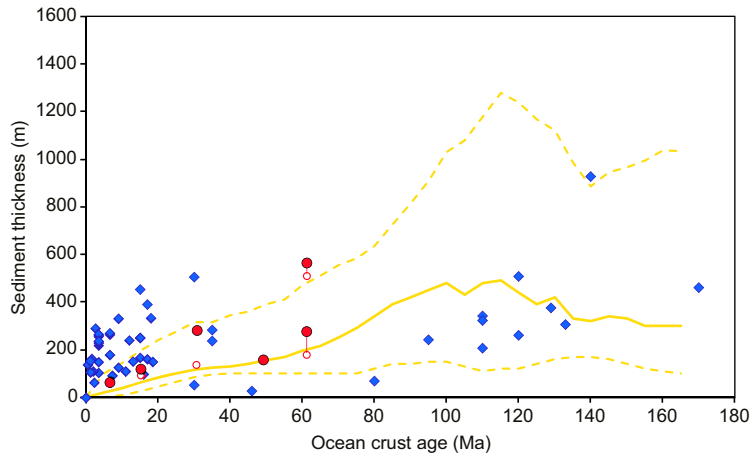

Figure F3. Sediment cover vs. crustal age for Expedition 390 and 393 sites. Solid circles = observed sediment thickness, open circles = sediment thickness expected based on site survey data, diamonds = sediment thicknesses at all DSDP/ODP/Integrated Ocean Drilling Program/IODP drill holes that cored more than 100 m into basement in intact oceanic crust and tectonically exposed lower crust/upper mantle, solid yellow line = global average sediment thickness vs. age, calculated as 25 My moving average of median sediment thickness of 5 Ma binned global compilation of sediment thickness vs. lithospheric age of Spinelli et al. (2004), yellow dashed lines = 25 My moving average of 25th and 75th percentiles of 5 Ma binned data.

Table T1. Summary of South Atlantic Transect proposed site operations achieved during Expedition 393 building on earlier activities during Expeditions 390C, 395E, and 390. SAR = sediment accumulation rate. NA = not applicable.

Site	Proposed site	Proposed primary/ alternate site	Operations: Previous expedition	Operations: Expedition 393	Hole	Latitude	Longitude	Water depth (m)	Age (Ma)	Half spreading rate (mm/y)	Estimated sediment thickness (m)
Drilled/Planned site											
U1559	SATL-13A	Primary	390C, 390	393	U1559B	30°15.6336′S	15°02.0941′W	3055	6.6	17.0	50
U1560	SATL-25A	Primary	395E	393	U1560B	30°24.2057′S	16°55.3702′W	3723	15.2	25.5	104
U1583	SATL-33B	Primary	NA	393	U1583F	30°42.6175′S	20°26.0336′W	4210	30.6	24.0	138
U1558	SATL-43A	Primary	390C	393	U1558D	30°53.7814′S	24°50.4822′W	4334	49.2	19.5	148
U1556	SATL-53B	Primary	390C, 395E, 390	NA	U1556B	30°56.5244′S	26°41.9472′W	5002	61.2	13.5	180
U1557	SATL-56A	Alternate	390C, 395E, 390	NA	U1557D	30°56.4651′S	26°37.7892′W	5011	61.2	13.5	510
U1561	SATL-55A	Alternate	395E	NA	U1561A	30°43.2902′S	26°41.7162′W	4910	61.2	13.5	126

Site	APC/XCB cored hole: Hole	Expedition	Observed sediment thickness (m)	Actual average SAR (m/My)	Total penetration (m)	Installed reentry system: Hole	Expedition	Casing shoe depth (mbsf)
U1559	U1559A	390C	64.0	9.70	66.2	U1559B	390C	55.3
U1560	U1560A	395E	120.2	7.91	122.5	U1560B	395E	122.0
U1583	U1583C	393	104.5	3.46	107.5	U1583F	393	Free-fall funnel
U1558	U1558A	390C	158.9	3.23	163.9	U1558D	390C	146.1
U1556	U1556A	390C	278.0	4.54	283.8	U1556B	390C	284.2
U1557	U1557B	390C	564.0	9.22	574.0	U1557D	390C/395E	571.6
U1561	U1561A	395E	46.0	0.75	49.0	NA	NA	NA

Site	RCB cored hole: Hole	Expedition	Cored interval top (mbsf)	Cored interval bottom (mbsf)	Cored interval thickness (m)	Recovered length (m)	Average recovery (%)	Sediment/ basement interface depth (mbsf)	Basement penetration (m)
U1559	U1559B	393	58.9	107.9	42.9	12.8	26	65.0	42.9
U1560	U1560B	393	124.0	314.0	190.0	74.8	39	123.0	190.0
U1583	U1583F	393	101.0	239.5	138.5	45.7	33	109.7	129.8
U1558	U1558D	393	150.0	370.3	220.3	100.8	46	166.8	203.5
U1556	U1556B	390	291.0	633.2	342.2	191.87	56	291.3	341.9
U1557	U1557D	390	575.6	684.7	109.1	71.28	65	564.8	119.9
U1561			NA	NA	NA	NA	NA	NA	NA

2. Background

2.1. Geologic setting

The SAT expeditions operated in the Leg 3 transect region (~31°S) but occupied a transect of new sites selected to (1) target basement formed along the same crustal flow line at similar spreading rates (~13–25 mm/y half rate; Table **T1**) and (2) recover sections of slow-spreading crust of comparable ages to the ocean crust reference sections in DSDP Hole 504B on the Costa Rica Rift (7 Ma; Shipboard Scientific Party, 1993a) and Ocean Drilling Program (ODP) Hole 1256D on the Cocos plate (15 Ma; Shipboard Scientific Party, 2003b; Expedition 309/312 Scientists, 2006; Expedition 335 Scientists, 2012), which are located in intermediate- and superfast-spreading crust, respectively.

The site locations were chosen to optimize the recovery of material required to achieve our multidisciplinary objectives. Thick sediment cover is typically targeted by scientific ocean drilling to maximize the resolution of paleoceanographic records. Thick sediment sequences are also often required to install the seafloor infrastructure required for deep-ocean drilling. This has led to a bias in DSDP/ODP/Integrated Ocean Drilling Program/IODP sampling of in situ upper ocean

crust (for depths >100 m into basement) toward regions with anomalously thick sediment (Figure F3). Rapid deposition of sediment in such areas soon after the crust is formed seals the volcanic rocks of the ocean crust from bottom seawater, resulting in anomalously hot basement temperatures, and may result in premature cessation of hydrothermal circulation. Consequently, the SAT sites target locations where the sediment cover is close to the global average for their crustal ages (Spinelli et al., 2004, Olson et al., 2016; Straume et al., 2019; Figure F3), even though this decision reduces the resolution of the paleoceanographic records. However, because seafloor roughness is greater in slow-spreading ocean basins than in fast-spreading basins (Spinelli et al., 2004; Kardell et al., 2019; Christeson et al., 2020), there are significant variations in sediment thickness and the continuity of sediment blanketing along the SAT. Indeed, the concept of an average sediment thickness is perhaps not useful in regions where significant proportions of the crust have little or no sediment. Volcanic rocks crop out at all ages along the transect (Estep et al., 2019), and these topographic variations likely impact the crustal hydrogeology. Consequently, Expedition 390 occupied two sites on 61 Ma crust to investigate the variability in duration and extent of hydrothermal alteration due to basement topography at a given crustal age: Site U1556, which is blanketed by 278 m of sediment, and Site U1557 in a more thickly sedimented (564 m) portion of the same local sediment basin (see figure F4 in Coggon et al., 2022a). Site U1557 also provides a higher resolution paleoceanographic record at this oldest crustal age. An additional short hole was drilled on 61 Ma crust (Expedition 395E Site U1561). The sediment sections cored at the 61 Ma sites cover key Paleogene hyperthermals, including the Paleocene/Eocene Thermal Maximum (PETM). Additionally, the underlying basement records the cumulative hydrothermal alteration of the uppermost crust across the entire SAT.

Following Expedition 390 operations, Expedition 393 was then freed to target the younger sites that form the age transect across the western flank of the Mid-Atlantic Ridge. The 7 Ma site (U1559) provides the young end-member for investigating the evolution of hydrothermal and microbiological systems with crustal age and allows comparison with similar-aged intermediate spreading rate crust from Hole 504B (Shipboard Scientific Party, 1993a). The 31 Ma (Site U1583) and 49 Ma (Site U1558) sites fill critical gaps in our ocean crust and deep biosphere sampling with respect to basement age and major changes in ocean chemistry (Coggon et al., 2010). The 15 Ma site (U1560) was chosen for comparison to superfast spreading rate crust from Hole 1256D (Shipboard Scientific Party, 2003b; Expedition 309/312 Scientists, 2006; Expedition 335 Scientists, 2012).

2.1.1. DSDP Leg 3 drilling results

During Leg 3, 10 sites were drilled in the equatorial and South Atlantic Ocean between Senegal and Brazil (Shipboard Scientific Party, 1970), including 7 sites along a transect across the Mid-Atlantic Ridge that penetrated to basement (Sites 14–20; Figure F1). The basal sediment ages are within a few million years of the inferred magnetic anomaly ages, which are consistent with a half spreading rate of ~20 mm/y since 76 Ma. Recovery in the cored intervals was typically high (>98%), but the sediments were only spot cored, and there are significant gaps between cored intervals (Shipboard Scientific Party, 1970). The cores recovered along the Leg 3 transect make up an almost continuous Lower Cretaceous to Pleistocene composite stratigraphic section (Shipboard Scientific Party, 1970). All sites yielded calcareous sediments with calcareous nannoplankton and planktic foraminifera. Basalts (0.05–2 m penetration) were recovered from each site, and they comprise variably altered extrusive rocks with common glass and some calcium carbonate veins.

2.2. Seismic studies and site survey data

The SAT is located along a crustal flow line at ~31°S where fracture zones are far apart and magnetic lineations are clear (Figure F1). The Crustal Reflectivity Experiment Southern Transect (CREST) cruise aboard the research vessel (R/V) *Marcus G. Langseth* conducted a detailed geophysical survey across the western Mid-Atlantic Ridge flank along this crustal flow line (Reece et al., 2016). The CREST survey included a 1500 km multichannel seismic reflection profile from the ridge crest to the Rio Grande Rise (RGR) spanning 0–70 Ma crust, two shorter ridge-crossing profiles spanning 0–7 Ma crust, and five ridge-parallel profiles at 6.6, 15, 31, 49, and 61 Ma. Ocean-

bottom seismometer profiles were acquired coincident with the ridge-parallel profiles. Gravity, magnetics, multibeam bathymetry, and backscatter data were also acquired.

Crustal accretion along the northern Mid-Atlantic Ridge is complex in places, and there are significant regions where spreading is accommodated by amagmatic extension by detachment faults that exhume sections of deep lithosphere to form oceanic core complexes (OCCs; Mallows and Searle, 2012) with a characteristic domal structure. However, the 2013 SoMARTherm survey found no OCCs between 25° and 33°S (Devey, 2014). This finding, combined with the relatively well defined marine magnetic anomalies on the southern Mid-Atlantic Ridge flanks (Meyer et al., 2017; Pérez-Díaz and Eagles, 2017a, 2017b), is consistent with accretion of intact magmatic crust. Because the ~31°S SAT follows a crustal flow line through a relatively long spreading segment away from major transform faults, a Penrose-type stratigraphy of lavas overlying dikes and gabbros is predicted to have been accreted along the transect (Penrose Conference Participants, 1972).

Kardell et al. (2019) calculated ages and spreading rates from magnetic data acquired during the CREST cruise (Figure **F4**). Ages of the SAT sites are estimated at 6.6, 15.2, 30.6, 49.2, and 61.2 Ma with half spreading rates of 17.0, 25.5, 24.0, 19.5, and 13.5 mm/y, respectively (Table **T1**). If a half spreading rate of 20 mm/y is used to define the transition between slow and intermediate spreading rates (Perfit and Chadwick, 1998), then the SAT sites formed at slow to intermediate spreading rates.

Seismic imaging along the CREST transect shows an abundance of unsedimented or thinly sedimented, exposed basement outcrops that may allow the ingress and egress of seawater and ridge flank hydrothermal fluids at all crustal ages from 0 to 65 Ma. This suggests that the crust is never fully sealed by sediment at these ages (Estep et al., 2019) and that there may be long-lived and ongoing connection between the oceans and uppermost basaltic crust with implications for biogeochemical exchanges and subsurface microbial activity. This is in strong contrast to recent hydrogeologic and hydrothermal alteration research in the Pacific that has focused on regions and sites with thick continuous sediment blankets and few outcrops of volcanic rocks (e.g., Juan de Fuca Ridge [Hutnak et al., 2006; Fisher and Harris 2010] and eastern equatorial Pacific [Langseth et al., 1983, 1988; Mottl, 1989; Mottl et al., 1983; Hutnak et al., 2008]).

Seismic Layer 2A exhibits relatively slow seismic velocities but a steep gradient of increasing velocities with depth (e.g., Houtz and Ewing, 1976) and is generally interpreted to correspond to the porous and permeable uppermost igneous portion of the oceanic crust. In the SAT region, based on seismic velocities, Layer 2A is imaged in crust from the Mid-Atlantic Ridge crest out to 48 Ma crust but is not present in older crust toward the RGR (Estep et al., 2019). Along the CREST SAT survey line, velocities at the top of basement increase rapidly from 2.4 km/s at 0 Ma to 4.2 km/s at 6 Ma and then continue to increase gradually to 4.9 km/s at 58 Ma (Kardell et al., 2019). The presence of unsedimented basement outcrops, persistent imaging of Layer 2A, and continued velocity increase at the top of basement are consistent with fluid circulation within the upper crust

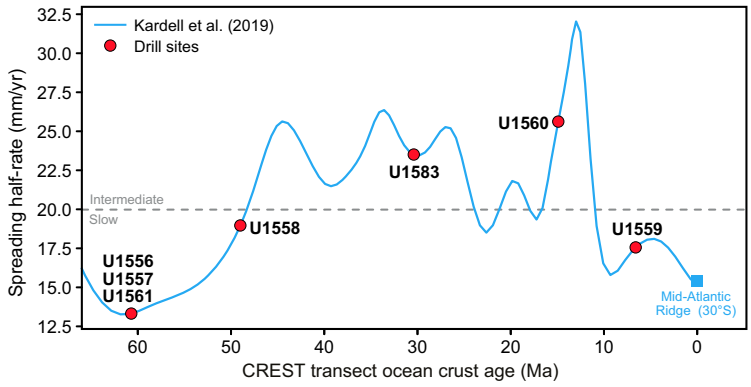

Figure F4. Ages and spreading rates along CREST transect. Blue line = cubic interpolation of rates calculated from table S3 in Kardell et al. (2019), red circles = estimated values at SAT drill sites.

that continues to at least 48–58 Ma (Estep et al., 2019; Kardell et al., 2019, 2021). The seismic transect ends just east of the eastern margin of the RGR, which may have affected the thermal history of the lithosphere and the structure of the crust on the western end of SAT.

The SAT sites were all positioned in localized sedimentary basins imaged on the seismic reflection profiles with unsedimented basement ridges within 1–2 km of most sites (see figure F4 in Coggon et al., 2022a). Actual sediment thicknesses at SAT sites increased from 64 m at the youngest (7 Ma) Site U1559 to 564 m at the oldest (61 Ma) Site U1557. However, Site U1561, which is also located on 61 Ma crust, is close to an exposed ridge and consequently encountered only 46 m of sediment before reaching the oceanic crust.

3. Scientific objectives

3.1. Objective 1 (primary): quantify the timing, duration, and extent of ridge flank hydrothermal fluid-rock exchange.

Hydrothermal circulation at MORs and across their vast ridge flanks influences tectonic, magmatic, and microbial processes on a global scale; is a fundamental component of global biogeochemical cycles of key elements and isotopes (e.g., O, S, Mg, Fe, Li, B, Tl, and ^{87}Sr); and facilitates geologic CO_2 sequestration within the ocean crust (e.g., Alt and Teagle, 1999). The chemical and isotopic composition of seawater reflects the dynamic balance between riverine inputs from the continents, burial of marine sediments, and hydrothermal exchanges with the ocean crust (e.g., Palmer and Edmond, 1989; Vance et al., 2009). Ocean crust is young and chemically relatively homogeneous compared to continental crust, and its chemical exchanges with seawater are limited to a few relatively well known reactions. Consequently, hydrothermal contributions to ocean chemistry are simpler to reconstruct than riverine inputs (Coggon and Teagle, 2011; Davis et al., 2003; Vance et al., 2009; Antonelli et al., 2017). Knowledge of the rates and magnitudes of hydrothermal exchanges will help us to decipher the changing global conditions responsible for past variations in seawater chemistry such as mountain building, changes in seafloor spreading rate, large igneous province emplacement, changing climate, and evolution of biological systems. Building this knowledge requires ocean basin–wide transects across ridge flanks with different hydrogeologic histories.

Conductive heat flow deficits indicate that, on average, hydrothermal exchange persists at low temperatures (generally ≪100°C) to 65 Ma on the ridge flanks (Stein and Stein, 1994; Figures **F2**, **F5**). Given the vast extent of the ridge flanks, the hydrothermal fluid flux through them is many orders of magnitude greater than that through high-temperature (~400°C) axial systems (Mottl, 2003) and is likely important for elements for which fluid-rock exchange occurs at low temperatures (e.g., Mg, K, S, Li, B, C, and H_2O). Hydrothermally altered ocean crust provides a time-integrated record of geochemical exchange with seawater manifested through changes in its chemical and isotopic composition, mineral assemblages, and physical properties (e.g., porosity, permeability, and seismic velocities). The intensity of seawater-basalt exchange depends on the crustal age, architectural and thermal history, sediment cover, and spreading rate. Consequently, hydrothermal contributions to global geochemical cycles depend on the global length of slow-, intermediate-, and fast-spreading ridges and the age-area distribution of the ridge flanks, which have varied significantly throughout the Phanerozoic (Müller et al., 2008). However, the impact of these variations on geochemical cycles is uncertain because the magnitude and spatial and temporal distribution of crust-seawater hydrothermal exchanges are poorly quantified. For example, the role of MOR spreading in controlling past atmospheric CO_2 and hence climate remains controversial (Alt and Teagle, 1999; Berner et al., 1983; Gillis and Coogan, 2011; Staudigel et al., 1989) because of uncertainties regarding the rate, extent, and duration of hydrothermal $CaCO_3$ precipitation due to our sparse sampling of intermediate age ocean crust (Figure **F5**). The hydrothermal carbonates that sequester CO_2 in the ocean crust also record the composition of the fluids from which they precipitate (Coggon et al., 2004) and provide an exciting opportunity to develop medium-resolution records of past ocean chemistry (e.g., Mg/Ca and Sr/Ca) (Coggon and Teagle, 2011; Coggon et al., 2010; Rausch et al., 2013), which integrates past changes in major Earth system processes such

as plate tectonics, mountain building, and climate. However, this approach is limited by sparse sampling of ocean crust of a variety of ages.

Knowledge of the controls on the extent, rate, and duration (Coogan et al., 2016; Harris et al., 2014) of natural CO_2 sequestration along the SAT will assist efforts to assess the feasibility of geo-engineered CO_2 sequestration within the ocean crust (e.g., Goldberg et al., 2008; Marieni et al., 2013). The permeable upper ocean crust is of particular interest because it constitutes a vast potential reservoir for CO_2 trapping in areas where the crust is isolated from the oceans by low-permeability sediments (Marieni et al., 2013) or permanent storage through carbonate mineralization (Matter et al., 2016).

Drilling experiments on the Juan de Fuca Ridge flank were a key investigation of hydrothermal evolution across a ridge flank but were restricted to young (<3.6 Ma), intermediate-spreading (29 mm/y half spreading rate) heavily sedimented crust (Shipboard Scientific Party, 1997; Expedition 301 Scientists, 2005; Expedition 327 Scientists, 2011). There is a dearth of holes in 20–140 Ma intact in situ MOR crust and no significant penetrations (>100 m) of 46–110 Ma crust (Figure **F2**; Expedition 335 Scientists, 2012). Consequently, the critical thermal, hydrogeologic, chemical, and microbial transitions across the ridge flanks remain unknown (Figure **F5**). Our current sampling of in situ upper ocean crust (>100 m) is biased toward areas with anomalously thick sediment for their crustal ages (Figure **F3**). The majority of holes in ocean crust older than 35 Ma penetrate intermediate or fast spreading rate crust. The recovery of uppermost basement sections along the SAT across slow/intermediate-spreading Mid-Atlantic Ridge crust was planned to address these sampling gaps with respect to age, spreading rate, and sediment thickness. In addition, knowledge of the controls on the extent, rate, and duration of natural CO_2 sequestration along the SAT will

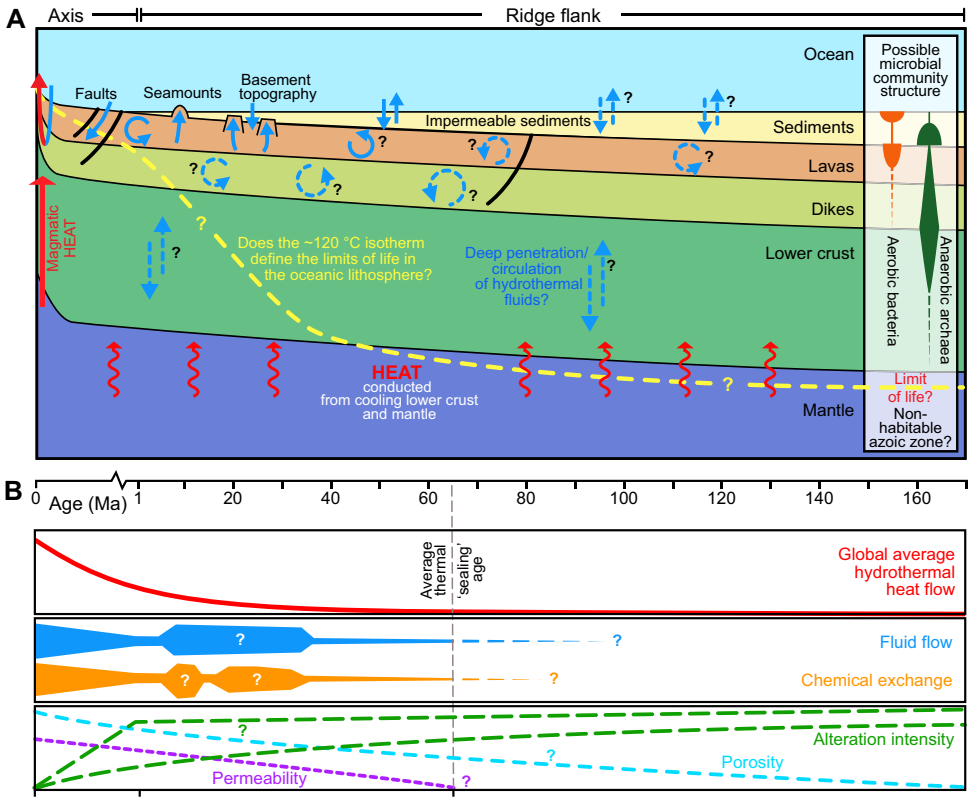

Figure F5. A. Schematic architecture of MOR flank (not to scale) illustrating parameters that may influence intensity and style of hydrothermal alteration and hypothetical trajectory of 120°C isotherm with crustal age. Arrows indicate heat (red) and fluid (blue) flow. B. Calculated global hydrothermal heat flow anomaly, which decreases to 0 by 65 Ma on average, and hypothetical variations in fluid flow and chemical exchange and crustal properties that could be measured to investigate intensity and style of ridge flank hydrothermal circulation (e.g., porosity, permeability, and two possible scenarios for alteration intensity). (After Coggon and Teagle, 2011; Expedition 335 Scientists, 2012; and an original figure by K. Nakamura, AIST.)

assist in assessing the properties and processes that govern the flow and storage of carbon in the subseafloor.

The hydrothermal alteration of thinly sedimented slow/intermediate-spreading ocean crust recovered along the SAT will be investigated using a combination of petrologic and geochemical analyses, radiometric dating, and detailed quantitative core logging of rock types, alteration features, and veins integrated with continuous wireline geophysical data with the following aims:

- To determine the nature, rates, magnitudes, distribution, and duration of hydrothermal alteration across the ridge flank;
- To investigate the effect of titanomagnetite/titanomaghemite alteration on the magnetic anomaly signal to elucidate its origin;
- To compare hydrothermal alteration of the uppermost slow/intermediate-spreading crust with crust of similar ages produced at faster spreading ridges (e.g., Holes 504B and 1256D);
- To evaluate the effect of changes in global spreading rates and the age-area distribution of the seafloor on hydrothermal contributions to global biogeochemical cycles; and
- To investigate signatures of changing ocean chemistry in the hydrothermal record and develop medium-resolution records of past ocean chemistry using hydrothermal minerals (following Coggon et al., 2010).

Shipboard description and analyses combined with detailed postexpedition research will allow us to address the following hypotheses:

- Hydrothermal chemical exchange persists beyond 20 My of crustal formation.
- Basement topography and sedimentation history affect the rate and duration of hydrothermal alteration.

3.2. Objective 2 (primary): investigate sediment- and basement-hosted microbial community variation with substrate composition and age.

Scientific ocean drilling has revealed that microorganisms, including Archaea, Bacteria, viruses, and eukaryotic fungi and protists are present, intact, and metabolically active in uncontaminated deep subsurface sediment and basalt. Knowledge about subseafloor microbial communities has grown exponentially since the initial microbiological investigations by DSDP in the 1980s, but only ~4% of ODP/Integrated Ocean Drilling Program/IODP sites have been sampled, documented, or archived for microbiological purposes (Figure **F6**) (Kallmeyer et al., 2012; Orcutt et al., 2014). Determining microbial community composition and physiological capabilities along the SAT will provide insights into the role of microbes in mineral alteration, hydrocarbon formation, and global biogeochemical cycles.

In sediments, the number of microbial cells present is estimated to equal that in the entire oceanic water column (Kallmeyer et al., 2012). However, the amount of biomass stored in the deep subsurface remains contentious because microbial cell abundance in subseafloor sediment varies by approximately five orders of magnitude (Figure **F6**) with significant geographic variation in the structure of subseafloor communities (Inagaki et al., 2006). Most studies have focused on relatively high biomass continental shelf systems (Inagaki and Orphan, 2014). Holocene efforts, including Integrated Ocean Drilling Program Expeditions 329 (South Pacific Gyre; Expedition 329 Scientists, 2011) and 336 (North Pond; Expedition 336 Scientists, 2012), investigated lower biomass sedimentary systems underlying oceanic gyres. Crucially, no data have been collected from the South Atlantic Gyre (Figure **F6**). Hence, postexpedition analyses of the cores recovered during the SAT expeditions will refine the global biomass census and improve our understanding of the global carbon cycle.

The presence or absence of oxygen in marine sediments has profound implications for the quantity, diversity, and function of microbial communities. Oxygen penetration depth varies between oceanic regions and settings, ranging from only a few millimeters in areas with high rates of microbial respiration, such as on continental shelves, to the entire sediment column in extremely low biomass sediments, such as the relatively thin sediments beneath the South Pacific Gyre

(D'Hondt et al., 2015). Extrapolation of an observed global relationship between oxygen penetration and sedimentation rate and thickness indicates South Atlantic Gyre sediment may be oxic to basement (D'Hondt et al., 2015). During Leg 3, oxygen was not measured, but pore water sulfate was detected near the basement. However, sediment organic carbon concentrations along the SAT are intermediate to those of North Pond, where oxygen penetrated tens of meters below seafloor and nitrate was present to basement, and Nankai Trough, where oxygen was depleted by 3 meters below seafloor (mbsf) and sulfate was depleted by 19 mbsf (Figure **F7**; Expedition 336 Scientists, 2012; Tobin et al., 2009; Orcutt et al., 2013; Reese et al., 2018). These results indicate that oxygen is unlikely to extend to the basement at sites along the SAT, contrary to model predictions (D'Hondt et al., 2015), and that the classical redox succession of oxygen respiration followed by nitrate reduction, potentially followed by metal reduction, may be present. However, oxygen may be reintroduced at the bottom of the sediment column because of oxygenated fluid flow from the uppermost volcanic basement, which is the case at North Pond (Expedition 336 Scientists, 2012). The recovery of the sediment package across the South Atlantic Gyre allows us to investigate the relationships between oxygen penetration, biomass, and carbon limitation of microbial activity.

Drilling allows us to compare the phylogenetic diversity, functional structure, and metabolic activity of South Atlantic Gyre communities with results from previously studied regions. By exploiting the variations in sediment carbon composition expected across the subsiding MOR flank, we can examine the response of autotrophy versus heterotrophy to carbonate chemistry. Additionally, previous studies of the sedimentary deep biosphere have explored community diversity based on site-to-site or downhole (age) comparisons, often implicitly assuming a similar starter community that colonized the seafloor and whose structure and function subsequently changed in response to evolving geochemical conditions or burial depth. However, recent work suggests energy limitation may preclude replication (Lever et al., 2015; Lomstein et al., 2012) and thus limit community changes. The SAT age-transect approach allows us to test this assumption directly by investigating the impact of burial depth and chemical zonation on sediment of the same age and hence the same starter community.

Given the dearth of basement holes in ocean crust of intermediate age before the SAT expeditions, it is no surprise that there were no microbiological samples across the critical ridge–flank transitions in basement properties that may affect microbial communities prior to the SAT expeditions (Figure **F5**). Most of the biological alteration of subseafloor basalts is thought to occur within 20 My of crustal formation (Bach and Edwards, 2003). However, microbiological investigations of

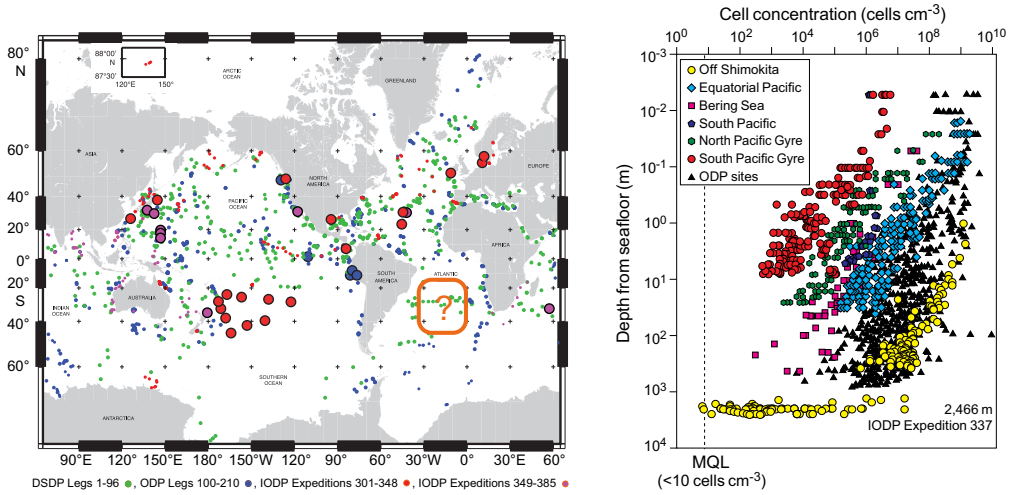

Figure F6. Left: global distribution of DSDP/ODP/Integrated Ocean Drilling Program/IODP drill sites. Larger circles = sites where microbiological samples were taken. Right: microbial cell abundance vs. depth at sampled sites, which reveals over five orders of magnitude of variation in biomass-depth trends, depending on geographic origin of samples (after D'Hondt et al., 2019). MQL = minimum quantifiable limit. South Atlantic represents a crucial gap in knowledge (orange box with question mark), and sampling proposed here will be used to groundtruth models predicted from current biomass database. Note that symbol colors between diagrams are not related because they are derived from different sources.

oceanic basement have focused on young (<10 Ma) crust (Jungbluth et al., 2013; Lever et al., 2013; Mason et al., 2010; Orcutt et al., 2011) or older (>65 Ma) lava associated with hotspot volcanism along the Louisville Seamount Trail (Expedition 330 Scientists, 2012; Sylvan et al., 2015). Basement outcrops that penetrate the relatively impermeable sediment provide permeable conduits that facilitate subseafloor fluid circulation in older basement (Wheat and Fisher, 2008). Fluid flow across the sediment/basement interface can produce redox gradients that provide recharge of depleted electron acceptors (e.g., oxygen and nitrate) to basal sediments, as observed above 3.5 and 8 Ma ocean crust on the Juan de Fuca Ridge flank (Engelen et al., 2008) and at North Pond (Orcutt et al., 2013), respectively. However, the extent and duration of fluid flow through this interface across the ridge flanks remains unknown (Figure **F5**). The recovery of the uppermost basaltic basement from 7 to 61 Ma along the SAT enables us to determine whether microbial populations are indeed present in basement older than 20 Ma where hydrothermal flow persists across the ridge flanks and to investigate the nature, extent, and duration of communication between the sedimentary and crustal biosphere for the first time.

The SAT expeditions were designed to sample subseafloor populations of Bacteria, Archaea, viruses, and microbial eukaryotes in both the sedimentary and upper crustal ecosystems across the aging Mid-Atlantic Ridge flank, quantify their biomass by cell enumeration, identify them using molecular biology methods, measure the stable isotopic composition (C, N, and S) of sediment and basement to relate processes to geochemistry, measure their metabolic activities using a variety of incubation assays, and resolve their physiological adaptations with omics-based approaches with the following aims:

- To evaluate cell abundance and community activity in the low-energy subseafloor biosphere of the South Atlantic Gyre and refine estimates of global subseafloor sedimentary microbial abundance;

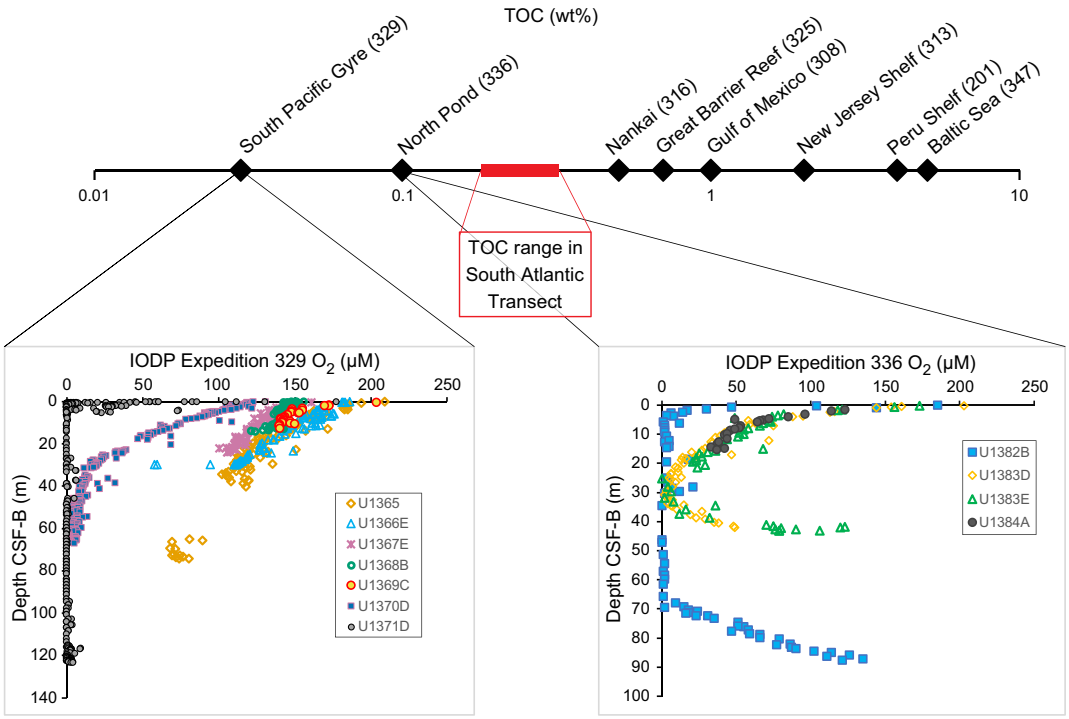

Figure F7. Comparison of predicted range of weight percent TOC for proposed SAT study area with other areas where scientific ocean drilling has conducted microbiological investigations (expedition numbers in brackets; data following Andrén et al., 2015; Shipboard Scientific Party, 2003a; Expedition 329 Scientists, 2011; Expedition 336 Scientists, 2012; Expedition 308 Scientists, 2006; Tobin et al., 2009; Expedition 313 Scientists, 2010; Expedition 325 Scientists, 2011). Proposed drill sites have higher TOC concentrations than South Pacific Gyre, where oxygen penetrated to basement, and North Pond, where oxygen penetrates tens of meters into the seafloor in Holes U1383D, U1383E, and U1384A, but lower than Nankai Trough, where pore water oxygen is consumed less than 5 m below seafloor, based on pore water Mn concentrations.

- To resolve model predictions about the depth of oxygen penetration into sediment from overlying seawater and into the bottom of the sediment package from oxygenated fluid in basement;
- To evaluate the role of subseafloor microbes in sediment biogeochemistry and basement alteration and hence global biogeochemical cycles; and
- To investigate how aging of the ocean crust influences the composition of the crustal biosphere, particularly the effects of changing oxidation state and permeability on microbial abundance, diversity, and function.

The SAT samples will also allow us to test the following hypotheses:

- South Atlantic Gyre microbial communities share membership and function with both oligotrophic sediments, like those found at North Pond, and open-ocean systems with higher organic matter input, such as Nankai Trough, given the intermediate organic carbon content of the SAT sites.
- Microbial community structure and diversity depends on the starter community (and hence sediment age) rather than subsequent selection driven by burial or chemical zonation.
- Crustal biomass decreases with increasing basement age, and communication between the sedimentary and crustal biosphere ceases with the cessation of hydrothermal flow and sealing of the basement.
- Microbial diversity increases within subseafloor basalts with basement age as previously demonstrated in basalts exposed on the seafloor (Lee et al., 2015; Santelli et al., 2009).

3.3. Objective 3 (secondary): investigate the responses of Atlantic Ocean circulation patterns and the Earth's climate system to rapid climate change, including elevated atmospheric CO_2 during the Cenozoic.

Climate change due to anthropogenic CO_2 emissions poses significant and imminent threats to global society and the biosphere. Knowledge of past ocean circulation patterns and temperatures is essential to understand the operation of Earth's climate system and required to improve the efficacy of numerical models in simulating intervals of high pCO_2. High pCO_2 intervals are commonly characterized by relatively shallow lysocline and calcite compensation depths (CCDs) resulting in poor preservation of calcareous microfossils used to generate paleoceanographic records and reconstruct past climates. This problem can be overcome by coring sediment deposited on basement slightly older than the targeted sediment age that accumulated prior to thermal subsidence of the seafloor below the CCD. More continuous composite stratigraphic sequences can be obtained by drilling multiple sites along a crustal age transect, a strategy successfully employed during ODP Leg 199 (Shipboard Scientific Party, 2002) and Integrated Ocean Drilling Program Expedition 320/321 (Pälike et al., 2012). The Walvis Ridge depth transect sampled during ODP Leg 208 demonstrated the dynamic nature of the Cenozoic CCD and lysocline in the eastern South Atlantic (Shipboard Scientific Party, 2004) and the value of redrilling DSDP transects to collect more complete records of Earth's history. Although spot cored, Leg 3 sites in the western South Atlantic demonstrated moderate to excellent carbonate preservation along the SAT (The Shipboard Scientific Party, 1970) and the area's suitability for high-resolution paleoclimatic and paleoceanographic reconstructions through key intervals of rapid climate change (Figure **F8**; Cramer et al., 2009; Zachos et al., 2001, 2008), including the PETM and other short-lived hyperthermals, early and middle Eocene climatic optima, the onset of Antarctic glaciation across the Eocene–Oligocene Transition (EOT), multiple Oligocene and the Miocene glaciation events (Oi and Mi events), the Miocene climatic optimum and Monterey Carbon Excursion, the Middle Miocene climate transition, Pliocene warmth, and the onset of Northern Hemisphere glaciation.

Global ocean circulation transfers heat and nutrients around the globe, both influencing and responding to changes in Earth's climate system (Broecker, 1991; Stommel, 1961; Wunsch, 2002). The western intensification of ocean currents means that by characterizing western portions of major ocean basins using drilling transects, records of deepwater mass properties and thus the development of modern thermohaline circulation can be constructed. The western South Atlantic

is the main northward flow path of Antarctic Bottom Water (AABW) and southward flow path of North Atlantic Deep Water (NADW) and their precursor water masses. Consequently, the SAT expeditions will provide complementary data needed to constrain the evolution of thermohaline circulation patterns and climate change as the Drake Passage and Southern Ocean opened, the northern NADW gateway opened, and the Tethys Ocean became restricted to thermohaline circulation. In particular, the SAT cores will assist in establishing how high-latitude sea surface (and hence deep ocean) temperatures and the CCD varied in response to pCO_2 changes and ocean acidification (Barker and Thomas, 2004; Barrera et al., 1997; Billups, 2002; Bohaty et al., 2009; Cramer et al., 2009; Frank and Arthur, 1999; Kennett and Stott, 1991; Scher and Martin, 2006; Thomas et al., 2003; Wright et al., 1991). Together the complementary records from western North Atlantic sediments (Integrated Ocean Drilling Program Expedition 342; Norris et al., 2014) and the SAT will provide an exceptional record of the evolution of Atlantic overturning circulation through the Cenozoic.

A novel, direct way to compare paleoceanographic reconstructions of past high pCO_2 to modern conditions is to recover sediments along transects of water column data collected by the WOCE. The SAT constitutes a paleo-WOCE line following the western portion of WOCE Line A10 (Figure **F9**), providing access to paleoceanographic records of southern- and northern-sourced deep and bottom waters. We will test models of bipolar deepwater evolution (e.g., Borrelli et al., 2014; Cramer et al., 2009; Katz et al., 2011; Tripati et al., 2005) using stable and radiogenic isotope analyses of sediments recovered from these key western South Atlantic sites.

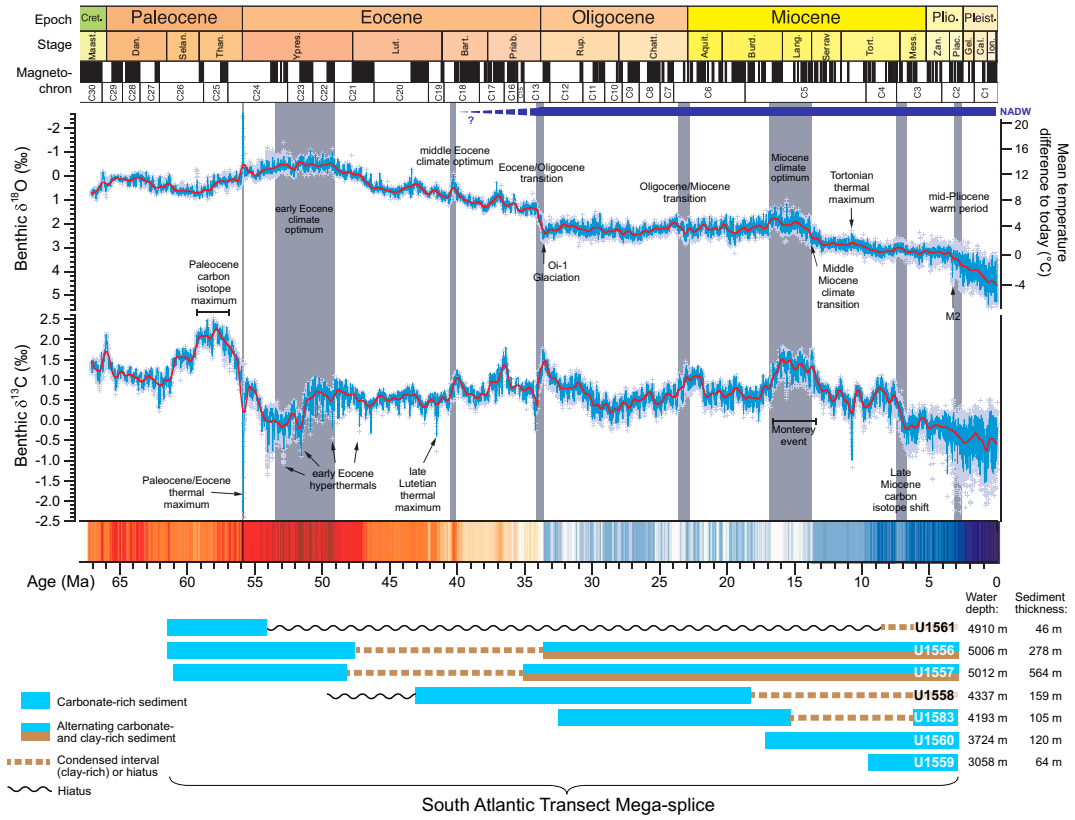

Figure F8. Composite deep-sea benthic foraminiferal $\delta^{13}C$ and $\delta^{18}O$ records showing both gradual and abrupt changes in global climate during Cenozoic, with key events highlighted by vertical bars (modified from Westerhold et al., 2020). Red and blue climate stripes show departure from average Cenozoic temperature in 100 ky time bins, with red representing warmer than average temperatures and blue colder than average. A rich paleoceanographic record of these changes has been accessed by drilling the SAT sites. Bars on bottom show 7 SAT sites, present water depth, and intervals of Cenozoic climate history they sampled. The deepest sites will generally contain carbonate-rich sediments (blue) in the older part, deposited when site was closer to ridge crest and shallower than CCD, transitioning up to carbonate-poor sediment (brown) in the younger part as each site subsided below CCD. Sites on younger oceanic crust will recover younger carbonate-rich sediments. Together, these sites represent a megasplice that recovered the last 61 My of Earth's climate history from an understudied region of the ocean.

The Walvis Ridge depth transect (Shipboard Scientific Party, 2004) revealed a dramatic 2 km shoaling of the CCD during the PETM due to the acidification of the ocean from massive carbon addition followed by a gradual recovery (Figure **F10**) (Zachos et al., 2005; Zeebe et al., 2008). Given chemical weathering feedbacks, the recovery of the CCD should have resulted in a transient overdeepening of the CCD (Dickens et al., 1997). Collectively, the SAT sites will provide additional data for reconstructing changes in the position of the lysocline and CCD in the western South Atlantic that are essential for constraining the timing of gateway events and the history of Northern Component Water (NCW) and Southern Component Water (SCW), which were the precursors to NADW and AABW, and the nature of Atlantic basin responses to climate change relative to the Pacific.

Microfossils provide a critical archive of ocean and climate history, including long-term changes (e.g., early Eocene warmth, Cenozoic cooling, and Pliocene warmth) and abrupt events (e.g., early Paleogene hyperthermals and multiple glaciation events). The SAT expeditions were designed to recover complete sedimentary sections along paleo-WOCE Line A10, exploiting the thermal subsidence of the ocean crust along the transect to provide material for high-resolution proxy records including benthic and planktic foraminiferal geochemistry, micropaleontological assemblages, orbitally tuned age models, neodymium isotopes, and alkenone $\delta^{13}C$ and boron isotope pCO_2 reconstructions with the following aims:

- To reconstruct the evolution of deepwater masses over the past 61 My to assess contributions of NCW and SCW in the early Paleogene western South Atlantic (Kennett and Stott, 1990), document the influence of the openings of the Drake and Tasman Passages on South Atlantic deepwater circulation, and reconstruct the overall development of modern thermohaline circulation;

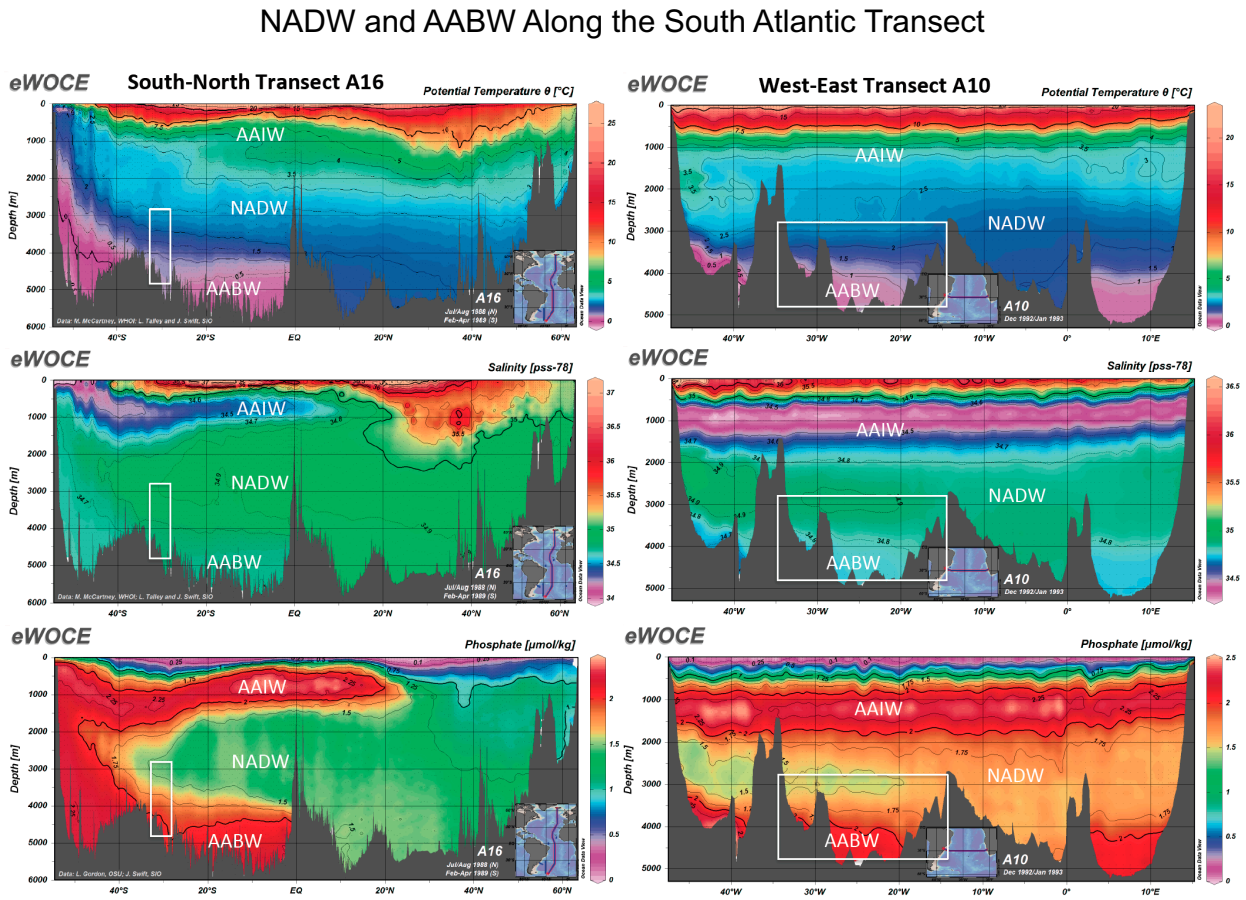

Figure F9. WOCE temperature, salinity, and phosphorus profiles along south–north Transect A16 through western South Atlantic Basin and west–east Transect A10 at 30°S close to location of SAT (data from WOCE; **http://www.ewoce.org**). Rectangles show approximate coverage of SAT. AAIW = Antarctic Intermediate Water.

- To provide high-resolution constraints on CCD and carbonate chemistry changes of the deep western Atlantic, particularly during transient hyperthermals and other intervals of global warmth;
- To reconstruct the Cenozoic history of the South Atlantic subtropical gyre by monitoring proxies of productivity and paleobiogeography of plankton, rates of speciation/extinction relative to the equatorial zone and higher latitudes, and changes in biodiversity and subtropical ecosystem dynamics; and
- To evaluate the response of subtropical planktic and benthic biota to changing environmental conditions such as global warming, ocean acidification, or fertility patterns during intervals of rapid climate change through the Cenozoic.

The recovered sediment sections will also allow us to test the following hypotheses:

- Low-latitude sites were potential sources of deepwater formation at times of global warmth and high atmospheric pCO_2.
- The strength of the coupling between the climate and the carbon cycle varied through the Cenozoic.
- The lysocline and CCD responded differently on the western side of the Mid-Atlantic Ridge compared to the Walvis Ridge record due to changing deep/bottom water sources, gateway configurations, and flow paths.

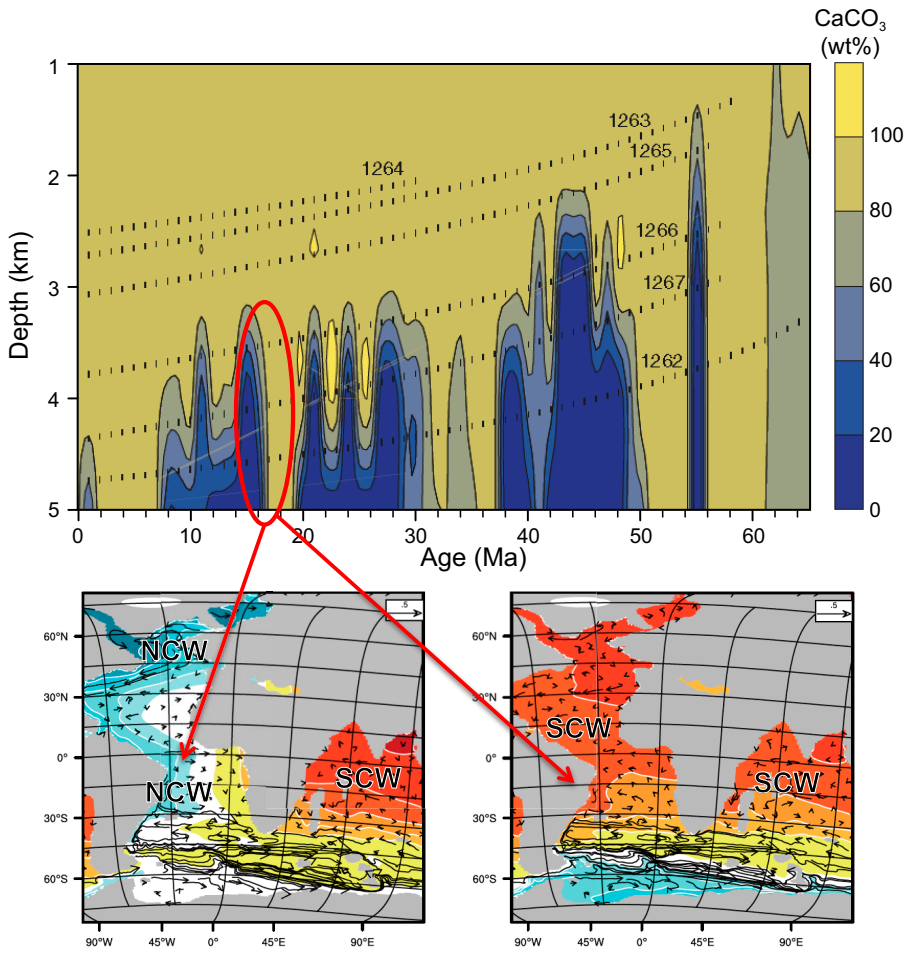

Figure F10. Top: percent carbonate in depth transect of drill sites recovered during Leg 208 on Walvis Ridge, eastern South Atlantic (Shipboard Scientific Party, 2004). Position of lysocline and CCD were dynamic during Cenozoic related to changing deepwater circulation, productivity, and ocean acidification associated with PETM. Bottom: modeled relative water mass age during mid-Miocene climatic optimum (Coggon et al., 2020). Red oval = correlative changes in carbonate chemistry on Walvis Ridge. Colors represent benthic age, which is a $\delta^{13}C$-like tracer; red = old water, blue = young water. Left: mode with NCW on. Right: NCW off. The SAT, near 31°S, is expected to capture changes in these two modes of deepwater formation.

- The subtropical gyre cut off the delivery of heat to Antarctica as the Antarctic Circumpolar Current developed through the late Eocene–Oligocene.

3.4. Connections to the 2050 Science Framework

Given its multidisciplinary essence, the SAT campaign will advance the full spectrum of the 2050 Science Framework including each of the seven interconnected Strategic Objectives (SOs) and five Flagship Initiatives (FIs) (Koppers and Coggon, 2020). For example, SAT Objective 1 explores hydrothermal alteration and fluid-rock exchange during crustal aging through the recovery of upper crustal sections (>100 m) along a crustal age transect. This aspect of the project directly relates to the 2050 Science Framework SO2 The Oceanic Life Cycle of Tectonic Plates and SO6 Global Cycles of Energy and Matter, as well as FI2 Probing the Deep Earth. Documenting the impact of fluid-rock exchange on the composition and physical properties of the crust as a function of its age provides insights into key properties of old crust entering subduction zones, such as hydration state, seismic velocity, and strength, to inform studies of hazards generated along convergent plate margins (SO7 Natural Hazards Impacting Society and FI3 Assessing Earthquake and Tsunami Hazards).

Quantifying the abundance and diversity of microbial life in ocean crust and the overlying nutrient-limited sediment environments (SAT Objective 2) will help determine the impact of biological activity in geochemical cycles and improve our understanding of the limits of life in the lithosphere. This knowledge will contribute to SO1 Habitability and Life on Earth, SO6 Global Cycles of Energy and Matter, and FI5 Exploring Life and its Origins. SAT Objective 3 investigates the responses of Atlantic Ocean circulation patterns and the Earth's climate system to rapid climate change. This objective relates to SO3 Earth's Climate System, SO4 Feedbacks in the Earth System, and SO5 Tipping Points in Earth's History, as well as FI1 Ground Truthing Future Climate Change and FI4 Diagnosing Ocean Health by examining the ocean's past responses to climate events, including hyperthermals, changes in oxygenation, and acidification, to look ahead to future impacts on Earth's climate and ecosystems.

The SAT project also embraced new technologies and approaches to core description and objective quantification of recovered cores through the analysis of high-resolution images of external core surfaces and the application of machine learning approaches (e.g., Enabling Element 4 Technology Development and Big Data Analytics). The ambitious operational goals of the SAT project align with the 2050 Science Framework and emphasize, as stated in the framework, that achieving these scientific objectives "requires continued developing of drilling, coring, logging, observatory, and laboratory tools and techniques." Overall, the mission of the 2050 Science Framework for scientific ocean drilling is to guide "multidisciplinary subseafloor research into the interconnected processes that characterize the complex Earth system and shape our planet's future." The breadth of the interrelated science addressed by the SAT project exemplifies such investigation of the interconnected Earth by IODP.

4. Operational strategy

The original operational strategy for Expeditions 390 and 393 is described in detail in the *Scientific Prospectus* (Coggon et al., 2020) and was updated in the *Scientific Prospectus Addendum* (Coggon et al., 2022b) following the completion of engineering Expeditions 390C and 395E. In brief, the SAT intended to drill six sites located at five different crustal ages (~7, 15, 31, 49, and 61 Ma), with two of the sites located in the same localized sedimentary basin on 61 Ma crust where significant basement topography results in variable sediment thickness (~180 and 640 m thick at proposed Sites SATL-53B and SATL-54A, respectively). At each of the six sites, we planned the following operations to achieve our scientific objectives and establish legacy boreholes for future basement experiments:

1. Recover a complete sediment section by coring three advanced piston corer (APC)/extended core barrel (XCB) sediment holes at each crustal age to allow compilation of complete paleoceanographic records across core breaks in the sediment sections using stratigraphic correla-

tion and to provide sufficient material for whole-round microbiological and pore water sampling,
2. Recover the sediment/basement interface using the XCB system,
3. Install a drill-in reentry cone and casing to ~5 meters subbasement (msb),
4. Core to ~250 msb, and
5. Collect wireline geophysical logging data through the basement sections.

4.1. Depth of basement drilling

To fully quantify the extent and duration of ridge flank hydrothermal exchange, we required our sampling of the upper basement to be as representative as possible of the entire extrusive crust. A systematic downward decrease in the extent of oxidative hydrothermal alteration is not observed through all previously drilled upper crustal sections (Shipboard Scientific Party, 2003b), and the permeability of the extrusive crust is highly heterogeneous and not always greatest at the top of the basement (Becker et al., 2013; Shipboard Scientific Party, 2003b). Commonly, fluid flow in the upper crust is channeled along specific horizons of enhanced permeability (Harris et al., 2015; Neira et al., 2016). At many drill sites globally, the fluid temperature–depth distribution recorded by hydrothermal carbonate veins, typically one of the last hydrothermal phases to form, indicates the circulation of cool (<100°C) ridge flank fluids through at least the upper 300 m (Coggon et al., 2010). If there is a depth limit to off-axis fluid circulation, sufficient basement drilling is required to establish what it is and how it varies across the ridge flanks; therefore, we need to achieve the maximum possible basement penetration in the time available. Consequently, our target was to core ~250 m into the uppermost basaltic ocean crust at each site along the transect.

5. Preexpedition engineering and coring operations

SAT Expeditions 390 and 393 were originally scheduled for October–December 2020 and April–June 2021, respectively. In 2020 and 2021, the global COVID-19 pandemic resulted in the postponement of several IODP expeditions, including Expeditions 390 and 393. In response, the ship was used to conduct preparatory work for postponed expeditions that did not require a science party aboard but could be carried out by the ship's crew and a team of technicians from the *JOIDES Resolution* Science Operator (JRSO). Two of these expeditions (390C and 395E) were in service of the SAT drilling project to reduce the operational risks and expedite basement drilling during the postponed Expeditions 390 and 393 by coring one hole through sediment to basement and installing a cased reentry system <5 m into basement in a second hole at each of the six proposed primary SAT sites. All basement drilling was deferred to Expeditions 390 and 393.

During Expedition 390C, which sailed in October–December 2020 (Estes et al., 2021), the sediment section at four of the SAT sites (U1556–U1559) was cored. The contact with basalt was slightly deeper than estimated at all sites (Table **T1**), likely because of a slight underestimation of the in situ seismic velocities. At 61 Ma Site U1556, basalt was encountered at 278 mbsf, significantly deeper than expected (180 mbsf). If the sediment had also been thicker than expected (640 m) at proposed Site SATL-54A ~2.5 km west of Site U1556, the casing length required would have exceeded the drill string weight limit for the water depth (~5 km). Therefore, alternate proposed Site SATL-56A replaced Site SATL-54A and was drilled as Site U1557. The site is ~6.5 km east of Site U1556 in the same localized sedimentary basin, where the basement contact was estimated to be 510 mbsf and encountered at 564 mbsf.

The reentry systems were to be installed using the Dril-Quip running tool, which permits later extension of casing. However, there were difficulties installing casing into basement with this system (Estes et al., 2021) similar to difficulties that had been reported during previous operations using the Dril-Quip system (e.g., Fryer et al., 2018). The extra time taken for troubleshooting meant that reentry installations could not be completed at all sites, and a second expedition was planned. Expedition 395E (April–June 2021; Williams et al., 2021) completed additional SAT preparatory work at Sites U1556, U1557, and U1560. Following installation of reentry systems at Sites U1556 and U1560 and extending casing at Site U1557, there was insufficient time to core and install a reentry system at proposed Site SATL-33B (on 31 Ma crust). Instead, a single APC/XCB

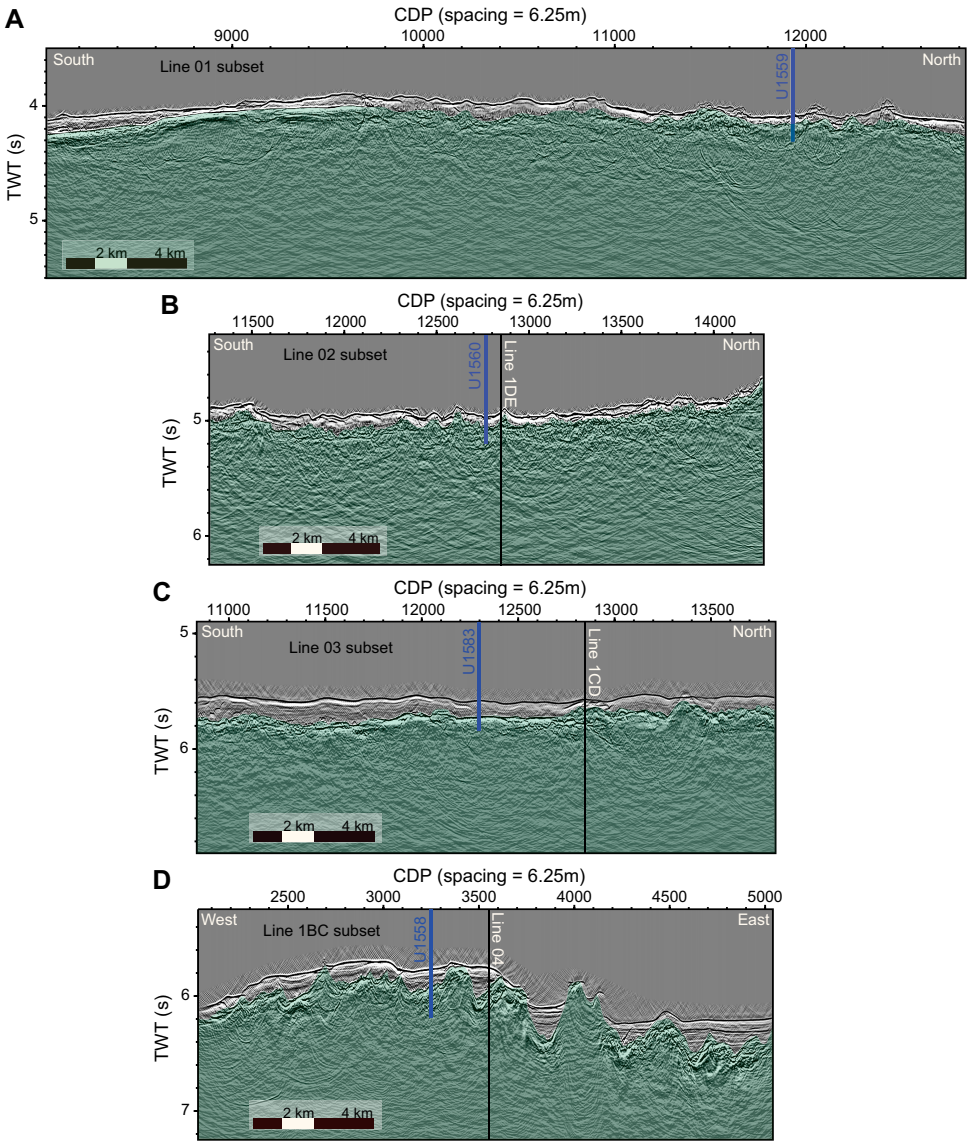

Figure F11. A–D. Seismic reflection profiles for SAT sites occupied during Expedition 393.

hole was cored at an alternate site adjacent to Sites U1556 and U1557, overlying 61 Ma crust (Site U1561; proposed Site SATL-55A; Figure **F11**; Table **T1**). Proposed Site SATL-33B was the only primary SAT site at which no operations were conducted prior to Expeditions 390 and 393.

6. Expedition 390C and 395E principal results

Because there was no shipboard science party on the ship during engineering Expeditions 390C and 395E, no cores were described during the expeditions. Instead, the Expedition 390C and 395E cores are considered part of the joint Expeditions 390 and 393 and were described in detail by the expeditions' shipboard science parties in combination with new cores recovered from each site. Although a range of physical properties and chemical analyses were conducted during Expeditions 390C and 395E, sediment microbiological sampling was not possible. Core catcher samples were collected for distribution to the Expedition 390 and 393 micropaleontologists and these allowed the development of preliminary biostratigraphic age models on shore ahead of Expeditions 390 and 393. A summary of the engineering expedition shipboard data is provided in the Expedition 390C and 395E *Preliminary Reports* (Estes et al., 2021; Williams et al., 2021), but all data generated

during the preexpedition engineering operations along with the descriptions of the Expedition 390C and 395E cores made during Expeditions 390 and 393 are combined with the results of Expeditions 390 and 393 and presented in the relevant site reports. The Expedition 390C and 395E geochemical data provided a valuable guide for chemical and microbiological sampling during Expeditions 390 and 393.

7. Revised Expedition 390 and 393 operational strategy

The successful installation of five of the six planned reentry systems along the SAT prior to Expeditions 390 and 393 significantly decreased the operational risk of the SAT expeditions. The time savings due to operations already completed were partially offset by the need to sail to and from Cape Town, rather than from Cape Town to Montevideo for Expedition 390 and from Montevideo to Montevideo for Expedition 393. These lengthier voyages added additional transit time to both expeditions. Extra time was also required to recore the thicker than expected sediments. The operations plans for the rescheduled Expeditions 390 and 393 were revised to account for these changes (Coggon et al., 2022b; Table **T2**; Figure **F12**). The failure of one of the electromagnetic

Table T2. Expedition 393 hole summary. * = between casing shoe at 122 mbsf and hole total depth at 124 mbsf (determined during Expedition 395E). DSF = drilling depth below seafloor. NA = not applicable. MM = missed mudline, water depth not directly determined.

Hole	Proposed site	Age (Ma)	Half spreading rate (mm/y)	Distance from MAR (km)	Latitude	Longitude	Water depth (m)	End of Exp. 393 depth (m)	Total penetration DSF (m)	Ocean crust penetration (m)	Depth to basement DSF (m)	Sediment/ basement interface core, section	Drilled interval (m)
U1559B	SATL-13A	6.6	17.0	130	30°15.6336′S	15°02.0941′W	3055	107.9	49.0	42.9	65.0	3R-1, 9 cm	NA
							Site U1559 totals:	107.9	49.0	42.9			NA
U1560B	SATL-25A	15.2	25.5	315	30°24.2057′S	16°55.3702′W	3723	316.1	192.2	193.1	~123*	NA	NA
U1560C	SATL-25A	15.2	25.5	315	30°24.2005′S	16°55.3703′W	3724	129.3	129.3	0.3	129.0	18X-2, 0 cm	2.0
							Site U1560 totals:	445.4	321.5	193.4			2.0
U1583A	SATL-33B	30.6	24.0	652	30°42.6060′S	20°26.0340′W	MM	NA	9.1	NA	NA	NA	NA
U1583B	SATL-33B	30.6	24.0	652	30°42.6062′S	20°26.0341′W	MM	NA	9.4	NA	NA	NA	NA
U1583C	SATL-33B	30.6	24.0	652	30°42.6011′S	20°26.0343′W	4215 (MM)	107.5	107.5	1.5	106.0	13X-1, 0 cm	NA
U1583D	SATL-33B	30.6	24.0	652	30°42.6288′S	20°26.0340′W	MM	NA	9.5	NA	NA	NA	NA
U1583E	SATL-33B	30.6	24.0	652	30°42.6285′S	20°26.0340′W	4210	105.2	105.2	NA	NA	NA	NA
U1583F	SATL-33B	30.6	24.0	652	30°42.6175′S	20°26.0336′W	4210	239.5	239.5	129.8	109.7	3R-1, 0 cm	101.0
							Site U1583 totals:	452.2	480.2	131.3			101.0
U1558D	SATL-43A	49.2	19.5	1067	30°53.7814′S	24°50.4822′W	4334	370.3	220.2	203.5	166.8	4R-1, 0 cm	NA
U1558E	SATL-43A	49.2	19.5	1067	30°53.7922′S	24°50.4822′W	MM	NA	9.5	NA	NA	NA	NA
U1558F	SATL-43A	49.2	19.5	1067	30°53.7923′S	24°50.4757′W	4337	177.2	177.2	1.2	176.0	24X-CC, 16 cm	3.0
							Site U1558 totals:	547.5	406.9	204.7			3.0
							Expedition 393 totals:	1553.0	1257.6	572.3			106.0

Hole	Cored interval (m)	Core recovered (m)	Recovery (%)	Total cores (*N*)	APC cores (*N*)	HLAPC cores (*N*)	XCB cores (*N*)	RCB cores (*N*)	Start date (2022)	Start time UTC (h)	End date (2022)	End time UTC (h)	Time on hole (h)	Time on hole (days)
U1559B	49.0	12.8	26.2	12	0	0	0	12	19 Jun	1115	23 Jun	1230	97.2	4.05
Site U1559 totals:	49.0	12.8	26.2	12	0	0	0	12					97.2	4.1
U1560B	192.2	74.8	38.9	40	0	0	0	40	19 Jul	0124	28 Jul	2355	238.6	9.94
U1560C	127.3	122.8	96.4	17	10	5	2	0	28 Jul	2355	30 Jul	1926	43.4	1.81
Site U1560 totals:	319.5	197.5	67.7	57	10	5	2	40					282.0	11.8
U1583A	9.1	9.1	100.4	1	1	0	0	0	06 Jul	0324	06 Jul	1615	13.0	0.54
U1583B	9.4	9.4	99.8	1	1	0	0	0	06 Jul	1615	06 Jul	1800	1.7	0.07
U1583C	107.5	110.2	102.5	13	12	0	1	0	06 Jul	1800	07 Jul	1540	21.6	0.9
U1583D	9.5	10.0	105.7	1	1	0	0	0	07 Jul	1540	07 Jul	1730	1.9	0.08
U1583E	105.2	105.2	100.0	12	12	0	0	0	07 Jul	1730	10 Jul	0430	59.0	2.46
U1583F	138.5	45.8	33.1	28	0	0	0	28	10 Jul	0430	18 Jul	0845	196.3	8.18
Site U1583 totals:	379.2	289.7	90.2	56	27	0	1	28					293.5	12.2
U1558D	220.2	100.8	45.8	38	0	0	0	38	28 Jun	0035	05 Jul	0524	172.8	7.2
U1558E	9.5	10.0	105.0	1	1	0	0	0	25 Jun	1130	26 Jun	0515	17.8	0.74
U1558F	174.2	164.3	94.3	23	9	9	5	0	26 Jun	0515	28 Jun	0035	43.4	1.81
Site U1558 totals:	403.9	275.1	81.7	62	10	9	5	38					234.0	9.8
Expedition 393 totals:	1151.6	775.2	66.4	187	47	14	8	118					906.7	37.8

brakes on the drawworks during Expedition 390 resulted in a premature curtailment of science operations and early return to Cape Town to enable repairs (Coggon et al., 2022a). Consequently, Expedition 393 operational plans were further refined to enable basement coring at the youngest (6.6 Ma) Site U1559 (Tables **T2**, **T3**).

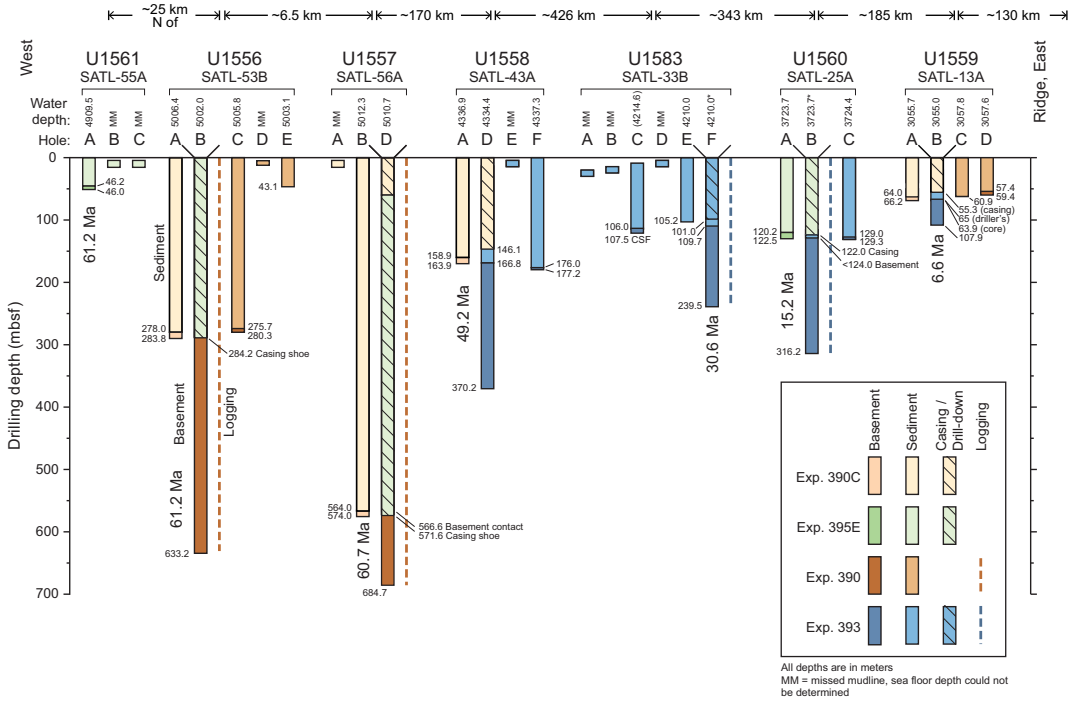

Figure F12. Scientific ocean drilling operations completed during SAT Expeditions 390C, 395E, 390, and 393.

Table T3. Comparison of South Atlantic Transect proposed targets with operational achievements at end of Expedition 393. Proposed objectives: * = achieved, † = mostly achieved, ‡ = partially achieved, ** = not achieved. NA = not applicable. (Continued on next page.)

Site information	Sediment coring	Basement depth (msb)	Wireline operations	Legacy installations
Site U1559 (proposed Site SATL-13A); 6.6 Ma				
Proposal/*Scientific Prospectus* 2020	3× APC to basement	250	2× FMS + triple combo + UBI	Reentry cone case near basement
Expeditions 390C and 395E	390C-U1559A†	250	2× FMS + triple combo + UBI	390C-U1559B
Scientific Prospectus Addendum 2022				*
Revised operational plan May 2022	390-U1559C, 390-U1559D*	250	2× FMS + triple combo + UBI	*
Achieved—end of Expedition 393	*	43**	No logging**	*
Site U1560 (proposed Site SATL-25A); 15.2 Ma				
Proposal/*Scientific Prospectus* 2020	3× APC to basement	250	2× FMS + triple combo + UBI	Reentry cone case near basement
Expeditions 390C and 395E	395E-U1560A†	250	2× FMS + triple combo + UBI	395E-U1560B*
Scientific Prospectus Addendum 2022	2× APC			*
Revised operational plan May 2022	1× APC	150	2× FMS + triple combo + UBI	*
Achieved—end of Expedition 393	393-U1560C†	193†	2× FMS + triple combo + UBI‡	*
Site U1583 (proposed Site SATL-33B); 30.6 Ma				
Proposal/*Scientific Prospectus* 2020	3× APC to basement	250	2× FMS + triple combo + UBI	Reentry cone case near basement
Expeditions 390C and 395E				
Scientific Prospectus Addendum 2022	3× APC	250	2× FMS + triple combo + UBI	Reentry cone case near basement
Revised operational plan May 2022	2× APC	250		Free-fall funnel
Achieved—end of Expedition 393	393-U1583C, 393-U1583E‡	129.8‡	1× FMS + triple combo‡	393-U1583F**
Site U1558 (proposed Site SATL-43A); 49.2 Ma				
Proposal/*Scientific Prospectus* 2020	3× APC to basement	250	2× FMS + triple combo + UBI	Reentry cone case near basement
Expeditions 390C and 395E	390C-U1558A	250		390C-U1558B*
Scientific Prospectus Addendum 2022	2× APC	250		*
Revised operational plan May 2022	1× APC	175		*
Achieved—end of Expedition 393	393-U1558F‡	203.5†	No logging**	Reentry system destroyed**

Table T3 (continued).

Site information	Sediment coring	Basement depth (msb)	Wireline operations	Legacy installations
Site U1557 (proposed Site SATL-56A); 61.2 Ma				
Proposal/*Scientific Prospectus* 2020	APC/XCB to basement	250	2× FMS + triple combo + UBI	Reentry cone case near basement
Expeditions 390C and 395E	390C-U1557B*			390C/395E-U1557D*
Scientific Prospectus Addendum 2022		247		*
Revised operational plan May 2022				*
Achieved—end of Expedition 390		118‡	Triple combo‡	*
Site U1556 (proposed Site SATL-53B); 61.2 Ma				
Proposal/*Scientific Prospectus* 2020	APC/XCB to basement	250	2× FMS + triple combo + UBI	Reentry cone case near basement
Expeditions 390C and 395E	390C-U1556A*			395E-U1556B*
Scientific Prospectus Addendum 2022		350		*
Revised operational plan May 2022	1× APC/XCB			*
Achieved—end of Expedition 390	390C-U1556A, 390-U1556C, and 390-U1556E*	353*	*	Reentry system lost**
Site U1561 (proposed Site SATL-55A); 61.2 Ma				
Proposal/*Scientific Prospectus* 2020	Alternative site 1× APC	NA	NA	NA
Expeditions 390C and 395E	395E-U1561A*			
Scientific Prospectus Addendum 2022				
Revised operational plan May 2022				
Achieved—end of Expedition 390	395E-U1561A*			

8. South Atlantic Transect drill sites

The SAT drilled during Expeditions 390C, 395E, 390, and 393 comprises the following seven sites from youngest to oldest:

- Site U1559 (proposed Site SATL-13A; Expeditions 390C, 390, and 393) is located nearest to the Mid-Atlantic Ridge on 6.6 Ma crust formed at a half spreading rate of 17 mm/y and overlain by ~64 m of sediment. This site provides a comparison to young intermediate spreading rate ocean crust drilled in reference Hole 504B (6.9 Ma; spreading rate of 36 mm/y; 275 m of sediment).
- Site U1560 (proposed Site SATL-25A; Expeditions 395E and 393) is located on 15.2 Ma crust formed at 25.5 mm/y and overlain by ~120 m of sediment. This site provides a comparison to reference superfast spreading rate ocean crust at Site 1256 (15 Ma; spreading rate of 220 mm/y; 250 m of sediment).
- Site U1583 (proposed Site SATL-33B; Expedition 393) is located on 30.6 Ma crust formed at 24 mm/y and overlain by ~105 m of sediment.
- Site U1558 (proposed Site SATL-43A; Expeditions 390C and 393) is located on 49.2 Ma crust formed at 19.5 mm/y and overlain by ~159 m of sediment.
- Site U1556 (proposed Site SATL-53B; Expeditions 390C, 395E, and 390) is located on 61.2 Ma crust formed at 13.5 mm/y and overlain by ~278 m of sediment.
- Site U1557 (proposed alternate Site SATL-56A; Expeditions 390C, 395E, and 390) is located on 60.7 Ma crust ~6.5 km east of Site U1556 in the same localized sedimentary basin and has a sediment thickness of ~564 m.
- Site U1561 (proposed alternate Site SATL-55A; Expeditions 395E and 390) is located on 61.2 Ma crust ~22 km north of Site U1556 and has a sediment thickness of ~46 m.

9. Site summaries

9.1. Site U1559

9.1.1. Background and objectives

Site U1559 is located ~130 km west of the Mid-Atlantic Ridge at 30°15.63′S, 15°2.09′W in 3055 m of water (Figure **F1**). The basement at Site U1559 was predicted to have formed at ~6.6 Ma at a half spreading rate of 17 mm/y (Figure **F4**). The site is located on Seismic Line CREST01 at Common Depth Point (CDP) 11923 between the CREST06 and CREST1E/F crossing lines (Figures **F1**,

F11A, F13) where a reflector at ~4.15 s two-way traveltime (TWT) was interpreted to be the top of basement and was estimated to be at 50 mbsf (Figure F11A) but observed at 64 mbsf.

Site U1559 was occupied twice before operations during Expedition 393. In November 2020, Hole U1559A was cored during Expedition 390C (Figure F12) to 66.2 mbsf, contacting basement rocks at 63.9 mbsf, and drilled in a reentry system with 13⅜ inch casing in Hole U1559B (Figure F12) to 55.3 mbsf, with the hole itself extending to 58.9 mbsf. When Expedition 390 revisited the site in May 2022, Hole U1559C was cored to 60.9 mbsf and Hole U1559D was cored to 59.4 mbsf (Figure F12). The plan for Expedition 390 was to core 250 m into basement with the rotary core barrel (RCB) system in Hole U1559B and collect wireline geophysical logging data through the basement. However, a failure of the forward electromagnetic drawworks brake caused operations to be cut short, and the ship returned to Cape Town, South Africa, early. Instead, the Hole U1559B basement objectives were postponed to the present expedition.

Site U1559 forms the young crustal end-member of the SAT and will be compared to older crustal material cored at Expedition 390/393 sites further from the ridge axis. The site is similar in age to Hole 504B in the eastern equatorial Pacific (6.9 Ma) that formed at an intermediate rate (36 mm/y half spreading rate) and is covered by 275 m of sediment. Science objectives at Site U1559 are to (1) investigate the history of the low-temperature hydrothermal interactions between the aging ocean crust and the evolving South Atlantic Ocean and quantify past hydrothermal contributions to global geochemical cycles, (2) collect samples of the sediment- and basalt-hosted deep biosphere beneath the low-productivity South Atlantic Gyre that will be used to refine global biomass estimates and investigate microbial ecosystems' responses to variable condition, and (3) construct paleoceanographic records of carbonate chemistry and deepwater mass properties across the western South Atlantic through key Cenozoic intervals of elevated atmospheric CO_2 and rapid climate change.

Expedition 393 reoccupied Hole U1559B (Figure F12) but deepened it only 49.0 m into relatively fresh basaltic lava flows of the upper ocean crust and recovered 12.8 m of hard rock core. Very slow rates of drilling (<0.7 m/h, absolute; 0.8 m/h rotational) and low rates of recovery (~26%) may in part reflect heavy damage to the RCB bit even after a short duration of rotation (52.7 h) and are perhaps displayed in the commonly flared deformation of the basalt cores recovered.

9.1.2. Operations

Previous operations in Holes U1559A and U1559B (Figure F12) are described in the Expedition 390C *Preliminary Report* (Estes et al., 2021), and Expedition 390 operations in Holes U1559C and U1559D (Figure F12) are described in the Site U1559 summary from that expedition (**https://iodp.tamu.edu/scienceops/sitesumm/390_393/390_ss1559.html**).

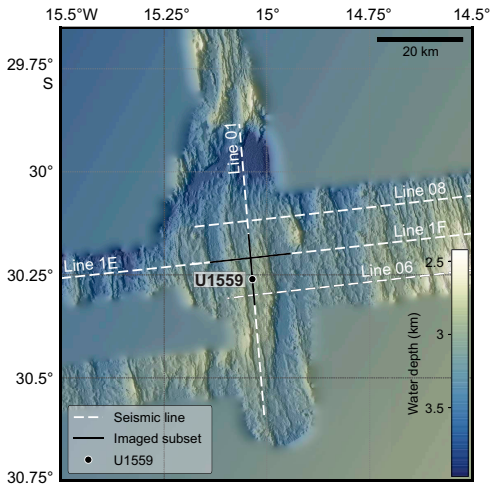

Figure F13. Site U1559 bathymetry (Christeson and Reece, 2020). Seismic reflection profiles were acquired during CREST cruise (Reece et al., 2016).

The R/V *JOIDES Resolution* departed Repair Quay 3 in Cape Town, South Africa, on 11 June 2022, with the last line released at 0949 h. We stopped just outside the harbor to test the 50 kVA uninterruptible power supply system under different levels of electrical load and then started the sea voyage to Site U1559 at 1455 h. Much of the transit was completed at reduced speed because of rough seas and high winds, and at times the heading had to be adjusted. Sea conditions began to improve on 18 June, allowing the ship to increase to full speed for the final two days of the transit. The ship completed the 1713 nmi voyage in 7 days and 23 h at an average speed of 9 kt. The ship's thrusters were lowered at 1220 h on 19 June, beginning operations in Hole U1559B.

An RCB bottom-hole assembly (BHA) was made up and run to 3031 meters below rig floor (mbrf). The top drive was picked up and a pipe pig was pumped through the drill string to clean rust from the inside. The ship maneuvered for reentry into Hole U1559B, which had been established and cased during Expedition 390C in November 2020 (Figure **F12**). We reentered Hole U1559B at 0143 h on 20 June and washed to 58.9 mbsf, the bottom of the existing hole. Cores 2R–13R penetrated from 58.9 to 107.9 mbsf and recovered 12.82 m (26.2%). Core 2R had no recovery and was drilled very quickly, indicating softer sediment above basalt. While drilling Core 3R, the drillers encountered basement at approximately 65 mbsf. Coring proceeded through Core 11R with a rate of penetration of about 1 m/h. While drilling Core 12R, penetration slowed to under 0.5 m/h with recovery decreasing. After 9% recovery of distinctively undergauge, poor quality core in Core 13R, it was decided to terminate coring and retrieve the bit to the ship. There was significant damage to the core guides and bit cones, some of which had been ground down to the bearings, creating a large 20 cm diameter hemispheroidal void where once there were cones and cutting buttons. Similar damage had been seen during recent operations drilling young basalts during IODP Expedition 395C in Holes U1562B and U1554F. Recovery in Hole U1559B was low and penetration was slow in part because of the fresh and fractured hard young ocean floor basalts being drilled but also because the ~65 m of sediment cover meant that the BHA extended ~100 m above seafloor, limiting the weight that could be applied to the bit. However, serious bit damage was clearly an issue, probably for some days. Early diagnosis and identification of warning signs of this style of bit failure require investigation. The ship was secured for transit and switched from dynamic positioning (DP) to cruise mode at 1232 h on 23 June, ending operations at Site U1559.

COVID-19 mitigation protocols were in effect from arrival in Cape Town until 24 June.

9.1.3. Principal results

Site U1559 targeted ~6.6 Ma upper oceanic crust, the youngest to be drilled along the SAT. Sediments recovered from Site U1559 during engineering Expedition 390C and fully staffed science Expedition 390 are described in the Expedition 390 *Preliminary Report* (Coggon et al., 2022a). Basal sediments and a few meters of volcanic basement had been recovered from Holes U1559A and U1559D. During Expedition 393, Hole U1559B was advanced 43 m into basement, reaching 107.9 mbsf. Core pieces were mostly <10 cm in length.

9.1.3.1. Basement

9.1.3.1.1. Igneous petrology

Five lithostratigraphic units were identified comprising four main volcanic units and one thin sedimentary unit (Figure **F14A**). Volcanic Unit 2 is divided into three subunits (2A–2C) and Unit 5 is divided into two subunits (5A and 5B) based on volcanic emplacement style and subtle changes in phenocryst assemblages. No brecciated rocks were recovered. The uppermost volcanic rocks are aphyric microcrystalline basalt sheet flows with some planar glassy margins and vuggy vesicular patches (Unit 1). These are underlain by sparsely plagioclase-phyric microcrystalline to fine-grained basalt pillow lavas (Subunit 2A) with common curved and planar glassy margins. Rare fresh olivine phenocrysts are present from 73.9 mbsf (Subunit 2B), and the absence of curved glassy margins from 83.7 mbsf suggest the lowermost lavas of this unit are sheet flows (Subunit 2C). Unit 2 basalts are separated from Unit 4 basalts by a thin layer (~10 cm) of hydrothermally altered indurated calcareous sediment (Unit 3) with altered glass impregnated into both the upper and lower contact (~85.5 mbsf). The directly underlying lavas (Unit 4) are sparsely plagioclase-phyric microcrystalline to fine-grained basalt sheet flows with rare olivine phenocrysts with the absence of glass and relatively coarse holocrystalline grain size suggesting emplacement as a sheet

flow. Unit 5 (~100.7 mbsf) comprises sparsely plagioclase-phyric microcrystalline to fine-grained basalt sheet and pillow flows with rare olivine and clinopyroxene phenocrysts. The relative abundance of olivine over plagioclase phenocrysts in the final recovered pieces distinguishes Subunit 5B (104.34 mbsf). Despite this variation, distinctive sparse macroscopic plagioclase phenocrysts are common to all the volcanic units apart from aphyric Unit 1. Together with only modest differences in geochemistry determined by portable X-ray fluorescence (pXRF) analysis, this consistency suggests that all of the igneous lithologic units at Site U1559 belong to a single comagmatic sequence of relatively normal mid-ocean-ridge basalt (N-MORB) with subtle internal variations related to fractional crystallization and other magma chamber processes. The interpretation of significant intervals of sheet flows is somewhat atypical for a slow spreading ridge. However, given the poor recovery, it is possible that some sections of pillow basalts or breccia were not recovered. This potentially biased recovery must be carefully considered by subsequent studies seeking to compare hydrothermal exchange between this hole and others along the SAT.

9.1.3.1.2. Alteration petrology

Hydrothermal alteration in Hole U1559B is characterized by pervasive gray background alteration with a variety of different colored alteration halos throughout the cored interval (Figure **F14B**). The short penetration of Hole U1559B precludes the separation of alteration zones with depth, but a downhole evolution in alteration halo types is present and the recovery of a more oxidized pillow lava fragment at the base of the hole indicates we may have only just begun to capture the full sequence of alteration at this site and crustal age. All alteration is dominated by the formation of yellow-brown clay minerals that replace mesostasis and groundmass. Calcite replaces groundmass in some sections. Three halo types are present, and they show a downhole shift from mainly dark gray halos accompanied by orange-light brownish gray halos in the cores to 92 mbsf to an increasing abundance of orange-gray halos below 92 mbsf (Igneous Units 1 and 2 and uppermost Unit 4).

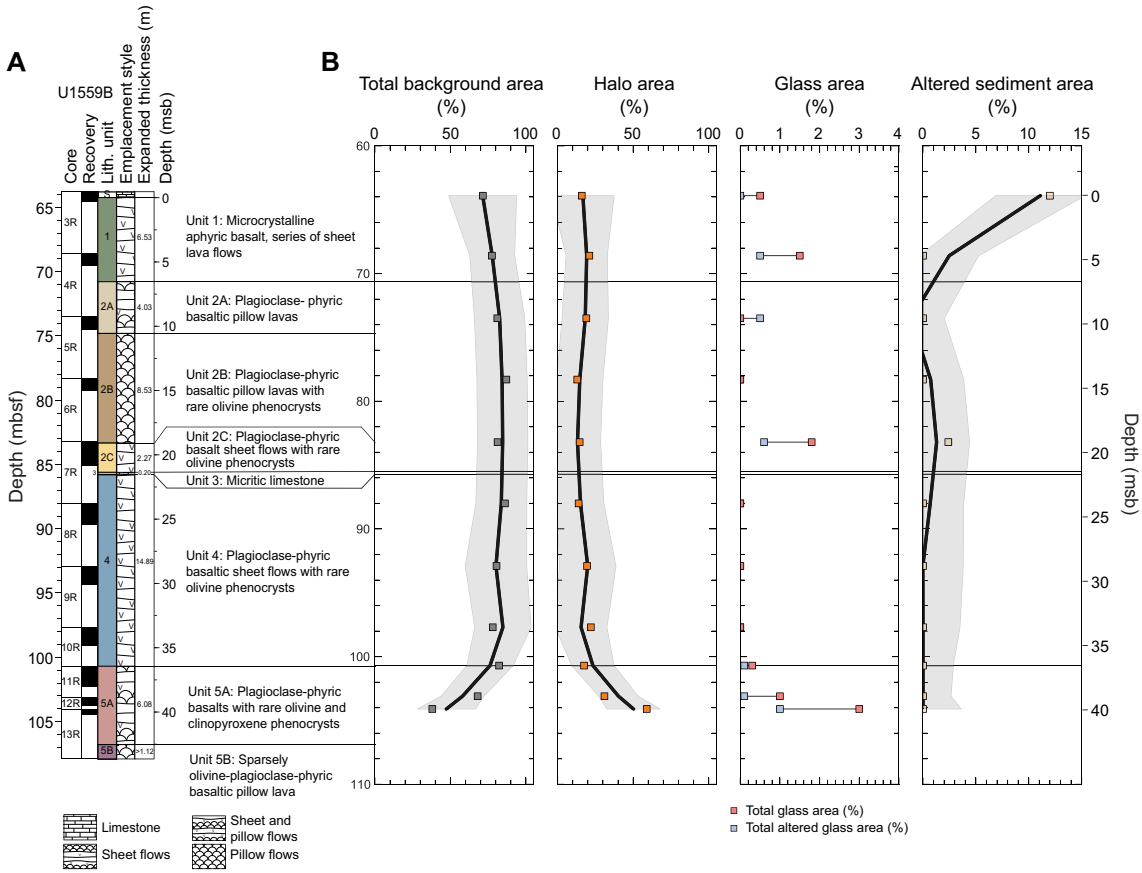

Figure F14. A. Stratigraphic column for igneous basement, Hole U1559B. Unit contact depths and thicknesses are expanded to account for <100% recovery. B. Area abundance of background alteration, alteration halos, fresh and altered glass, and altered sediment. Data are plotted at individual core level. Depths are CSF-A and plotted at top of cored interval. Black trend lines = locally weighted nonparametric regression (LOWESS), gray shading = 2σ of mean.

The earliest stage of alteration is the formation of dark gray alteration halos around fractures and veins. This is followed by the formation of the orange-light brownish gray and orange-gray halos. Crosscutting relationships are rare, and the sequence of later alteration is determined by crack-seal textures in veins that suggest that early clay-lined veins are reopened and filled by calcite.

9.1.3.1.3. Igneous geochemistry

Representative samples of basement cores from Hole U1559B were taken from the freshest portions of each lithologic subunit to obtain a downhole record of the primary magmatic conditions, along with one sample near the basalt/sediment contact. In addition, two Hole U1559B samples were prepared as matrix-matched check standards for use with direct core pXRF data collection throughout Expedition 393. Eight samples were measured for loss on ignition (LOI) and bulk rock geochemical analysis via inductively coupled plasma–atomic emission spectroscopy (ICP-AES). The unoxidized powders of these samples as well as powders of the reference billets of the two standards were also characterized for elemental abundances via pXRF. Hole U1559B basalts are exceptionally uniform in their major element compositions, with TiO_2 contents varying between 1.0 and 1.2 wt%, with high Cr (320–390 ppm) and low Ba (<1–6 ppm). In terms of basaltic rock type, they are olivine tholeiites per the Yoder and Tilley (1962) normative classification scheme. K/Zr ratios, which are a crude measure of alteration, are 10–18 in Hole U1559B samples, moderately higher than fresh South Atlantic mid-ocean-ridge basalt (MORB), which average 7.4.

9.1.3.1.4. Paleomagnetism

Paleomagnetic measurements on basement cores from Hole U1559B were performed to characterize the magnetic signature and retrieve initial information regarding the magnetic mineralogy. Continuous measurements of the remanent magnetization were conducted using the superconducting rock magnetometer (SRM) at 2 cm spacing. To avoid excessive noise and edge effects, we only measured pieces longer than 9 cm. Measurements of remanence were made before and after progressive alternating field (AF) demagnetization at steps of 5, 10, and 20 mT applied field strength. Measurements were also conducted on a total of 11 discrete cubes of 8 cm^3 volume (1 or 2 per core). Paleomagnetic experiments included anisotropy of magnetic susceptibility (AMS), remanence before and after AF or thermal demagnetization, and isothermal remanent magnetization (IRM) acquisition.

Paleomagnetic SRM results reveal a clear principal component at 20 mT demagnetization. Inclination values of these components are predominantly positive, which indicates a reversed polarity. The distribution of inclinations is approximately Gaussian with mean values around 38°. This is about 11° less than the geocentric axial dipole (GAD; ±49.1°) at 30°S. Discrete sample measurements revealed clear characteristic remanent magnetization (ChRM) that has inclinations similar to the SRM results. Discrete sample results confirm a reversed polarity magnetization, which is in contrast to the normal polarity expected for the 6.6 Ma basement age at Site U1559 based on magnetic data collected during the CREST survey (Kardell et al., 2019). Considering the biostratigraphic datums at the sediment/basement interface, the crustal age is likely placed within the geomagnetic polarity Chron C3Ar (Gradstein et al., 2020), which is slightly older than the expected age for Site U1559. In addition, median destructive fields and IRM acquisition up to 1.2 T suggest that the dominant magnetic carriers are likely low-coercivity minerals (e.g., titanomagnetite and maghemite). AMS measurements indicate a dominant prolate fabric for the majority of samples with a well-defined subhorizontal magnetic foliation perhaps caused by flow emplacement. No systematic changes of the scalar parameters of AMS were found with depth in Hole U1559B.

9.1.3.1.5. Physical properties

Characterization of the basement physical properties at Site U1559 is primarily based on cores from Hole U1559B, with additional information from Holes U1559A, U1559C, and U1559D. Whole-round, section half, and discrete measurements were considered together to characterize the petrophysical signatures for the different volcanic units. In addition to these measurements, all whole-round cores were imaged using an X-ray image logger and ~30% of the recovered material was scanned using the DMT core scanner after identifying oriented core pieces with relatively cylindrical shapes.

Many of the hard rock whole-round measurements are impaired by the small, discontinuous core pieces recovered from Hole U1559B. These measurements therefore often underestimate the true physical properties of the material. Natural gamma radiation (NGR) in Hole U1559B is relatively low and consistent across units and ranges 0.2–2.1 counts/s (mean = 1.05 ± 0.36 [±1σ] counts/s). Pass-through magnetic susceptibility measured on whole-round cores ranges from 1–1054 instrument units (IU) (mean = 68.5 ± 112 IU). Discrete point magnetic susceptibility measurements from section halves range 1–1636 IU (mean = 97.6 ± 199 IU). Peaks in magnetic susceptibility are associated with Lithologic Unit 3 (thin indurated calcareous sediment layer), the base of Unit 4 (sheet flow), and Subunit 5A (mixed sheet and pillow flows).

Discrete bulk density measurements using moisture and density (MAD) range 2.79–2.90 g/cm^3 (Figure **F15**). Porosity is variable in Hole U1559B and ranges from 2.6% in the fine-grained sheet and pillow flows of Subunit 5A to 5.6% in the microcrystalline sheet flow of Unit 4 (Figure **F15**). *P*-wave velocity ranges from 5.46 km/s in Subunit 2A to 5.80 km/s in Unit 1 (mean = 5.63 ± 0.91 km/s) (Figure **F15**). The limited number of discrete samples (n = 11) from Hole U1559B do not show a clear relationship between alteration level and petrophysical parameters. The average thermal conductivity measured in basement samples was 1.78 ± 0.04 W/(m·K) (Figure **F15**). Together with heat flow estimates from the overlying sediment, this suggests a temperature gradient of about 40°C/km in the shallow basement at Site U1559 if the thermal regime is mostly conductive. These data are similar to measurements from ODP Hole 896A, near the 6.9 Ma ocean crust reference site in Hole 504B (see figure 76 in Shipboard Scientific Party, 1993b).

9.1.3.1.6. Microbiology

Microbiology sampling in basement in Hole U1559B focused on exploring evidence for life in the sediments and underlying volcanic basement, especially at the sediment/basement interface, using

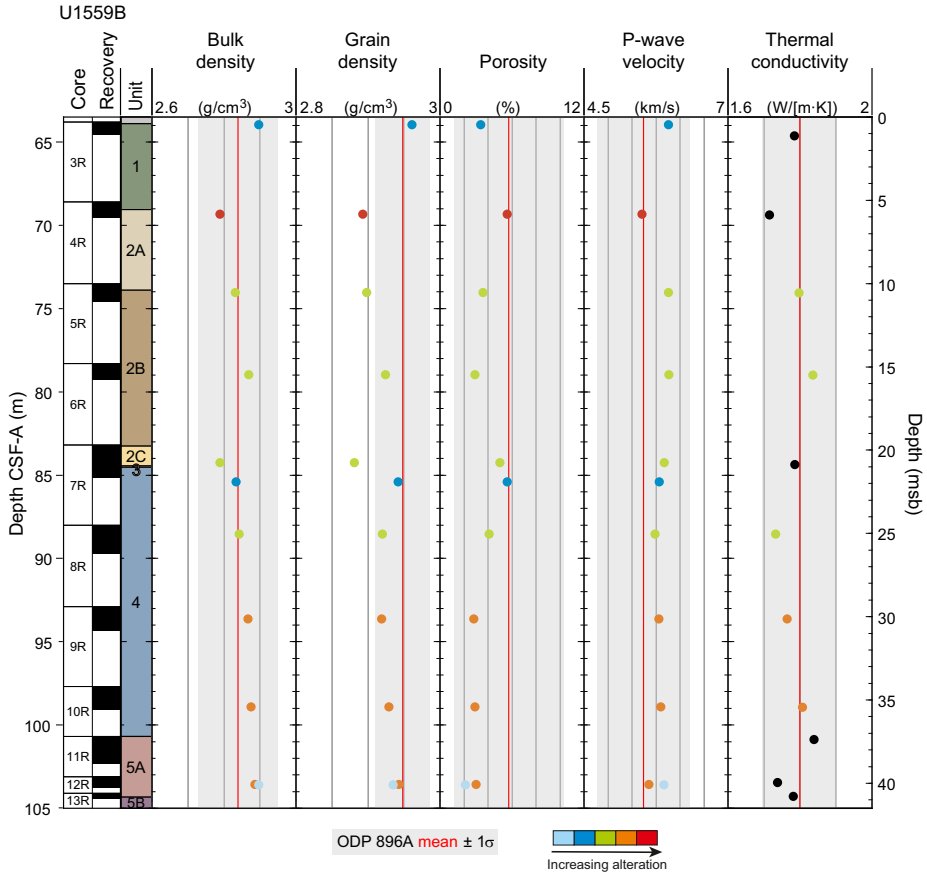

Figure F15. Comparison of physical properties of discrete samples, Holes U1559B and 896A. Range of data from Hole 896A (red line = mean value of each data type, shaded boxes = ±1σ). V_p shown is maximum velocity measured for each sample. Symbol colors represent alteration degree. Black symbols lack alteration degree description.

microscopy, culture-based approaches, and culture-independent approaches. In total, eight whole-round samples (5–13 cm long) representative of the different rock types and alteration styles that comprise the volcanic basement stratigraphy of Hole U1559B were collected for shipboard and shore-based microbiological analyses. All eight samples were tested for contamination, but no tracer was detected, most likely the result of the too small an amount of rock sample in the test vials. To determine the extent of microbial activity, viral production and ammonium enrichments were established that will be analyzed in shore-based laboratories postexpedition.

9.2. Site U1560

9.2.1. Background and objectives

Site U1560 is located ~315 km west of the Mid-Atlantic Ridge at 30°24.2057′S, 16°55.3702′W in 3723 m of water (Figure **F1**). The basement at Site U1560 was predicted to have formed at ~15.2 Ma at a half spreading rate of 25.5 mm/y (Kardell et al., 2019) (Figure **F4**), which is the highest spreading rate in the study region. The site is located on the north–south trending (356) CREST02 seismic crossing line at CDP 12770 about 0.4 km south of the main east–west (085) CREST1D/E seismic line (Figures **F1**, **F11B**, **F16**) where a reflector at ~5.07 s TWT was interpreted to be the top of basement and estimated to be at 104 mbsf (Figure **F11B**) and observed at ~120 mbsf.

Site U1560 was previously occupied in April 2021 during Expedition 395E with objectives to confirm the depth to basement by coring, conduct gas safety measurements, and set a reentry system consisting of a reentry cone and 10¾ inch casing (Williams et al., 2021). Hole U1560A was cored using the APC and XCB systems to 122.5 mbsf (Figure **F12**), finding the sediment/basement contact at 120.2 mbsf. The drill bit and casing assembly was drilled into Hole U1560B (Figure **F12**), setting the casing shoe at 122.0 mbsf and the base of the hole at 124.0 mbsf. Although the drill bit showed signs of wear, the underreamer and casing were in excellent condition; consequently, the top of basement in Hole U1560B was defined to be between those depths (~123 mbsf). Ten bbl of 15 lb/gal cement was pumped with the intention to fill the base of the hole and pipe to ~100 mbsf. Hole U1560C (Figures **F12**, **F17**) was drilled during Expedition 393 and volcanic rocks were encountered at 129 mbsf indicating significant basement topography over ~10 m.

The original operational objectives of Expedition 393 at Site U1560 were to core a single APC/XCB hole to basement (Hole U1560C) and to core and log ~250 m of basement volcanic rocks in Hole U1560B.

At 15.2 Ma, Site U1560 is the second to youngest location on the SAT and will be compared to older and younger crustal material cored at Expedition 390/393 sites. Site U1560 is of similar age

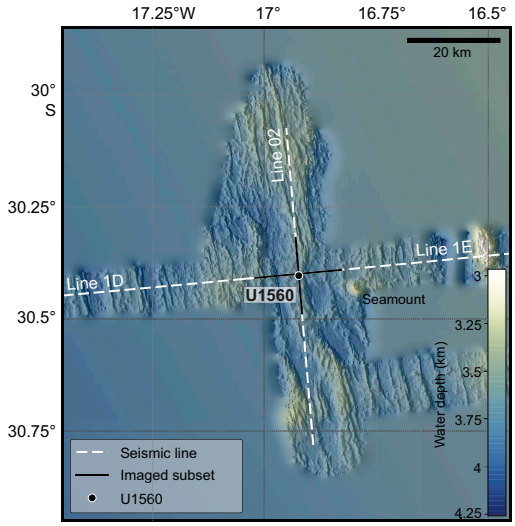

Figure F16. Site U1560 bathymetry (Christeson and Reece, 2020). Seismic reflection profiles were acquired during CREST cruise (Reece et al., 2016).

but contrasting environment to the deep drilling at the Superfast Site 1256 (Wilson et al., 2006; Expedition 309/312 Scientists, 2006; Expedition 335 Scientists, 2012) on crust that formed at the East Pacific Rise during an episode of superfast spreading rate in a region of high pelagic productivity and rapid sedimentation (Shipboard Scientific Party, 2003b).

Science objectives at Site U1560 are to (1) investigate the history of the low-temperature hydrothermal interactions between the aging ocean crust and the evolving South Atlantic Ocean and quantify past hydrothermal contributions to global geochemical cycles, (2) collect samples of the sediment- and basalt-hosted deep biosphere beneath the low-productivity South Atlantic Gyre that will be used to refine global biomass estimates and investigate microbial ecosystems' responses to variable conditions, and (3) construct paleoceanographic records of carbonate chemistry and deep water-mass properties across the western South Atlantic Ocean through key Cenozoic intervals of elevated atmospheric CO_2 and rapid climate change.

9.2.2. Operations

9.2.2.1. Transit

The ship completed the 187 nmi voyage to Site U1560 in 16 h at an average speed of 11.3 kt, arriving at 0130 h on 19 July 2022.

9.2.2.2. Hole U1560B

At 0130 h on 19 July 2022, we lowered the thrusters and started operations in Hole U1560B (Figures **F12**, **F18**). We assembled the RCB BHA with a new C-7 bit and lowered it to 3714 meters below sea level (mbsl). Guided by the subsea camera images, we reentered Hole U1560B at 0920 h on 19 July and lowered the bit to 124 mbsf, the base of the existing hole. No set cement was found by drilling except for a small 5 cm roller at the top of Core 2R. A turbid greenish cloud issued from the reentry cone on reentry.

We started coring in Hole U1560B at 1215 h on 19 July. Cores 2R–21R penetrated volcanic basement from 124.0 to 219.2 mbsf, recovering 38.4 m (40%). Ship heave reached over 4 m at times,

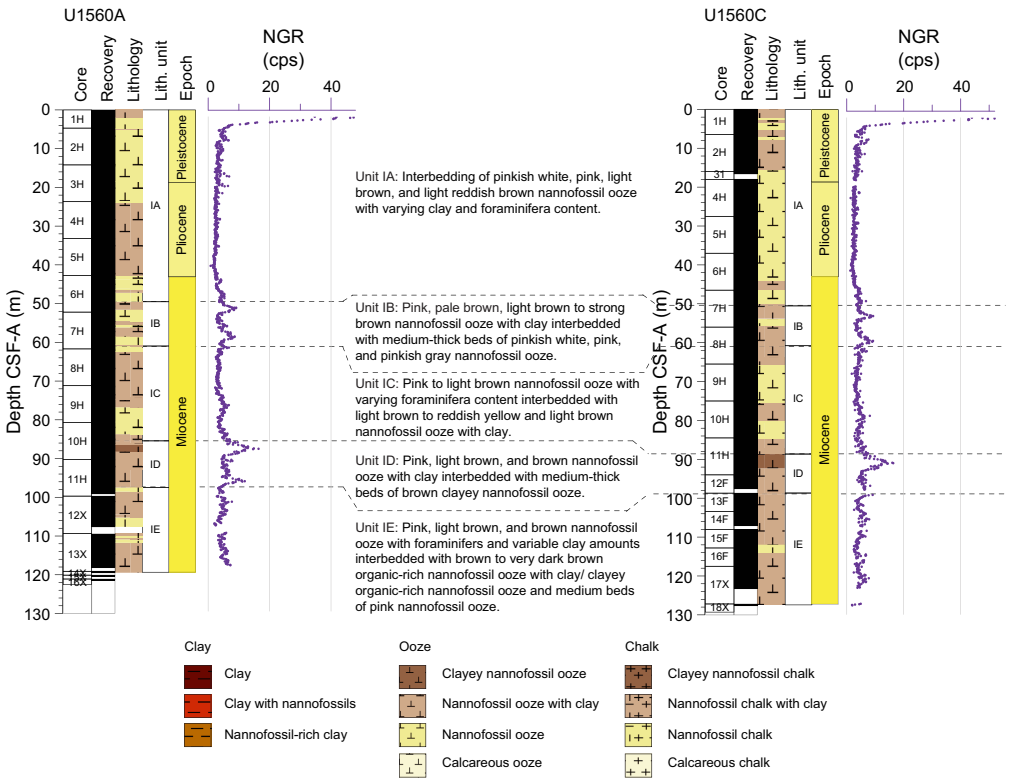

Figure F17. Lithostratigraphic summary of sediment units and correlation of full sediment sequences, Holes U1560A and U1560C. Dashed lines = correlation between units. cps = counts per second.

and up to 4 m of soft hole fill was reported between cores. Mud sweeps of 30–60 bbl were made after most cores to flush out cuttings and fill. All cores were half length (4.8–4.9 m). After cutting Core 21R, the bit had 52.3 h of drilling time. It was still cutting in-gauge, good recovery cores but would not last to the intended target depth; therefore, at 2325 h on 22 July, we started to raise the pipe to change to a new bit. There was 5,000–10,000 lb overpull at 128 mbsf (~5 msb), so the drillers rotated through this area to clear the tight spot. We deployed the subsea camera to observe the BHA coming out of the reentry cone, and the bit cleared the seafloor at 0250 h on 23 July. The BHA was racked in the derrick, the used bit and mechanical bit release (MBR) were removed, and a new MBR with a new C-7 bit and BHA were made up. At 1030 h, we started lowering the new bit down to the seafloor.

We redeployed the subsea camera and reentered Hole U1560B at 1955 h. We found 1 m of soft fill and restarted coring from 219.2 mbsf at 0030 h on 24 July. Cores 22R–41R penetrated from 219.2 to 316.2 mbsf and recovered 36.35 m (37%). There were no problems with torque, and a 30–60 bbl mud sweep was run after every core to flush out any cuttings. At 2320 h on 26 July, the decision was made to stop coring to leave time for downhole logging and a sediment hole at this site.

With ship heave increasing through the day to an extent where it would have not only posed problems for the downhole logging tools but also provided poor quality data, it was decided not to drop the RCB bit on the seafloor for logging. Instead, we decided to change to an APC/XCB polycrystalline diamond compact (PDC) bit and log through that to give time for the heavy seas to subside, as forecasted. The narrower diameter of the PDC bit (9⅞ inch compared to 11⅞₁₆ inch for a typical APC/XCB roller-cone bit) would allow the bit to reenter casing in Hole U1560B for downhole

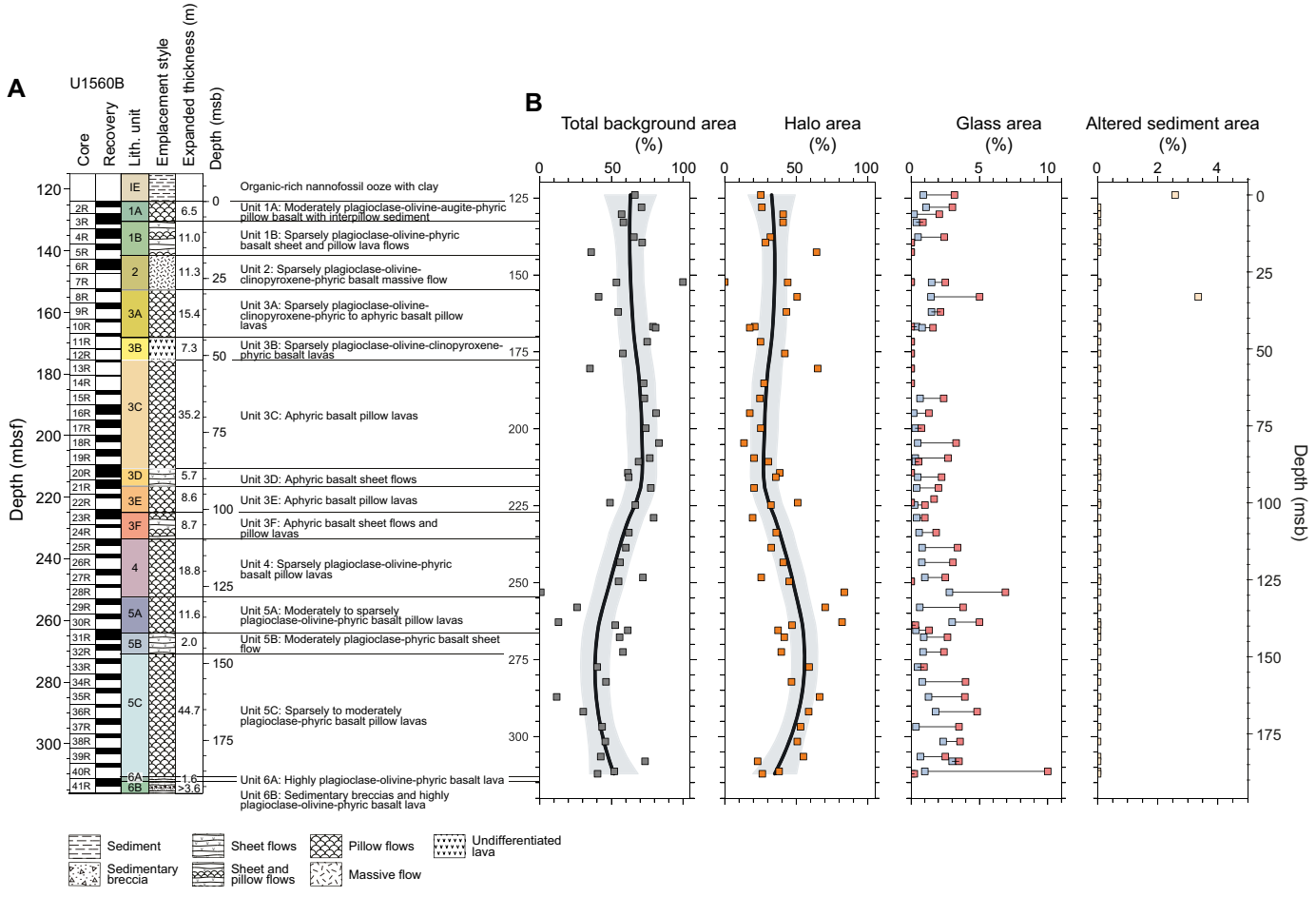

Figure F18. A. Stratigraphic column for igneous basement, Hole U1560B. Unit contact depths and thicknesses are expanded to account for <100% recovery. B. Area abundance of background alteration, alteration halos, fresh and altered glass, and altered sediment. Data are plotted at individual core level. Depths are CSF-A and plotted at top of cored interval. Black trend lines = locally weighted nonparametric regression (LOWESS), gray shading = 2σ of mean.

logging. The lockable float valve (LFV) was locked open to allow the logging tools to pass through. The RCB bit was raised to the ship, clearing the seafloor at 0225 h on 27 July and the rig floor at 0905 h. The bit, MBR, and RCB parts of the BHA were removed and replaced with an APC/XCB BHA. The RCB bit had been used for 42.5 drilling hours and had some wear to the inner teeth but was otherwise in good condition.

From 1115 h, we lowered the bit to the seafloor and deployed the subsea camera to guide reentry. At 1755 h, we reentered Hole U1560B and set the bit at 27.7 mbsf in the casing for downhole logging. From 2025 h, we assembled the triple combo downhole logging tool string, consisting of magnetic susceptibility, electrical resistivity, density, neutron porosity, and natural gamma tools. During drilling, hole conditions had not caused excessive torque and no tight spots were encountered while raising the RCB bit, so the hole seemed to be in good condition for logging. Therefore, the density tool source and the magnetic susceptibility tool were included in the tool string, unlike operations in Hole U1583F. We lowered the triple combo down the pipe, and it reached the base of the hole (316 mbsf), recording logging data down from the seafloor. The tool string completed one upward pass in the open hole (316–122 mbsf) and a second pass from 316 mbsf through the open hole and casing to the seafloor. The triple combo was raised back to the ship, and the Formation MicroScanner (FMS)-sonic tool string was assembled. At 0645 h on 28 July, we started to lower it down the pipe. The bottom of the tool was kept 5 m off the bottom of the hole (311 mbsf) to prevent damage to the bottom part of the FMS tool. The tool made two upward passes in the open hole. After the second pass, one of the caliper arms would not fully close, remaining open by 0.2 inch and causing difficulty at first when bringing the tool into the base of the BHA. However, after pumping to clear the hole and tool of potential debris, we were able to bring the tool string to the surface without damage. We assembled the Ultrasonic Borehole Imager (UBI) tool string, and at 1545 h we lowered it down the pipe. This tool string also reached 311 mbsf and made two upward passes in the open hole, and it was back on the rig floor at 2245 h. We rigged down the Schlumberger logging equipment and started pulling the bit out of Hole U1560B, clearing the seafloor at 2355 h.

In summary, Cores 393-U1560B-2R through 41R penetrated from 124.0 to 316.2 mbsf (192.2 m of basement rocks), recovering 74.8 m (39%). Of the two C-7 RCB bits deployed in Hole U1560B, the first bit drilled for 52.3 h over a 95.2 m interval with 38.44 m of recovery (40%) and the second bit drilled for 42.5 h over a 97.0 m interval recovering 36.35 m of basalt (38%). A total of 9.9 days (238.5 h) were spent on operations in Hole U1560B.

9.2.2.3. Hole U1560C

The ship was offset 10 m to the north in preparation for coring Hole U1560C (Figure **F17**). An XCB core barrel was deployed to close the LFV in the BHA, which had been set open for the previous day's downhole logging. The bit was set at 3721.7 mbsl, and we started Hole U1560C at 0245 h on 29 July 2022. Core 1H recovered 6.5 m of sediment, placing the mudline depth at 3724.7 mbsl. To correct the stratigraphic overlap with cores from Hole U1560A (Figure **F17**), cored in April 2021 during Expedition 395E, we drilled ahead 2.0 m from 16.0 mbsf (drilled interval 31). Cores 1H–15F penetrated from the seafloor to 112.8 mbsf and recovered 111.9 m (101%) of nannofossil ooze with varying amounts of clay and foraminifera. Advanced piston corer temperature (APCT-3) tool measurements were made on Cores 5H, 8H, and 11H. While taking the Core 11H APCT-3 measurement, the APC core barrel became stuck in the formation, and it required three drillover attempts and 160,000 lb of overpull to free it. The APC piston rods had twisted during the process, and as a result we switched over to half-length APC (HLAPC) coring from Core 12F. The drill crew worked between cores to straighten the piston rods for the full-length tool.

After Core 393-U1560C-16F reached 117.5 mbsf, we switched to the XCB coring system in anticipation of reaching basement at approximately the depth it was found in Holes U1560A (120.2 mbsf) and U1560B (~123 mbsf). Basement was eventually encountered at 129.0 mbsf in Hole U1560C, 9.8 m deeper than in Hole U1560A. The two holes are only 10 m lateral distance apart, and the difference in basement depth reflects the rugged basement surface topography that is typical of slow/intermediate spreading rate ridges. Core 17X drilled a further 0.3 m into the basement and recovered two ~5 cm pieces of basalt. It was the last core of the expedition. Cores 1H–17X cored from seafloor to 129.3 mbsf and recovered 122.75 m (96%). Nonmagnetic core barrels were

used on all APC and HLAPC cores, and all full-length APC cores were oriented using the Icefield MI-5 core orientation tool.

From 0530 h on 29 July, the rig floor team coated the core line and then raised the bit to the ship, clearing the seafloor at 0900 h and the rig floor at 1655 h. The BHA was disassembled and stowed for transit, and 115 ft of drill line was slipped and cut. We raised the thrusters and started the transit to Cape Town, South Africa, at 1930 h.

9.2.3. Principal results

Site U1560 targeted 15.2 Ma upper oceanic crust along the SAT. A complete sedimentary sequence comprising nannofossil ooze with varying amounts of clay and foraminifera was recovered from both Holes U1560A and U1560C (Figure **F17**), and uppermost basement rocks were recovered in both holes as well as in Hole U1560B. Hole U1560B advanced 192.2 m into basement and recovered a volcanic sequence of moderately to sparsely plagioclase ± olivine phyric pillow lavas and sheet and massive flows (Figure **F18A**). Most of the lavas show positive magnetic inclinations, but negative inclinations for rocks from Igneous Units 1 and 2 occur, hinting at a younger age for these flows. Core 393-U1560B-7R directly beneath the fine-grained basalt massive flow of Unit 2 was without recovery. Preliminary wireline logs hint at elevated natural gamma readings, suggesting the presence of strongly altered basalts that enjoyed prolonged direct exposure to ocean bottom waters at the southern Mid-Atlantic Ridge. The lowermost lavas in Hole U1560B are highly plagioclase-olivine-clinopyroxene phyric basalt lavas that include two tantalizing zones of sedimentary breccias comprising altered basalt and glass clasts in a matrix of indurated calcareous sediment, hyaloclastite, and zeolite.

9.2.3.1. Sediments

9.2.3.1.1. Sedimentology

Biogenic and minor amounts of siliciclastic sediments were recovered from two Holes U1560A and U1560C. Biogenic sediments consist primarily of nannofossil ooze with varying amounts of clay and foraminifera. Intervals with siliciclastic sediments include rare to common clays with variable nannofossil and foraminifera content. A single sedimentary Lithologic Unit I was defined at Site U1560 and was divided into five subunits (Figure **F17**). Subunit IA extends from the top of the hole to 49.5 m core depth below seafloor, Method A (CSF-A), in Hole U1560A and to 51.3 m CSF-A in Hole U1560C. It is Pleistocene to Late Miocene pinkish white, pink, light brown, and rarely light reddish brown nannofossil ooze with variable amounts of clay and foraminifera. Subunit IB is Late Miocene and extends from 49.5 to 61.0 m CSF-A in Hole U1560A and from 51.3 to 61.2 m in CSF-A in Hole U1560C, and it comprises pink, pale brown, light brown to dark brown nannofossil ooze with clay interbedded with 10–30 cm thick beds of pinkish white, pink, and pinkish gray nannofossil ooze. Subunit IC extends from 61.0 to 85.4 m CSF-A in Hole U1560A and from 61.2 to 89.3 m CSF-A in Hole U1560C and consists of Late Miocene pink to light brown nannofossil ooze with varying foraminifera content interbedded with light brown to reddish yellow and light brown nannofossil ooze with clay. Subunit ID extends from 85.4 to 96.4 m CSF-A in Hole U1560A and from 89.3 to 98.9 m CSF-A in Hole U1560C. It consists of Late to Middle Miocene pink, light brown, and brown nannofossil ooze with clay interbedded with medium–thick beds of brown clayey nannofossil ooze. Subunit IE extends from 96.4 and 98.9 m CSF-A in Holes U1560A and U1560C, respectively, to the sediment/basement interface. It consists of Middle Miocene pink, light brown, and brown nannofossil ooze with foraminifera and variable amounts of clay interbedded with brown to dark brown organic carbon–bearing nannofossil ooze with clay, brown to dark brown clayey organic carbon–bearing nannofossil ooze, and 10–30 cm thick beds of pink nannofossil ooze.

9.2.3.1.2. Biostratigraphy and age-depth model

Calcareous nannofossil and planktic foraminifera biostratigraphy was performed primarily on core catcher samples recovered from Holes U1560A and U1560C, examined both on shore and on board *JOIDES Resolution*. The mudline sample from Hole U1560C contains Late Pleistocene to recent planktic foraminifera, but ages based on nannofossils could not be determined because of contamination. Biostratigraphic analyses indicate that the Pliocene–Pleistocene occurs above 42.65 m core depth below seafloor, Method B (CSF-B), in Hole U1560A and above 43.24 m CSF-B

in Hole U1560C, with the Pliocene/Pleistocene boundary located at 20.42 m CSF-B in Hole U1560A and 20.56 m CSF-B in Hole U1560C. The Miocene/Pliocene boundary could not be determined precisely because index taxa were not observed for either nannofossils or foraminifera. However, the position of this boundary is approximated by a nearby nannofossil bioevent, the base of *Ceratolithus cristatus* (5.08 Ma), which occurs at 42.65 m CSF-B in Hole U1560A and 43.24 m CSF-B in Hole U1560C. Combined nannofossil and planktic foraminifera biostratigraphy indicates the presence of Early to Middle Miocene sediments below 45.80 m CSF-B in Hole U1560A and below 46.45 m CSF-B in Hole U1560C.

The most refined estimate for the age of basement comes from the micropaleontological analysis of the thin section (Sample 393-U1560B-2R-1, 83–85 cm) taken from indurated calcareous interpillow sediments. The sample contained preserved planktic foraminifera tests and amongst identified taxa were *Orbulina* spp., *Praeorbulina* spp., and *Trilobatus sicanus*. This provides narrow 14.4–15.1 Ma age constraints that agree with the projected crustal age of ~15.2 Ma for Site U1560.

Calcareous nannofossil and planktic foraminifera bioevents in conjunction with paleomagnetic data allowed for comprehensive hole age-depth models and calculation of linear sedimentation rates (LSRs). LSRs range 0.43–2.01 cm/ky in Hole U1560A and 0.29–2.24 cm/ky in Hole U1560C. In both holes, the highest LSRs occur throughout the Miocene–Pliocene interval, with values ranging 0.43–2.01 cm/ky in Hole U1560A and 0.49–2.16 cm/ky in Hole U1560C, whereas the lowest LSRs are recorded in the Pleistocene.

9.2.3.1.3. Sedimentary and pore water geochemistry

Samples from Holes U1560A and U1560C were analyzed for interstitial water (IW) and sediment geochemistry (Figure **F19**). In addition, headspace gas was measured in Hole U1560A during Expedition 395E. IW geochemical data from Holes U1560A and U1560C show an increase in Na, Cl, and Br in the upper ~20 m, remain uniform downhole for most of the section, and decrease to near seawater values in the lowermost ~25 m of Subunit IE. Measured pH is mostly uniform in

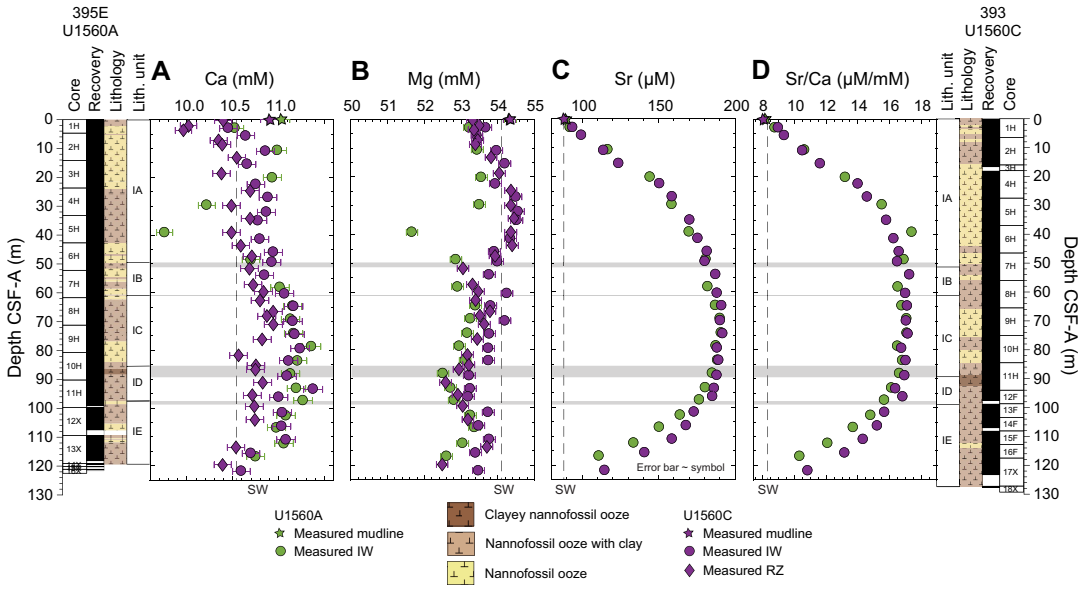

Figure F19. (A) Calcium, (B) magnesium, (C) strontium, and (D) Sr/Ca ratios, Holes U1560A and U1560C. Ca concentrations remain close to or above seawater (SW) value (dashed black line) throughout Holes U1560A (10.2–11.4 mM) and U1560C (10.5–11.4 mM), with good agreement in Ca concentrations between holes. Broad decrease in Mg concentrations is observed in Hole U1560A (54.3 mM at 0 m CSF-A to 52.6 mM at 116.86 m CSF-A), and values remain below seawater throughout sediment column. In Hole U1560C, Mg concentrations increase in Subunit IA (53.7–54.5 mM; ~3–27 m CSF-A), decrease in Subunits IB–ID (54.6–53.2 mM; ~27 to ~90 m CSF-A), and increase slightly in Subunit IE (up to 53.8 mM at 111.00 m CSF-A). In contrast to small changes observed in Ca and Mg profiles, Sr concentrations and Sr/Ca ratios vary significantly in both holes. Sr and Sr/Ca ratios increase in Subunit IA (Sr: ~90–180 μM; Sr/Ca: ~8–17 μM/mM), remain uniform throughout Subunits IB and IC (Sr: ~190 μM; Sr/Ca: ~17 μM/mM), and then decrease toward sediment/basement interface in both holes (Sr: ~110–115 μM; Sr/Ca: ~11 μM/mM). Seawater reference values correspond to International Association for the Physical Sciences of the Oceans (IAPSO) standard composition. RZ = Rhizon.

both holes and remains within the range of local bottom seawater (7.6–7.8), with the exception of the upper ~40 m in Hole U1560A (pH varies from 7.7 to 7.8). Alkalinity profiles are mostly indistinguishable between the two holes, and values remain uniformly higher than seawater between ~25 and 90 m CSF-A (~2.8–2.9 mM) before decreasing gradually toward near seawater values at the sediment/basement interface. In contrast to the small changes in the Ca and Mg pore water profiles, Sr concentrations and consequently Sr/Ca ratios vary significantly in both holes (~90–190 µM and ~8–17 µM/mM, respectively) (Figure **F19**), consistent with carbonate dissolution and recrystallization within the sediments. Increases in concentration relative to the mudline are observed for B (11%–13%), Li (2%–4%), Si (179%–215%), and K (7%–9%) at Site U1560, and all profiles behave similarly between Holes U1560A and U1560C. Silicate diagenesis within the sediment column, as well as chemical exchanges between sediment and basement, are likely responsible for the downhole variability observed in these elements. Sulfate concentrations in both holes show some variability in Subunit IA (~27–28 mM) but remain uniform below ~40 m CSF-A. Ammonium concentrations vary significantly between Holes U1560A (3.5–40.6 µM) and U1560C (7.5–20.3 µM), whereas Mn profiles are mostly similar (0.13–3.67 µM). Oxygen concentrations in Hole U1560C decrease in Subunit IA to near anoxic for much of the hole before increasing again to reach ~260 µM at the sediment/basement interface. Calcium carbonate is generally high in both holes, with the lowest values in the lowermost ~10 m of each hole. Total organic carbon (TOC) values in Hole U1560A are fairly uniform downhole (0.3 wt%), but concentrations in Hole U1560C are higher overall and gradually increase with depth (up to ~1.4 wt% near the top of Subunit IE). In Hole U1560C, TOC concentrations are low in the lowermost ~20 m of the sediment cover.

9.2.3.1.4. Paleomagnetism

Paleomagnetic measurements were conducted at 2 cm resolution on sediment archive-half sections from Holes U1560A and U1560C using the SRM. Remanent magnetization was measured before and after AF demagnetization steps at 5, 10, and 20 mT. Discrete measurements including AMS and AF demagnetization were conducted on a total of 26 (7 cm^3 J-cube) samples. IRM acquisition experiments were performed on 10 selected samples, at least once per lithologic subunit. Paleomagnetic measurements were used to construct the magnetostratigraphy for the sediment package at Site U1560.

A single remanent magnetization component could be defined after cleaning the drilling overprint with the 5 mT AF demagnetization step. The distribution of the 20 mT inclination is generally bimodal in both holes. The values are clustered around ±46° in Hole U1560A, whereas clusters centered at +43° and −45° were measured in Hole U1560C. Despite the presence of few intervals with shallow inclinations, generally clear positive and negative polarities can be detected, allowing good preliminary correlation to polarity chrons on the geomagnetic polarity timescale (GPTS). AF demagnetization of discrete samples up to a maximum of 160 mT allow us to isolate the ChRM with maximum angular deviation angles ranging 2.1°–14.0°. Inclinations from ChRM calculated for discrete samples confirm the values measured from the SRM used to construct the magnetostratigraphy. Preliminary ties to the GPTS reveal the Brunhes, Matuyama, and Jaramillo Chrons in the uppermost sediment column to ~8 m CSF-A in both Holes U1560A and U1560C. In both holes, the Pliocene/Pleistocene boundary is identified in Subunit IA at ~20 m CSF-A and the Miocene/Pliocene boundary is at the bottom of Subunit IA. The base of the sediment column was placed in Chron C5ADn (14.163–14.609 Ma; Gradstein et al., 2020), which agrees with the estimated basement age of ~15.2 Ma (Kardell et al., 2019).

Rock magnetic experiments were conducted on one or two samples for each lithologic subunit, revealing the dominance of low-coercivity minerals in the cores with no significant variations with depth or sediment type. AMS measurements reveal a well-defined oblate magnetic fabric characterized by a steeply inclined magnetic foliation, which might reveal deposition on a steep slope or subsequent tectonic tilting.

9.2.3.1.5. Physical properties

Characterization of the sediment physical properties at Site U1560 was primarily based on cores from Hole U1560C, with additional information from Hole U1560A. A correlation framework and splice were developed for the site that considers NGR, gamma ray attenuation (GRA), magnetic susceptibility, and magnetic inclination from each hole. The correlation resulted in an almost con-

tinuous spliced record to 138 m core composite depth below seafloor (CCSF), with a total core gap of ~4 m.

Whole-round measurements of NGR range 1–52 counts/s but are mostly lower than 10 counts/s throughout Hole U1560C (mean = 5 ± 4 counts/s). A few peaks (10 and 20 counts/s) stand out in the middle portion of the sequence (within Subunit IB and at the Subunit IC/ID boundary). In particular, peaks in Subunit IB reflect its clayey nannofossil ooze lithology. In both holes, the elemental concentrations of K and Th display trends that are similar to the NGR total counts. U shows the lowest concentration of the radioactive components. These well-defined features were used as tie points for stratigraphic correlation.

Magnetic susceptibility from the Whole-Round Multisensor Logger (WRMSL) mimics the NGR trends, ranging 1–60 IU, although it is scattered toward higher values in the lower part of Subunit IE, likely due to drilling disturbance caused by the XCB system. Discrete point magnetic susceptibility shows a downhole trend similar to the WRMSL record, with some higher peaks in the upper part of Subunit IA. For both magnetic susceptibility measurements, the lower values are consistent with the nannofossil ooze. Bulk density based on GRA ranges 1.4–1.9 g/cm^3 over the interval measured and is uniform with depth. The highest density interval is recorded in the upper part of Subunit IC (60–65 m CSF-A), up to 1.9 g/cm^3, which also corresponds to a peak in *P*-wave velocity.

MAD analyses were performed on 25 discrete samples to measure porosity and density. Porosity shows a decreasing trend from ~70% to ~60% in the first 15 m but stays relatively constant at ~60% to the bottom of Hole U1560C. There is a small interval with 45% porosity that corresponds to the highest bulk density at 106 m CSF-A but the sedimentologic cause remains unclear. *P*-wave velocity data range 1.5–1.6 km/s with a mean of 1.53± 0.02 km/s and is invariant downhole other than an increase from 1.55 to 1.6 km/s in the uppermost 15 m.

Shear strength is relatively uniform in the lower part of Subunit IA and Subunits IC–IE around values of 8–10 kN/cm^2, shows higher values in the upper part of Subunit IA, and the highest value is in Subunit IB (30 kN/cm^2). Compressional strength decreases from the seafloor to ~75 mbsf from 2.0 to 0.1 kg/cm^2 (mean = 1.1 ± 0.5 kg/cm^2), below which it shows a scattered trend around 1 kg/cm^2 down to the sediment/basement interface. Most samples have a thermal conductivity of ~1.2 W/(m·K) with the highest measurements from Subunit IC (1.34 ± 0.02 W/[m·K]). Using the thermal conductivity data and formation temperature measurements from Holes U1560A and U1560C, the vertical conductive heat flow for Site U1560 is estimated to be 22 mW/m^2.

9.2.3.1.6. Microbiology

Microbiology sampling in sediments at Site U1560 during Expedition 393 occurred in Hole U1560C and was focused on exploring evidence for microbial life in the sediments using microscopy, culture-based approaches, and culture-independent approaches. From Hole U1560C, one microbiology whole-round sample (5–10 cm long) was collected from each 9.5 m core. These whole-round samples were subsampled for different shipboard and shore-based scientists. Additional personal whole-round cores for specialized shore-based analyses were also taken. A total of 14 routine whole rounds were taken and subsequently sampled, and an additional 35 whole rounds were taken for personal shore-based analyses.

Multiple microbiology analyses were started shipboard during Expedition 393 on sediment samples from Site U1560. To study the extent of viral activity and dynamics between viruses and other microbial life (Bacteria and Archaea), virus-induced microbial mortality and prophage induction experiments were performed on subsamples taken from five microbiology whole-round cores throughout the sediment column. To study the microbial activity at the sediment/basement interface, ammonium enrichment incubation experiments were started with the deepest sediment cores in Hole U1560C, along with the uppermost basement samples.

9.2.3.2. Volcanic rocks

9.2.3.2.1. Igneous petrology

Holes U1560A–U1560C all recovered volcanic basement, but only Hole U1560B penetrated deeply into basement. During Expedition 393, Hole U1560B was cored from the pilot bit depth at 124 mbsf and advanced a further 192.2 m to 316.2 mbsf, recovering ~75 m of basalt (~39%) (Figure

F18A). This recovery was generally sufficient for unit boundaries, lava types, and volcanic emplacement styles to be determined with confidence throughout most of the hole, although low to zero core recovery in critical parts of the sequence means some important transitions were not recovered (e.g., Core 7R; 147–153 mbsf). Similarly, the extent of sedimentary breccias and other fragile or broken formations from throughout the hole remain uncertain. Some clarification may come from the careful analysis of drilling and wireline logging information and paleomagnetic conglomerate tests.

Hole U1560B recovered a volcanic sequence composed of six main volcanic and units. Unit 1 is divided into two subunits (1A and 1B), Unit 3 is divided into six subunits (3A–3F), Unit 5 is divided into three subunits (5A–5C), and Unit 6 is divided into two subunits (6A and 6B). Unit 1 directly underlies basal sedimentary Subunit IE and consists of sparsely to moderately plagioclase-olivine-phyric pillow lavas with some intervening sheet flows and interpillow sediments near the interface. Unit 2 is a sparsely plagioclase-olivine-augite-phyric massive flow, with a fine- to medium-grained interior, and between 6 and 11 m thick depending on the unrecovered material in Core 7R (see Figure F18A). Unit 3 consists mostly of pillow lavas with phenocryst abundances that grade from sparsely phyric to aphyric. Unit 3 is the most primitive of Hole U1560B in terms of Cr/Ti ratios. Unit 4 consists of sparsely plagioclase-olivine-phyric basalt pillow lavas, with a composition transitional between Unit 3 and Unit 5. Subunits 5A and 5C consist of moderately to sparsely plagioclase-olivine-phyric pillow lavas, separated by two or three sheet lava flows (Subunit 5B). Basalts in Unit 6 are highly plagioclase-olivine-clinopyroxene-phyric and may provide a relatively fresh protolith for comparison with other, more strongly altered highly phenocryst-rich basalts recovered at other sites along the SAT. Hole U1560B ends in Subunit 6B, which contains highly plagioclase-olivine-clinopyroxene phyric lavas with two tantalizing sedimentary breccias of basalt and glass clasts in a matrix of indurated calcareous sediment and hyaloclastite.

Lava composition assessed by pXRF varies significantly downhole, with geochemical boundaries largely corresponding to the petrologically defined boundaries. Incompatible element concentrations and Zr/Ti ratios are mostly consistent with an N-MORB-like composition for the lavas at Site U1560, although higher Zr/Ti in Subunits 3A and 3B and Unit 6 nudge toward enriched MORB (E-MORB) and warrant further investigation. The recurring sequence of chemostratigraphic units, with a central primitive, aphyric lava unit as was noted for Sites U1558 and U1583 is also present at Site U1560.

9.2.3.2.2. Alteration petrology

Hole U1560B records fluid/rock reactions over the range of spatial contexts expected for uppermost basement, albeit with only limited recovery of breccias. The secondary minerals forming (predominantly various clays, carbonate, Fe oxyhydroxides, and zeolites) are consistent with reactions at low temperatures with seawater-derived fluids. There are three distinctive alteration zones downhole in Hole U1560B, recognized by broad shifts in mineralogy and abundance of alteration features. The uppermost 25 m of the igneous rocks in Hole U1560B are characterized by the presence of green clay filling vesicles in the background rocks and alteration halos in the massive flows as well as the low abundance of alteration halos (<20%) and few carbonate veins (Figure F20). From 25 to 250 msb, the proportion of halos remains similar, but orange halos dominate the overall halo abundance. This zone in Hole U1560B also hosts the most carbonate veins whereas green clay is restricted to massive flows. From below 250 msb, there is a marked increase in the abundance of brown halos of variable alteration intensity. The lowermost part of the hole (below 250 msb) is carbonate vein poor but zeolite veins are more abundant than higher in the section. This overall change in dominant characteristics is in part controlled by the volcanic architecture of the upper crust, such as the association of green clay with massive flow, but also reflects hiatuses in volcanism that exposed parts of the crust to direct contact with seawater for prolonged periods of time as recorded by the brown halo zones.

9.2.3.2.3. Igneous geochemistry

For the Hole U1560B basement cores, representative samples were taken from the freshest portions of each lithologic subunit to obtain a downhole record of the primary magmatic conditions, along with one sample near the basalt/sediment contact. A sample of intercalated sediments/breccia fill was taken to better understand the basalt-sediment chemical exchanges that occurred as

new lavas erupted. A total of 27 samples were measured for LOI and bulk rock geochemical analysis via ICP-AES and powder pXRF to complement the huge number of direct pXRF analyses taken directly on the split core surface.

Basalt compositions show strong variability downhole that is evident in both the pXRF surface data and in the ICP-AES data. In terms of basaltic rock type, the freshest Site U1560 samples classify as olivine tholeiites per the Yoder and Tilley (1962) normative classification scheme. TiO_2 contents vary between 1.3 and 1.7 wt%, which is consistent with moderate to large amounts of crystallization before eruption. The Hole U1560B basalts are moderately altered, with elevated abundances of K_2O and Rb, but lower abundances overall than those seen at older sites. K_2O shows only a slight increase downhole from 0.1 to 0.33 wt%. K/Zr ratios, a measure of relative K enrichment, range from MORB-like values of 7–9 up to 24.6. MgO shows evidence for Mg removal from the rocks via seafloor weathering. The lowest MgO samples are clustered near unit boundaries, suggesting locally more intensive reactions with seawater.

9.2.3.2.4. Paleomagnetism of volcanic rocks

Paleomagnetic measurements were conducted on archive halves of basement cores from Hole U1560B using the SRM at 2 cm intervals. Remanent magnetization before and after progressive AF demagnetization at 5, 10, and 20 mT were measured on pieces that are longer than 9 cm. Data resolution varied according to the core recovery rate in Hole U1560B (0%–84%). AF demagnetization and rock magnetic experiments were performed on cube samples, targeting representative levels of both fresh basalts and those with varying degree and type of alteration.

Natural remanent magnetization (NRM) intensity of volcanic rocks at Site U1560 varies between 8.65 and 0.04 A/m, with the highest values detected in volcanic units and some rocks showing

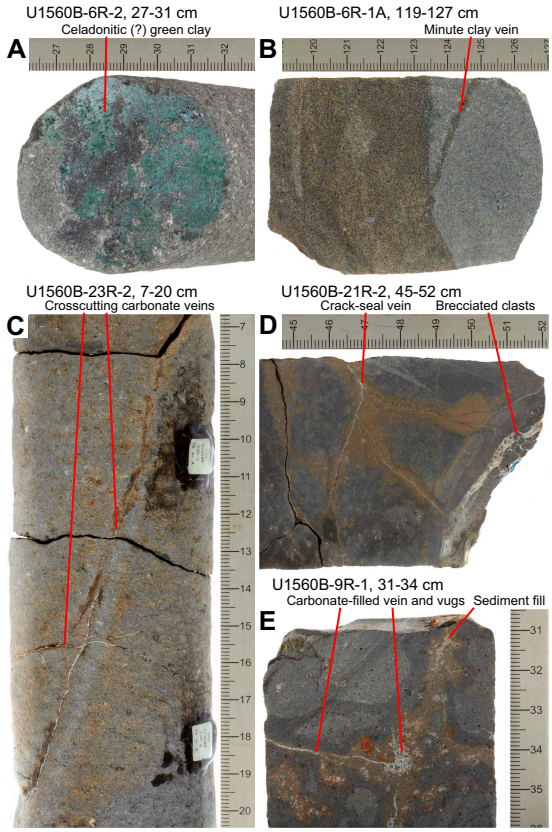

Figure F20. Vein types, Hole U1560B. A. Strong green vein, potentially composed of celadonite, on broken rock surface (6R-2, 27–31 cm). B. Submillimeter-wide clay vein with brown halo (6R-1, 119–127 cm). C. Several crosscutting narrow carbonate veins (23R-2, 7–20 cm). D. Branched carbonate veins with crack-seal texture and wider carbonate vein in which brecciated fragment of host rock are floating (21R-2, 45–52 cm). E. Carbonate-filled vein and vuggy space (9R-1, 31–34 cm). Also note vein filled with metamorphosed sediment.

unexpectedly high magnetic susceptibility values (>10^3 IU). The SRM results at the 20 mT demagnetization step show mean intensity values around 0.95 A/m and mostly positive inclination, which agrees with the expected reversed polarity for 15.2 Ma old basement. However, negative inclinations were also observed at the top of the basement, suggesting a significant younger age for Subunit 1A to Unit 2. Overall, the 20 mT inclination values are clustered around 64°, significantly steeper than the expected values calculated based on the GAD (±49.1° at 30°S).

A total of 28 discrete samples were subjected to AF demagnetization up to 190 mT to isolate the ChRM, which is generally well defined with maximum angular deviations between 0.5° and 11.3°. Locally, a secondary component was detected in pillow lava units. Rock magnetic experiments in fresh basalts reveal the dominance of low-coercivity minerals such as magnetite or maghemite. In contrast, heavily altered samples are characterized by a mixture of high- and low-coercivity minerals. These samples also revealed the lowest magnetic susceptibility and remanence intensity values. In addition, variations in magnetic mineral grain size were observed for units associated with different emplacement styles. The magnetic fabric of the volcanic rocks in Hole U1560B is mostly prolate showing a subhorizontal magnetic foliation with no visible correlation with the emplacement style.

9.2.3.2.5. Physical properties

Characterization of the basement physical properties at Site U1560 is primarily based on cores from Hole U1560B (for a total of 190 m), with additional information from Holes U1560A and U1560C, where only the uppermost basement was recovered. In Hole U1560B, NGR is 2.1 ± 0.7 (±1σ) counts/s and ranges 0.2–5.3 counts/s. The highest NGR is associated with sedimentary breccias, which have a mean NGR of 2.7 ± 1.3 counts/s. Basalts of all flow styles have lower mean NGR between 1.8 and 2.1 counts/s. Point magnetic susceptibility ranges 0–2595 IU. Five prominent peaks in magnetic susceptibility are associated with relatively fresh, fine-grained holocrystalline massive and sheet basalt flows. These peaks in magnetic susceptibility are also apparent in the wireline logging data. A total of 33 discrete samples were used for MAD and *P*-wave velocity measurements, and these samples were characterized in terms of their alteration, emplacement style, and groundmass grain size. Bulk density from MAD analysis ranges 2.08–2.89 g/cm^3, with the lowest densities measured from breccia matrix and pillow lava chilled margins with thin sedimentary intercalations. These samples also display the lowest *P*-wave velocity and the highest porosity. *P*-wave velocity ranges 3.85–5.89 km/s in Hole U1560B and is highest in Igneous Units 1 and 6 (mean = ~5.7 km/s). Units 2–4 have a mean *P*-wave velocity of ~5.4 km/s, but the lowest mean velocity is measured in Unit 5 (5.0 ± 0.6 km/s). Porosity ranges 2.0%–35.5%, but basaltic samples that are not associated with a chilled margin generally show porosities <10%. Thermal conductivity in the hole ranges 1.13–1.79 W/(m·K) with a mean of 1.63 ± 0.15 W/(m·K). There is a slight downhole increase in thermal conductivity from ~1.7 W/(m·K) at the top of the basement sequence to ~1.8 W/(m·K) at ~230 mbsf. Thermal conductivity values show two broad oscillations in the lower part of Hole U1560B, with relative minima at ~255 and 288 mbsf. Its overall trend mimics the *P*-wave pattern and is opposite to the porosity profile.

Three different wireline logging tool strings (triple combo with magnetic susceptibility, FMS-sonic, and UBI) were run successfully through the basement section in Hole U1560B, reaching the bottom of the hole at every pass and indicating overall good hole conditions. Some of the more outstanding features observed in the core measurements, such as high magnetic susceptibility values associated with massive flows in Unit 2 and smaller peaks in deeper units, are clearly recognized in the logs, and the generally good agreement between the logs and core measurements provide robust constraints for the stratigraphy of intervals with incomplete recovery (Figure **F21**). Two full passes each with the FMS (high-resolution resistivity images of the borehole wall) and UBI (360° acoustic images) may provide a comprehensive frame for core-log integration.

9.2.3.2.6. Microbiology

Microbiology sampling in volcanic rocks from Hole U1560B focused on exploring evidence for life in the basement, especially at the sediment/basement interface using microscopy, culture-based approaches, and culture-independent approaches. A total of 18 whole-round samples (9–14 cm long) from Hole U1560B were collected for microbiological analyses, and they represented all characterized lithostratigraphic units. After the exteriors of whole-round pieces were removed to

avoid material contaminated during coring, the remaining material was split into samples that were prepared for different microbiology analyses. Experiments were started shipboard to study microbial activity at the sediment/basement interface using ammonium enrichment incubations. These incubations focused on the uppermost basement samples to correspond with the deep sediment column samples described in the sediment section.

9.3. Site U1583

9.3.1. Background and objectives

Site U1583 is located ~652 km west of the Mid-Atlantic Ridge at 30°42.6175′S, 20°26.0336′W (Hole U1583F) in 4210 m of water (Figure **F1**). The basement at Site U1583 was predicted to have formed at ~30.6 Ma at a half spreading rate of 24 mm/y (Kardell et al., 2019; Christeson et al., 2020) (Figure **F4**). The site is located on the approximately north–south trending (355) CREST03 seismic crossing line at CDP 12300 about 3.3 km south of the main east–west (085) CREST1C/D seismic line (Figures **F1**, **F11C**, **F22**). A reflector at ~5.73 s TWT was interpreted to be the top of basement and estimated to be at 138 mbsf (Figure **F11C**) and observed at 106 mbsf.

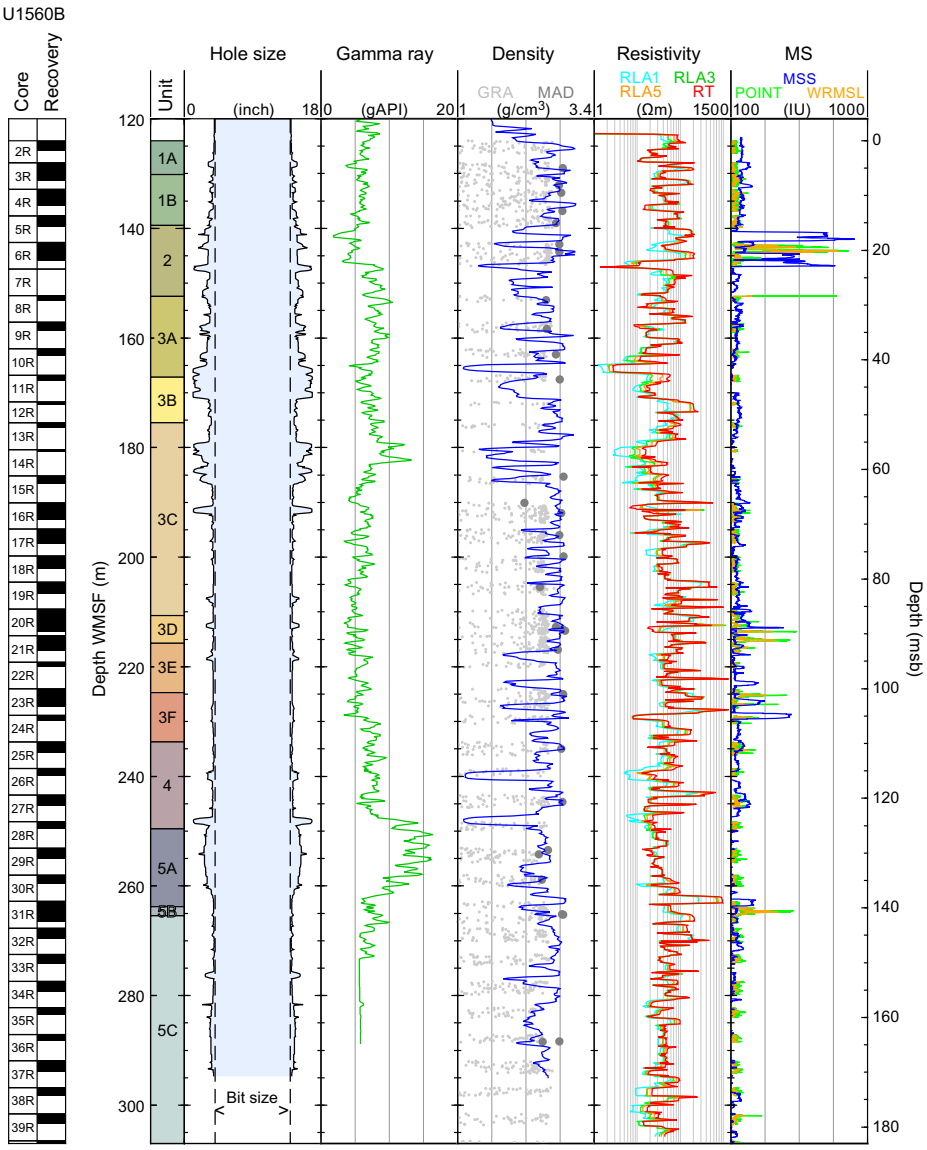

Figure F21. Summary of logging data recorded with triple combo logging string, Hole U1560B. RLA1, RLA3, and RLA5 = apparent resistivity from Computed Focusing Modes 1, 3, and 5, respectively; RT = true resistivity; MS = magnetic susceptibility; MSS = Magnetic Susceptibility Sonde; WRMSL = Whole-Round Multisensor Logger.

Site U1583 is a new site that has not been previously occupied. The original operational objectives of Expedition 393 at Site U1583 were to core two APC/XCB holes to basement and core and log ~250 m of basement volcanic rocks. At 30.6 Ma, Site U1583 is in the middle of the SAT and will be compared to older and younger sediments and igneous rocks cored during Expeditions 390 and 393. Science objectives at Site U1583 are to (1) investigate the history of the low-temperature hydrothermal interactions between the aging ocean crust and the evolving South Atlantic Ocean and quantify past hydrothermal contributions to global geochemical cycles, (2) collect samples of the sediment- and basalt-hosted deep biosphere beneath the low-productivity South Atlantic Gyre that will be used to refine global biomass estimates and investigate microbial ecosystems' responses to variable conditions, and (3) construct paleoceanographic records of carbonate chemistry and deep water-mass properties across the western South Atlantic Ocean through key Cenozoic intervals of elevated atmospheric CO_2 and rapid climate change.

While *JOIDES Resolution* was operating at Site U1583 at 1030 h on 6 July 2022, a tribute was held for Professor Dirk "Dick" Kroon, Regius Professor of Geology at the University of Edinburgh (Scotland), former IODP Science Evaluation Panel Co-Chair, and until recently Chair of the IODP Forum. Many colleagues from the international scientific ocean drilling community around the world joined the shipboard party in the minute's silence. A free-fall funnel labeled Dick Kroon 1957–2022 was dropped over Hole U1583F to enable coring and wireline logging operations during Expedition 393.

9.3.2. Operations

9.3.2.1. Transit

At 0530 h on 5 July 2022, we started the 227 nmi transit to Site U1583. The transit took 21.5 h at an average speed of 10.6 kt, and we arrived on site at 0300 h on 6 July.

9.3.2.2. Site U1583

The ship switched to DP mode at 0315 h on 6 July 2022, beginning operations in Hole U1583A. On site, we noted a 41 m seafloor depth discrepancy between the ship's precision depth recorder (PDR) 12 kHz estimate of 4234 mbsl and the prospectus estimate from the preexpedition seismic survey of 4193 mbsl. Sea conditions were rough, and ship heave was 3–4 m. The APC/XCB BHA was made up and lowered to 4228.5 mbsl, 4.5 m above the PDR estimated depth.

9.3.2.3. Holes U1583A and U1583B

At 1545 h on 6 July 2022, we started Hole U1583A; however, Core 1H recovered 9.14 m of sediment, indicating that the bit was below the seafloor when the piston was shot, so the mudline depth could not be determined. At 1715 h, we started Hole U1583B at approximately the same

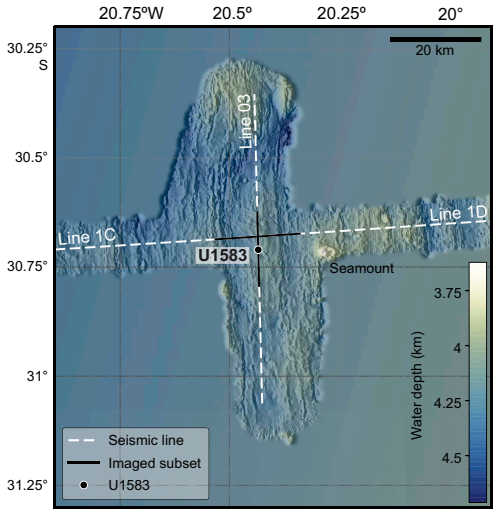

Figure F22. Site U1583 bathymetry (Christeson and Reece, 2020). Seismic reflection profiles were acquired during CREST cruise (Reece et al., 2016).

geographic location with the drill bit 5 m shallower; similarly, Core 1H was full, recovering 9.38 m of sediment, so the mudline depth again could not be determined.

9.3.2.4. Hole U1583C

The bit was raised 10 m shallower than the Hole U1583B shooting depth to 4213.5 mbsl, and the ship moved 10 m north. At 1845 h on 6 July 2022, we started Hole U1583C (Figure **F23**). Core 1H recovered 8.5 m of sediment, giving an apparent mudline at 4214.6 mbsl. We did not know at the time that this core was also shot from below the mudline. Coring continued with the full-length APC system with the Icefield orientation tool run on each core. Temperature measurements were taken on Cores 4H, 7H, and 10H. Core 12H hit hard rock when it was fired, based on some damage to the cutting edge of the APC shoe. The basement contact was subsequently confirmed when the bit encountered hard formation 2 m below the top of Core 12H at 104.5 mbsf. Core 12H recovered 8.02 m of sediment, an apparent 401% recovery, most of which was disturbed sucked-in sediment and is not in place. This basement depth was ~33.5 m shallower than expected from the site survey seismic interpretation of basement depth at ~138 mbsf. Cores 1H–12H penetrated from 0 to 104.5 mbsf and recovered 108.3 m (103%).

The XCB coring system was then deployed for Core 393-U1583C-13X, which penetrated 3 m to 107.5 mbsf and recovered 1.9 m (63%) of fresh microcrystalline basalt. The bit was then pulled out of the hole, clearing the seafloor at 1540 h on 7 July and ending Hole U1583C.

9.3.2.5. Hole U1583D

We started Hole U1583D 50 m south of Hole U1583C and 20 m south of the preexpedition site coordinates, which we reserved to be the location for hard rock coring in Hole U1583F. All holes at this site are located on a north–south line because the site sits on the edge of a north–south trending basin and the basement depth was anticipated to be more uniform in this direction compared to the east–west direction. Core 1H recovered 10.04 m of sediment, and the mudline depth could not be determined. Coring was terminated, and Hole U1583D ended at 1730 h on 7 July 2022.

9.3.2.6. Hole U1583E

We raised the bit by 5 m to 4204.5 mbsl, and at 1835 h on 7 July 2022 we started Hole U1583E (Figure **F23**) in the same location as Hole U1583D. Core 393-U1583E-1H recovered 4.03 m of sed-

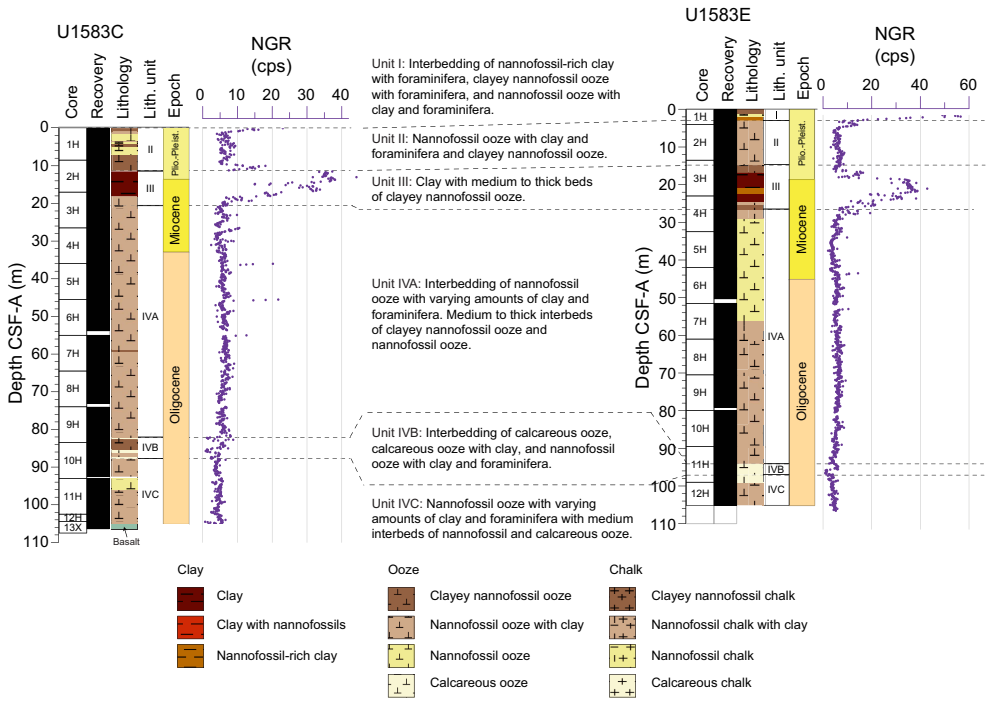

Figure F23. Lithostratigraphic summary of sediment units and correlation of full sediment sequences, Holes U1583C and U1583E. Dashed lines = correlation between units. cps = counts per second.

iment, placing the mudline at 4210.0 mbsl. This seafloor depth was 24 m shallower than the PDR depth and 17 m deeper than depth predicted from the preexpedition seismic survey. The difference from the seismic survey depth is consistent with observations at Sites U1556–U1560 along the transect, where mudline seafloor depths are 8–21 m deeper than the depth estimated from the seismic survey. While retrieving Core 2H, the core winch weight indicator showed that the core barrel became detached from the core winch line. An overshot was made up using a core catcher and an RCB core barrel. The barrel was lowered, and the APC core barrel was retrieved. Coring continued through Core 12H at 105.2 mbsf. All cores were full-length APC cores with the Icefield orientation tool run on all but two cores (3H and 4H). Temperature measurements were taken on Cores 3H and 8H.

After cutting Core 393-U1583E-12H, the APC core barrel could not be pulled back into the BHA. From 1230 to 1545 h on 8 July, we tried to free the barrel by pumping and washing over it, but it would not move. We decided to deploy the Kinley Cutter tool to cut the winch core line just above the APC corer. The Kinley Cutter was deployed at 1610 h, and the hammer/actuator was deployed at 1640 h. However, based on the core winch line tension, the Kinley wireline cutter and crimper had stopped before reaching the bottom of the drill string and cut partway down. Approximately 1560 m of core winch line was pulled up to the ship, and we then started to raise pipe. The drill pipe was pulled out of the hole to 2562 mbrf when the severing tool was found in Stand 83. A second Kinley Cutter was deployed to sever the remaining core winch line from the sinker bar assembly. This was unsuccessful, and the rig crew continued to pull the drill string out of the hole, cutting and removing the remaining core winch line at each stand. The second severing tool was found at the top of Stand 55. The rig crew continued to pull the drill string to the surface, cutting and removing the core winch line as before. The bit reached the rig floor at 0435 h on 10 July, ending Hole U1583E. The rig floor team then disassembled the lower part of the BHA and found that the APC core barrel assembly had stuck in the landing saver sub because a shear pin had become wedged between the landing seat and the core barrel. The APC cutting shoe was undamaged, showing that it had not hit basement, and Core 12H recovered 6.1 m of sediment after its long trip to the surface. Cores 1H–12H penetrated from the seafloor to 105.2 mbsf and recovered 105.2 m (100%).

9.3.2.7. Hole U1583F

At 1000 h on 10 July 2022, we began assembling the RCB BHA with a C-7 bit and then lowered it to 4174 mbsl, where we paused to slip and cut the drill line and pick up the top drive. At 0030 h on 11 July, we started Hole U1583F (Figure **F24A**) and washed down through most of the sediment column to 101 mbsf (drilled interval 11). Core 2R penetrated from 101.0 to 109.5 mbsf and recovered 6.4 m (76%) of clayey nannofossil ooze. At the start of drilling Core 3R, a hard formation was noted by the drillers at 109.7 mbsf, and the formation was subsequently confirmed to be basalt. Coring continued through Core 8R at 142.9 mbsf. With a hole in basement established, a free-fall funnel was deployed at 1450 h on 12 July to aid in reentry for downhole logging or a bit change, which was still a possibility at the time. Coring continued with a typical RCB half-core advance of 4.8 m. To test for microbiological contamination, perfluoromethyldecalin (PFMD) tracer was run continuously in the drilling fluid until the supply was exhausted on Core 12R. From Core 12R, there was up to 3 m of backfill in the hole after each core and the drill string experienced high torque at times. It was uncertain if the fill resulted from cuttings not being completely cleared from the hole or if new material was falling down from the borehole wall. We ran 30–60 bbl mud sweeps after every core to flush out the cuttings. The last five cores (25R–29R) averaged only 7% recovery, and the bit had been run for ~73 h of drilling time; therefore, coring was terminated at 1230 h on 16 July after recovering Core 29R. Basement Cores 3R–29R penetrated from 109.5 to 239.5 mbsf and recovered 39.4 m (30%).

To prepare for wireline logging in Hole U1583F, we ran a 75 bbl mud sweep and released the RCB bit at the bottom of the hole. We set the end of the pipe at 102.8 mbsf in sediment ~7 m above the basalt flow that forms the uppermost basement to avoid of the risk of dislodging rock pieces while the logging tools were below that depth. At 1730 h, we began to rig up the triple combo logging tool string, consisting of NGR, neutron porosity, density, and electrical resistivity tools. Because of the hole conditions and ~3 m ship heave, which is high for logging, the density tool source and magnetic susceptibility tool were not included in the tool string, and the density tool was used

only for the caliper log of borehole diameter. The tool string was lowered down the pipe, but at ~540 mbsl it developed an electrical fault and had to be raised back to the ship. The fault was found in the electrical resistivity tool (the lowermost tool of the tool string), which was then replaced with the backup resistivity tool.

We started to lower the triple combo from the rig floor again at 0045 h on 17 July. Logs were recorded on the downward pass, and the tool string reached to 237 mbsf, within 3 m of the bottom of the hole. Two logging passes were run in the open hole. During the first pass, the wireline heave compensator cut out about halfway up the open hole but logging continued to the top of basement. While descending for the second pass, the tool string encountered an obstruction at 182 mbsf and could not pass below it. We raised the triple combo to the rig floor, disassembled it, and assembled the FMS-sonic tool string. We lowered the FMS-sonic tool string to 182 mbsf and made a logging pass up to the top of basement at 109.5 mbsf. One FMS caliper arm sustained damage at ~160 mbsf, likely due to downward tool motion in the high heave conditions. Subsequently, the tool string could not go back down into basement, and overpull of approximately 8,000 lb was observed when trying to pull the tool string back into drill pipe. After pumping to remove any potential obstruction, the tool string still could not enter the pipe. Finally, we rotated the pipe 180°, and the tool string could be pulled in. When the tool string reached the rig floor, it was discovered that the FMS tool caliper arms had been damaged and one was missing. By 0000 h, we had disassembled the FMS-sonic tool string, ending downhole logging operations in Hole U1583F. The difficult borehole conditions and continuing high heave did not allow for the planned logging with the UBI tool string. We raised the pipe from 102.8 mbsf, clearing seafloor at 0035 h

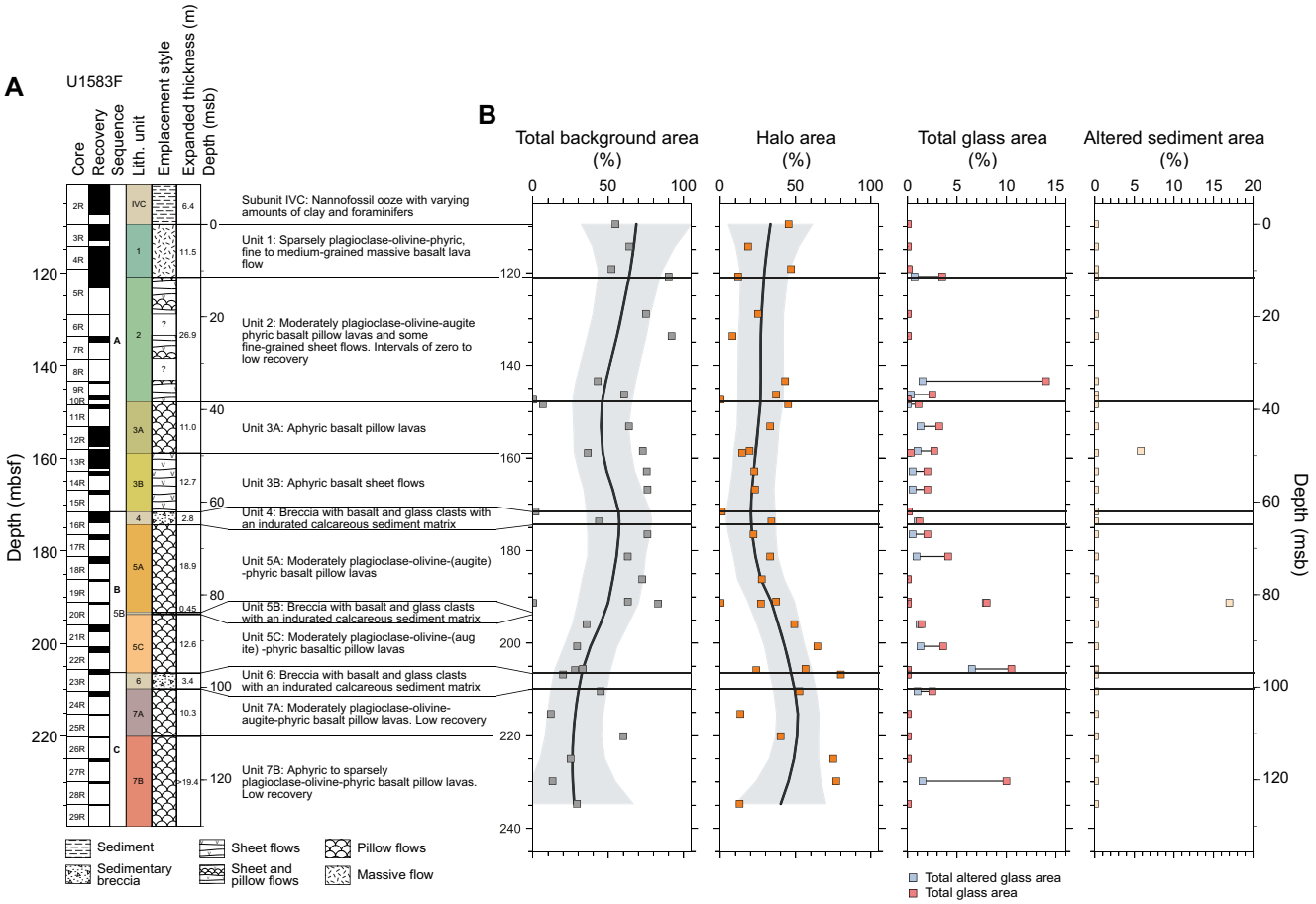

Figure F24. A. Stratigraphic column for igneous basement, Hole U1583F. Unit contact depths and thicknesses are expanded to account for <100% recovery. B. Area abundance of background alteration, alteration halos, fresh and altered glass, and altered sediment. Data are plotted at individual core level. Depths are CSF-A and plotted at top of cored interval. Black trend lines = locally weighted nonparametric regression (LOWESS), gray shading = 2σ of mean.

on 18 July. The BHA reached the ship at 0645 h and was disassembled. The rig floor was secured for transit by 0840 h, and we raised the thrusters and began the transit to Site U1560.

9.3.3. Principal results

Site U1583 targeted 30.6 Ma upper oceanic crust along the SAT. A near-complete sedimentary sequence was recovered from the combination of Holes U1583C and U1583E (Figure **F23**), and uppermost basement rocks were recovered in Hole U1583C as well as Hole U1583F. Hole U1583F advanced to a total depth of 239.5 m (Figure **F12**), ~130 m into volcanic rocks of the ocean crust, and recovered >39 m of basalt lavas and breccias with a recovery rate of ~30%.

9.3.3.1. Sediments

9.3.3.1.1. Sedimentology

Drilling at Site U1583 recovered 108.3 m of sediment and 1.89 m of volcanic rock in Hole U1583C and 105.2 m of sediment in Hole U1583E (Figure **F23**). The cores recovered from Holes U1583A–U1583F record four major sedimentary lithologic units (I–IV). Biogenic sediments consist primarily of calcareous nannofossil ooze with varying amounts of clay and foraminifera. Intervals with siliciclastic sediments have abundant clays with variable nannofossil and foraminifera content. Lithologic Unit I is composed of 3 m of Pliocene/Pleistocene sediments, consisting of interbedded nannofossil-rich clay with foraminifera and clayey nannofossil ooze, and was only recovered in Hole U1583E. Lithologic Unit II is composed of up to 11.3 m of Pliocene/Pleistocene sediments, predominantly beds of nannofossil ooze with clay and foraminifera interbedded with beds of nannofossil ooze with clay. Unit III consists of up to 11.9 m of clay and nannofossil ooze with varying amounts of clay. Unit IV is divided into three subunits (IVA–IVC). Subunit IVA is up to 64.4 m thick and consists of nannofossil ooze with clay and varying amounts of foraminifera. Subunit IVB is up to 6.1 m and consists of nannofossil ooze with clay and decimeter thick beds of calcareous ooze. Subunit IVC is up to 24.4 m thick and consists of nannofossil ooze with clay and varying amounts of foraminifera.

9.3.3.1.2. Biostratigraphy and age-depth model

Calcareous nannofossil and planktic foraminifera biostratigraphy of Site U1583 was performed primarily on core catcher samples examined on board *JOIDES Resolution* during Expedition 393. The mudline sample in Hole U1583E contains modern assemblages of planktic foraminifera and calcareous nannofossils. In contrast, the uppermost sediments in Hole U1583C contain a collection of recent to Late Pleistocene planktic foraminifera accompanied by Early Pleistocene calcareous nannofossils, confirming that the mudline was missed in this hole.

Biostratigraphic analyses indicate that the Pliocene/Pleistocene boundary occurs above 11.1 m CSF-B in Hole U1583C and above 13.5 m CSF-B in Hole U1583E (Figure **F25**), which corresponds to the sequence of brown nannofossil-rich clays and pink nannofossil oozes (Lithologic Units I and II, respectively). Dark clay sediments (Lithologic Unit III) below the Pliocene–Pleistocene sediments are ~6.6 m thick in Hole U1583C and 11.8 m thick in Hole U1583E and represent a condensed interval spanning roughly ~9 My across the Miocene/Pliocene boundary (Figure **F25**).

Biostratigraphic data indicate early Middle Miocene sediments occur between 14.8 and 36.0 m CSF-B in Hole U1583C and between 23.0 and 42.0 m CSF-B in Hole U1583E (Figure **F25**). The Oligocene is ~71.5 m thick in Hole U1583C and ~54.8 m thick in Hole U1583E and corresponds to the sequence of calcareous and nannofossil oozes (combined Lithologic Unit IV).

The most accurate determination for the age of the sediment/basement interface comes from the deepest sediment samples from Holes U1583C (Sample 12H-CC, 12–17 cm) and U1583E (Sample 12H-CC, 0–1 cm) that both contain *Sphenolithus distentus*, suggesting an age younger than 30.0 Ma (Figure **F25**). Planktic foraminifera assemblages in the same two samples contain *Subbotina angiporoides* and record the disappearance of *Paragloborotalia opima*, suggesting an age older than 30.8 Ma. These results are generally in good agreement with the projected crustal age of ~30.6 Ma at Site U1583.

Calcareous nannofossil and planktic foraminifera bioevents, in conjunction with paleomagnetic data, allowed for comprehensive hole age-depth models (Figure **F25**) and calculation of LSRs.

LSRs range 0.13–4.08 cm/ky in Hole U1583C and 0.06–7.29 cm/ky in Hole U1583E. In both holes, the highest LSRs consistently occurred within the Oligocene, with values ranging 0.29–4.08 cm/ky in Hole U1583C and 0.17–7.29 cm/ky in Hole U1583E. In contrast, the Neogene and Quaternary in both holes record the lowest sedimentation rates.

9.3.3.1.3. Sedimentary and pore water geochemistry

Samples from Site U1583 were mostly collected from Hole U1583C, with one additional water sample each from Holes U1583E (mudline) and U1583F (sediment/basement interface). Shipboard analyses included fluid chemistry, sediment geochemistry, and measurements of headspace gas. Pore fluid salinity is uniform at the seawater value (35) throughout Hole U1583C, although concentrations of Na, Cl, and Br are higher than in seawater below ~5 m CSF-A. Measured pH (7.5 ± 0.1 [2σ]; n = 13) is uniformly lower than local bottom seawater between ~3 and 56 m CSF-A and gradually increases (up to 7.8) between ~60 and 100 m CSF-A. Alkalinity values are much more variable and show a number of inflection points, including increases at the boundary between lithostratigraphic Units II (nannofossil ooze with clay and foraminifera) and III (clay with nannofossils and clayey nannofossil ooze) (2.0–2.5 mM) and the boundary between Subunits IVA (nannofossil ooze with clay and foraminifera) and IVB (calcareous and nannofossil oozes with clay and foraminifera) (2.2–2.5 mM). The transition from Units II to III is also marked by (1) an increase in Ca, Sr, and Sr/Ca and a decrease in Mg concentrations in pore fluids, consistent with the dissolution of biogenic carbonate and recrystallization of high-Mg inorganic calcite; and (2) significant increases in B (67%), Li (10%), Si (78%), and K (17%) concentrations, which are likely a result of diagenetic reactions involving detrital silicates and biogenic silica. The weak positive trend between SO_4 and Ca concentrations in Hole U1583C hints at a potential role for sulfate reduction within these sediments, which may also explain the concomitant downhole decrease in SO_4 and TOC content. NH_4 (3–17 µM) and Mn (0.63–2.86 µM) concentrations remain low throughout the sediment column, with the exception of two peaks observed in Unit III (clay with nannofossils and clayey nannofossil ooze) and Subunit IVB. Oxygen concentrations decrease between Unit II and Subunit IVA and reach a minimum value of 10.5 µM at ~22 m CSF-A before gradually increasing to 207.4 µM at ~99 m CSF-A. Calcium carbonate content is generally high throughout the hole, with the exception of Unit III, which has a difference of ~80 wt% between the top and bottom of

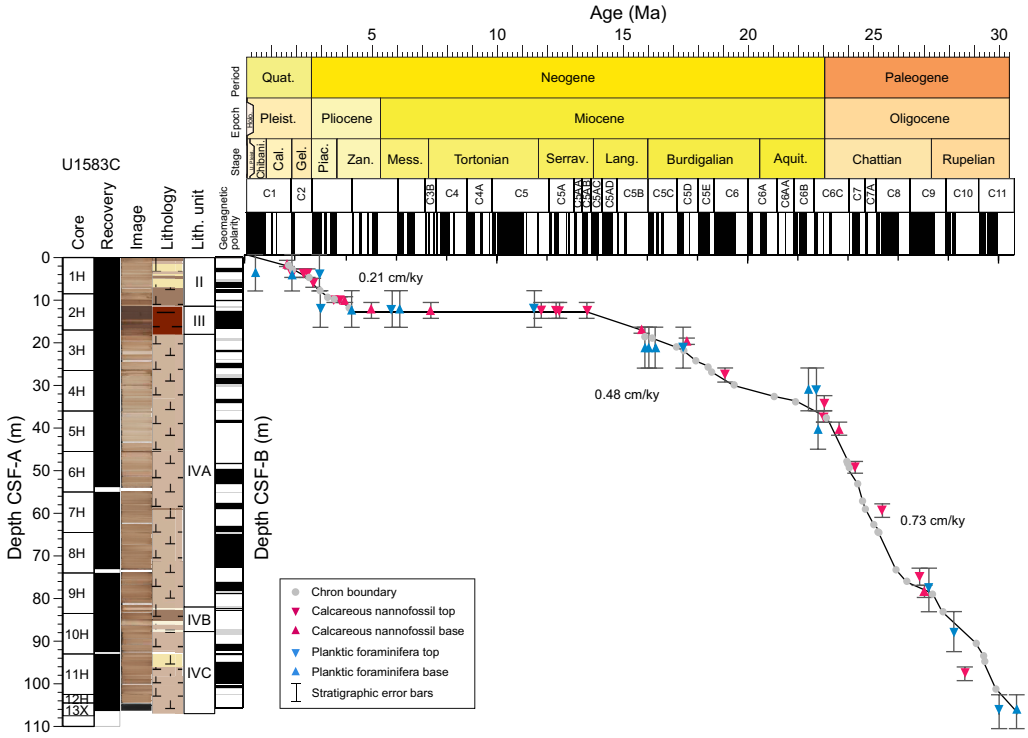

Figure F25. Age-depth model showing biostratigraphic and magnetostratigraphic datums, Hole U1583C. LSRs were averaged for Pleistocene, Pliocene, Miocene, and Oligocene.

the unit. Conversely, low TOC concentrations (<0.36 wt%) are measured in Hole U1583C and values gradually decrease toward the bottom of Subunit IVC (nannofossil ooze with clay and foraminifera), which is consistent with organic matter oxidation. A spike in TOC is seen in Subunit IVB, which coincides with increases in SO_4, NH_4, and Mn geochemical profiles. In Hole U1583C, headspace gas measurements for methane, ethane, propane, and higher molecular weight hydrocarbons were below detection limits.

9.3.3.1.4. Paleomagnetism

Continuous measurements of remanent magnetization were conducted on sediment cores from Holes U1583C and U1583E using the SRM at 2 cm intervals before and after progressive AF demagnetization of three steps (5, 10, and 20 mT). Discrete measurements including AMS and remanence after AF demagnetization were conducted on 25 cube samples. IRM acquisition experiments were performed on eight selected samples, which is at least one per lithologic unit. Paleomagnetic measurements provide constraint on the magnetostratigraphy for the entire sediment sequence at Site U1583.

Viscous overprints are almost completely removed at 20 mT demagnetization, and characteristic components can be observed at this stage. Inclination values of the revealed characteristic components (a.k.a. 20 mT inclination) show a bimodal distribution in both holes, where values are clustered around +57° and –54° in Hole U1583C and around +59° and –51° in Hole U1583E. Well-defined normal and reversed polarities in the 20 mT inclination are present in both Holes U1583C and U1583E, enabling age determinations by magnetostratigraphic correlations with polarity chrons on the GPTS. The topmost sediment sequence in Hole U1583E contains the Brunhes, Matuyama, and Jaramillo Chrons, which are absent in Hole U1583C. The Oligocene/Miocene boundary occurs in Subunit IVA at ~40 m CSF-A in Hole U1583C and ~45 m CSF-A in Hole U1583E. Paleomagnetic results at the bottom of the sediment sequence above the sediment/basement interface (between 100 and 110 m CSF-A) were placed in Chron C11r for Hole U1583C and Chron Cr11.2n in Hole U1583E. The relative ages of those chrons agree with the estimated basement age of ~30.6 Ma (Kardell et al., 2019).

Discrete samples were subjected to AF demagnetization up to a maximum of 130 mT. Most of the samples reveal a single remanent magnetization component after the 5 mT AF demagnetization step with maximum angular deviation angles spanning from 2.2° to 14.8°. Inclinations of ChRM components calculated from discrete sample measurements are consistent with the values measured from the SRM.

Mineralogy-related measurements were conducted on one or two discrete samples for each lithologic unit. IRM measurements reveal the dominance of low-coercivity minerals throughout the cored interval with no variations with depth or between lithologic units. AMS measurements show two different trends in the magnetic fabric with either a subvertical or a subhorizontal magnetic foliation. Samples showing subhorizontal magnetic foliation correspond to typical oblate sedimentary fabric. In contrast, the presence of samples characterized by a subvertical magnetic foliation might be related to either soft-sediment deformation or drilling disturbance.

9.3.3.1.5. Physical properties

Characterization of the sediment physical properties at Site U1583 was primarily based on cores from Hole U1583C, with additional information from Hole U1583E. Whole-round, section half, and discrete measurements were considered together to characterize the petrophysical signatures for the different lithologic units. All archive halves were imaged using an X-ray image logger. A correlation framework and a semicontinuous splice were developed for the site that consider NGR, GRA, magnetic susceptibility, and magnetic inclination from each hole.

Whole-round NGR measurements range 1–42 counts/s through the sedimentary section in Hole U1583C. NGR is relatively low in the nannofossil ooze (Units II and IV; ~5 counts/s) and high in clay-rich Unit III (15–42 counts/s; mean = 27 counts/s). Similarly, magnetic susceptibility ranges 1–126 IU and shows a downhole trend similar to the NGR record over the entire hole, with the highest values in Unit III (ranging 30–122 IU; mean = 78 IU). Bulk density based on GRA ranges 1.4–2.5 g/cm^3 over the interval measured and shows an overall gradual increase downhole due to increasing consolidation of sediments with depth. In MAD analyses, porosity shows an overall

decreasing trend from 65% at the top of Unit II to 55% in the bottom of Subunit IVA and then remains relatively constant through the bottom of Hole U1583C, and bulk density measured generally follows the GRA record. *P*-wave velocity ranges 1.45–1.72 km/s with a mean value of 1.54 ± 0.03 km/s, and increases downhole, which is likely due to sediment compaction. Shear strength is relatively uniform in nannofossil ooze with values of 15–16 kN/cm^2 and shows its highest value of 42 kN/cm^2 in clay-rich Unit III. Compressional strength is scattered between 0.1 and 1.0 kg/cm^2 (mean = 0.6 ± 0.3 kg/cm^2) throughout the sedimentary sections with no apparent downhole trend. Most samples have a thermal conductivity of ~1.3 W/(m·K), and the lowest measurements come from Unit III (0.93 W/[m·K]). The vertical conductive heat flow for Site U1583 was estimated to be 31 mW/m^2, based on three APCT-3 tool measurements and thermal conductivity. This value is lower than the modeled heat flow values for ocean crust of this age, requiring significant regional advection of heat by hydrothermal fluid circulation (cf. Kardell et al., 2022)

9.3.3.1.6. Microbiology

Microbiology sampling of sediments in Hole U1583C was focused on exploring evidence for microbial life using microscopy, culture-based approaches, and culture-independent approaches. One microbiology whole-round sample (5–10 cm long) was collected from each 9.5 m core. One additional sediment sample was taken from near the sediment/basement interface in Hole U1583F. A total of 13 routine microbiology whole rounds were taken and subsequently sampled for different shipboard and shore-based scientists, and an additional 33 whole rounds were taken for personal, specialized, shore-based analyses.

Two microbiology experiments were started shipboard during Expedition 393 on sediment samples from Site U1583. To study the extent of viral activity and dynamics between viruses and other microbial life (Bacteria and Archaea), virus-induced microbial mortality and prophage induction experiments were performed on samples taken from five microbiological whole-round cores throughout the sediment column. To study the microbial activity at the sediment/basement interface, ammonium enrichment incubation experiments were started with the deepest sediment cores in Holes U1583C and U1583F, along with the uppermost basement samples.

9.3.3.2. Volcanic rocks

9.3.3.2.1. Igneous petrology

Site U1583 was established above ~30.6 Ma ocean crust during Expedition 393, and Holes U1583C and U1583F recovered volcanic basement. The uppermost igneous rock encountered was an ~11 m thick massive basalt lava flow intersected by Holes U1583C and U1583F at 107.5 and 109.7 mbsf, respectively, some 30 m shallower than predicted by seismic site surveys (Kardell et al., 2019; Christeson et al., 2020). Only Hole U1583F advanced deeply into basement, reaching 239.6 mbsf (129.8 msb) with ~30% recovery (Figure **F24A**).

Hole U1583F intersected three volcanic sequences: A, B, and C with 62, 35, and 33 m expanded thicknesses, respectively, separated by two sedimentary breccia units (Units 4 and 6) with thicknesses estimated between 0.8 and 3.4 m (Figure **F24A**). The upper Sequence A (109.7–171.6 mbsf) consists of Unit 1, an 11 m thick massive lava flow, Unit 2 made of moderately plagioclase-olivine-augite phyric pillow lavas and sheet flows, and the aphyric Unit 3, which is markedly more primitive than all the other lavas in the hole. The middle Sequence B is capped by sedimentary breccia Unit 4 and consists of moderately plagioclase-olivine (± augite) phyric pillow basalts and another thin breccia horizon. The lower Sequence C is again capped by a sedimentary breccia (Unit 6) above sparsely to moderately plagioclase-olivine phyric pillow basalts that are chemically and lithologically similar to Sequence B.

Lava compositions assessed by pXRF downhole vary both gradationally and in a stepwise fashion across petrologically defined unit boundaries. Incompatible element concentrations and Zr/Ti ratios are consistent with a relatively primitive N-MORB-like lava composition at Site U1583. In contrast to the sequence stratigraphy defined by the presence of sedimentary breccias, pXRF measurements reveal that Unit 3 has a uniquely primitive composition in Hole U1583F, splitting the hole into three major chemostratigraphic units: Units 1 and 2, Unit 3, and Units 4–7.

9.3.3.2.2. Alteration petrology

Hole U1583F records fluid/rock reactions over the full range of spatial contexts expected for uppermost basement. The secondary minerals forming are predominantly various clay minerals, calcium carbonate, Fe oxyhydroxides, and zeolites that are consistent with reactions at low temperatures between basalt and seawater or seawater-derived ridge flank hydrothermal fluids. In Hole U1583F, it is possible to identify zones of alteration that have distinctive characteristics. The uppermost 70 m of the hole are characterized by the presence of green clay filling vesicles (in background and in alteration halos) and a generally low abundance of alteration halos (<30% of core surface) and background alteration dominates (Figure **F24B**). This zone also hosts the most calcium carbonate and carbonate abundance increases downhole through this zone. From 40 to 70 msb, complex multicolored halos occur that exhibit both diffuse and sharp halo sequences that are variably mutually overprinting. These multihalos are best observed through the changing sequences of vesicle fillings. From 70 msb, green clay in vesicles is absent and the abundance of carbonate filled veins decreases. These changes are accompanied by an increased modal proportion of alteration halos, with the prominence of brown halos increasing downhole. From 95 msb, halos are most commonly orange and there is a slight increase in carbonate veins.

9.3.3.2.3. Igneous geochemistry

For Hole U1583F basement cores, representative samples were taken from the freshest portions of each lithologic subunit to obtain a downhole record of the primary magmatic conditions, along with one sample near the sediment/basalt contact. In addition, one sample of the intercalated indurated calcareous sediment/breccia matrix was taken to better understand the sediment-basalt chemical exchanges that occurred as new lavas erupted. A total of 17 samples were measured for LOI and bulk rock geochemical analysis via ICP-AES. The unoxidized powders of these samples were characterized for elemental abundances via pXRF to complement additional pXRF measurements made directly on the cut core surfaces.

In terms of basaltic rock type, the freshest Site U1583 basalts classify as olivine tholeiites following the Yoder and Tilley (1962) normative classification scheme. Basalt compositions show variability downhole that is most evident in the pXRF surface data. TiO_2 contents vary between 1.3 and 1.5 wt%, which is consistent with a moderate amount of magmatic crystallization before eruption. The Hole U1583F basalts are moderately altered, with elevated abundances of K_2O and Rb. K_2O shows a gradual increase downhole from 0.1 wt% to as high as 0.48 wt%. K/Zr ratios are overall lower than those seen in the older SAT sites, ranging to values similar to those seen at Site U1559 (≈ 6.6 Ma). MgO shows clear evidence for Mg removal from the rocks via seafloor weathering, with the lowest MgO samples clustered near horizons of volcano-sedimentary breccias, suggesting locally more intensive reactions with seawater.

9.3.3.2.4. Paleomagnetism of volcanic rocks

Continuous measurements of remanent magnetization were performed at a resolution of 2 cm intervals on basement cores of Hole U1583F using the SRM before and after progressive AF demagnetization at 5, 10, and 20 mT. Only core pieces longer than 9 cm were measured. Discrete magnetic measurements were performed on 20 cube samples taken predominantly from fresh background basalts with some samples displaying different styles and intensities of hydrothermal alteration.

The SRM results indicate that viscous overprints are mostly removed, and primary components can be clearly observed at the 20 mT demagnetization step. The primary components predominantly show positive inclination, which indicates reversed geomagnetic polarity at this latitude (30°S). Inclination values are clustered around 45.4°, agreeing with the calculated GAD (±49.1°). Based on the age of the sediments at the sediment/basement interface, the basement at Site U1583 can be placed in reversed Chron C11r with a basal age of 30.59 Ma (Gradstein et al., 2020). However, in brecciated intervals some rocks present negative inclinations, suggesting either extensive overprinting of the primary remanent magnetization by a secondary component or rotation of the clasts.

A subset of 20 discrete samples were subjected to AF demagnetization up to 190 mT step to isolate the ChRM. Discrete sample measurements mostly revealed well-defined ChRM with maximum

angular deviation between 0.3° and 14.8°. A few samples show a more stable secondary component, as the ChRM is revealed after the 25 mT step. Experiments to determine the magnetic mineralogy were conducted on a selected number of samples to define the possible relationships with igneous units and alteration types. Most of the samples show the dominance of low-coercivity minerals as titanomagnetite. A few altered basalts and the breccias do not reach saturation at the maximum applied field of 1200 mT, implying a significant contribution of high-coercivity minerals such as hematite. AMS measurements reveal different magnetic fabric shapes depending on the emplacement style of igneous units.

9.3.3.2.5. Physical properties

Whole-round, section half, and discrete measurements characterize the petrophysical signatures for the different igneous units. In addition to these measurements, ~77% of the recovered material was scanned using the DMT core scanner after identifying oriented core pieces with relatively cylindrical shapes. Selected archive-half sections with breccia were imaged using an X-ray image logger.

NGR in Hole U1583F is relatively low in the basalts (Unit 2, 3, 5, and 7) at around 2 counts/s and higher in the sedimentary breccias: 5.1 ± 2.7 counts/s in Unit 4 and 4.0 ± 1.5 counts/s in Unit 6. Discrete point magnetic susceptibility measurements range 1–2910 IU and are highest in the massive flows of Unit 1 (mean = 610) and sheet flows of Unit 3 (mean = 196). A total of 23 discrete sample cubes were used for *P*-wave velocity and MAD analyses and were described in terms of their alteration, emplacement style, and groundmass grain size. Bulk density ranges 2.05–2.90 g/cm^3 with the breccia samples having lower densities than the basalts. Breccias also have the lowest *P*-wave velocity and the highest porosity. Basalt with stronger alteration have higher porosity, lower *P*-wave velocity, lower bulk density, and lower grain density. Most basalt samples have a porosity <10%, although one sample of a strongly altered basalt from a brown halo has a porosity of 12.1%. *P*-wave velocity shows a general decreasing trend with depth in Hole U1583F and ranges 4.87–6.00 km/s. Lower *P*-wave velocity toward the bottom of the hole is likely driven by the higher prevalence of altered basalts in Units 5–7. Thermal conductivity in the basement at Site U1583 ranges 1.23–2.00 W/(m·K), with the lowest values found in Units 4 and 6 (sedimentary breccias) and higher mean values between 1.6 and 1.7 W/(m·K) in basalt flows.

9.3.3.2.6. Downhole logging

After completion of coring, two downhole logging tool strings were deployed in Hole U1583F (see operations, above). Sea state was marginal for logging (up to 3 m heave) and affected the operations. However, the logging data, in particular the resistivity log, are still of good quality (Figure **F26**) and will help constrain the major units identified in the volcanostratigraphy.

9.3.3.2.7. Microbiology

Microbiology sampling from volcanic rocks in Hole U1583F was focused on exploring evidence for life in the basement, especially at the sediment/basement interface using microscopy, culture-based approaches, and culture-independent approaches. Nine whole-round samples (10–17 cm long) from Hole U1583F and one whole-round sample (15 cm) from Hole U1583C, reflecting all the major igneous characteristics and units, were collected for microbiological analyses. Following the careful removal of potentially contaminated core exteriors, the remaining material was split into subsamples that were prepared for different microbiology analyses. Experiments were started shipboard to study microbial activity at the sediment/basement interface using ammonium enrichment incubations. These incubations focused on the uppermost basement samples to correspond with the deep sediment column samples described in the sediment section.

To determine the extent of contamination of microbiology samples, the perfluorocarbon tracer (PFT) PFMD was injected into drilling fluid during Hole U1583F coring until the tracer ran out after Core 12R. Microbiologists then collected samples from both the exterior and interior of core intervals selected for microbiology analysis, as well as core catcher rubble, to quantify the presence of PFMD. PFMD was detected from a majority of the exterior samples, with an average concentration of 46 ppb/g and a median concentration of 48 ppb/g of rock when detected. The tracer was not detected in the interior microbiology samples, suggesting no to minimal drilling contamination of the samples.

9.4. Site U1558

9.4.1. Background and objectives

Site U1558 is located ~1067 km west of the Mid-Atlantic Ridge at 30°53.78′S, 24°50.48′W in 4334 m of water (Figures **F1**, **F27**). The basement at Site U1558 was predicted to have formed at ~49.2 Ma at a half spreading rate of 19.5 mm/y (Kardell et al., 2019) (Figure **F4**). The site is located on Seismic Line CREST1B/C at CDP 3252 about 3.4 km west of Crossing Line CREST04 (Figures **F1**, **F11D**, **F27**) where a reflector at ~5.94 s TWT was interpreted to be the top of basement and estimated to be at 148 mbsf (Figure **F11D**) and observed at 158.9 mbsf.

Site U1558 was previously occupied in November 2020 during Expedition 390C (Figure **F12**) with objectives to confirm the depth to basement by coring, conduct gas safety measurements, and set a reentry system consisting of a reentry cone and 13⅜ inch casing (Estes et al., 2021). Hole U1558A was cored by the APC and XCB systems to 163.9 mbsf (Figure **F12**), finding the sediment/basement contact at 158.9 mbsf. Holes U1558B and U1558C marked unsuccessful attempts to drill in and release the reentry system using the Dril-Quip running tool. While lowering the reentry system for Hole U1558D, the reentry cone and mud skirt became detached from the casing and fell to

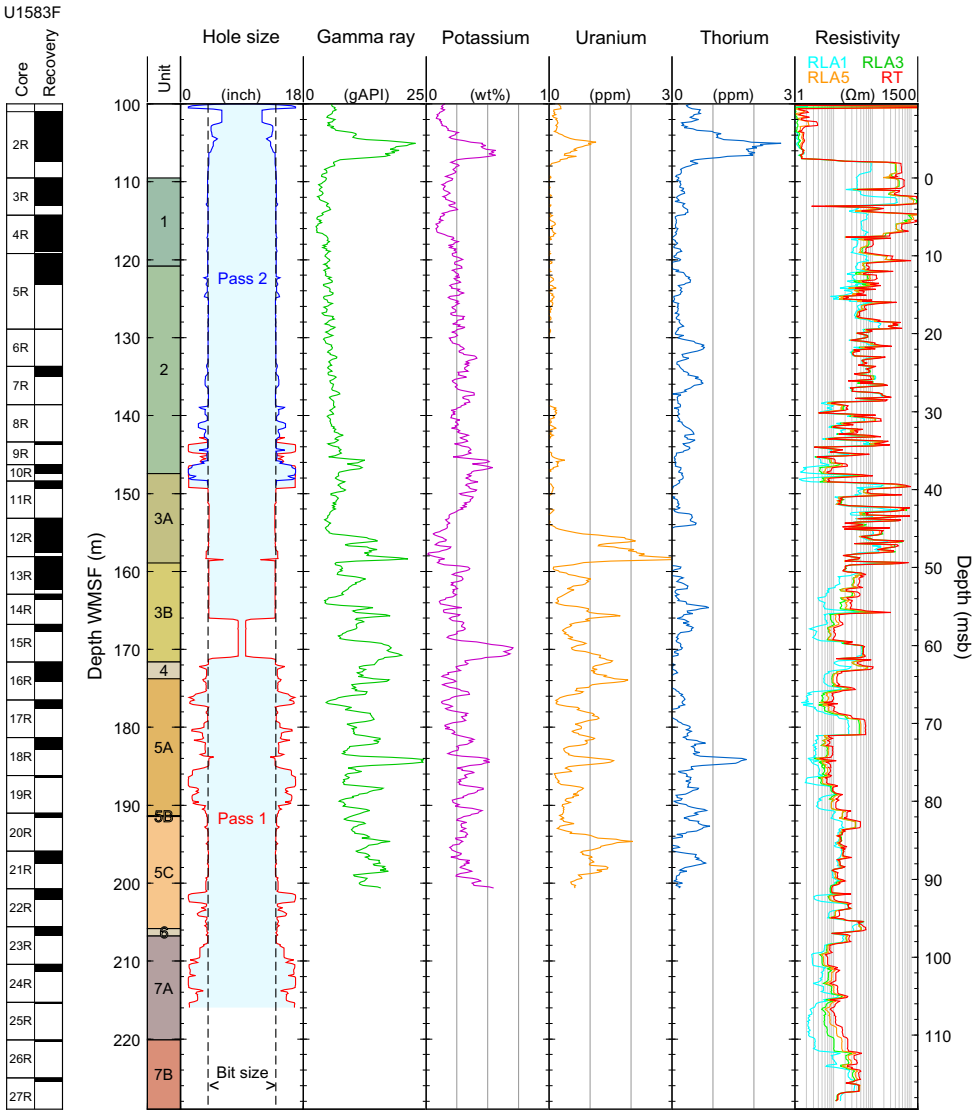

Figure F26. Summary of logging data recorded with triple combo logging string, Hole U1583F. Caliper is combination of two upward passes that were made. RLA1, RLA3, and RLA5 = apparent resistivity from Computed Focusing Modes 1, 3, and 5, respectively; RT = true resistivity.

the seafloor the right way up and within a few meters of the intended location. The drill bit and casing assembly was lowered through the cone and was drilled into Hole U1558D, setting the casing shoe at 146.1 mbsf and the base of the hole at 150.0 mbsf.

The original operational objectives of Expedition 393 at Site U1558 were to core a single APC/XCB hole to basement and core and log ~250 m of basement volcanic rocks in Hole U1558D.

At 49.2 Ma, Site U1558 is the second oldest location of the SAT and will be compared to older and younger crustal material cored at Expedition 390/393 sites. Science objectives at Site U1558 are to (1) investigate the history of the low-temperature hydrothermal interactions between the aging ocean crust and the evolving South Atlantic Ocean and quantify past hydrothermal contributions to global geochemical cycles, (2) collect samples of the sediment- and basalt-hosted deep biosphere beneath the low-productivity South Atlantic Gyre that will be used to refine global biomass estimates and investigate microbial ecosystems' responses to variable conditions, and (3) construct paleoceanographic records of carbonate chemistry and deep water-mass properties across the western South Atlantic Ocean through key Cenozoic intervals of elevated atmospheric CO_2 and rapid climate change.

9.4.2. Operations

During Expedition 393, three holes were cored at Site U1558. Hole U1558E consisted of one APC core that missed the mudline. Hole U1558F was cored by the APC and XCB systems to 177.2 mbsf (Figure **F28**), with the sediment/basement contact at 176.0 mbsf. In Hole U1558D, the sediment/basement contact was found at 166.8 mbsf and the volcanic sequence was cored by the RCB system to 370.2 mbsf (203.4 msb) (Figure **F29A**). Unfortunately, while withdrawing the bit out of Hole U1558D to prepare for wireline logging, the reentry cone and some casing were pulled out of the seafloor by the BHA, ending operations in that hole. The cased SAT holes were intended to be legacy holes for potential future deepening or other operations, but this is no longer possible at this site. This damage also precluded wireline logging of the volcanic sequences.

9.4.2.1. Transit

The ship completed the 508 nmi transit from Site U1559 to Site U1558 in 46.5 h (1.9 days), arriving on site at 1125 h on 25 June 2022. The ship was switched to DP mode, beginning operations at Site U1558.

9.4.2.2. Hole U1558E

An APC/XCB BHA was assembled and deployed to 4321 mbrf. A pipe pig was circulated down through the drill pipe to remove any rust from the extra ~1300 m of pipe required to reach the seafloor at Site U1558 compared to the shallower Site U1559 drilled previously. Heavy weather

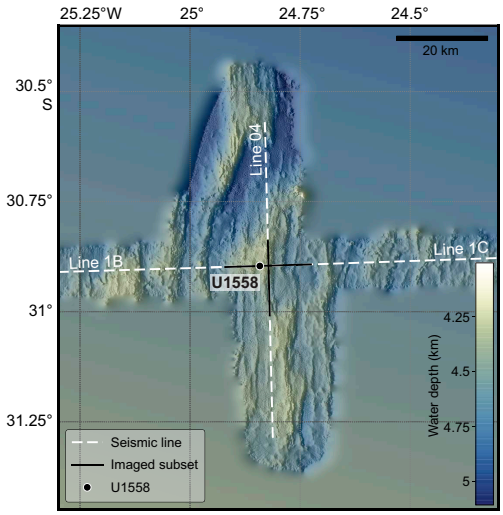

Figure F27. Site U1558 bathymetry (Christeson and Reece, 2020). Seismic reflection profiles were acquired during CREST cruise (Reece et al., 2016).

and sea conditions delayed the start of coring in Hole U1558E by 3 h, waiting for the ship's heave to subside. The ship was positioned 20 m south of Hole U1558D. At 0440 h on 26 June 2022, Core 393-U1558E-1H penetrated 9.5 m and recovered 9.97 m (105%), but there was no mudline. Therefore, Hole U1558E was terminated at 0515 h.

9.4.2.3. Hole U1558F

The ship was offset 10 m east of Hole U1558E (50 m southeast of Hole U1558A), and we started Hole U1558F at 0610 h on 26 June 2022 (Figure F28). Coring started with the full-length APC, and a seafloor depth of 4337.3 mbsl was established based on the mudline in Core 1H. After Core 3H, we drilled ahead 3 m in an effort to offset gaps in the stratigraphy recovered from Hole U1558A during Expedition 390C. APC coring continued through Core 393-U1558F-10H at 86.9 mbsf, where 80,000 lb of overpull was required to free the barrel, marking APC refusal depth. All full-length APC cores were oriented, and the APCT-3 tool was deployed on Cores 3H, 6H, and 10H. Unfortunately, the advance in Core 10H was overdrilled by 4.7 m, and core is missing from Hole U1558F from 82.2 to 86.9 mbsf. The HLAPC system was deployed for Cores 11F–19F. Core 19F at 129.2 mbsf needed to be freed by drilling over the core barrel, marking HLAPC refusal depth. The XCB coring system was deployed for Cores 20X–24X. The driller noted a formation change at 176.0 mbsf, and drilling was terminated at 177.2 mbsf approximately 1.2 m into volcanic rocks. Cores 1H–24X penetrated from 0 to 177.2 mbsf and recovered 164.3 m (94%). The drill string was recovered to the ship, and the drill bit cleared the rotary table at 0035 h on 28 June, ending Hole U1558F.

9.4.2.4. Hole U1558D

We then made up the RCB BHA with a new TransCo C-4 RCB bit and following a slip and cut, lowered it to Hole U1558D, where a reentry system had been installed in November 2020 during

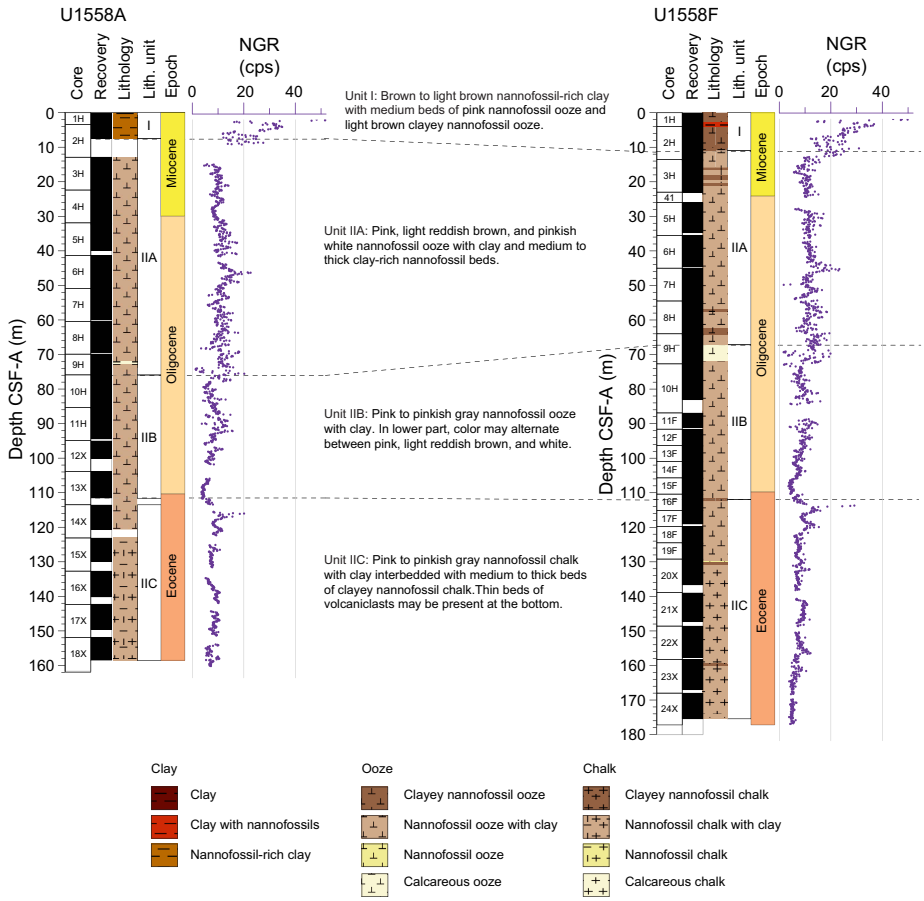

Figure F28. Lithostratigraphic summary of sediment units and correlation of full sediment sequences, Holes U1558A and U1558F. Dashed lines = correlation between units. cps = counts per second.

Expedition 390C (Figure **F12**). Guided by the subsea camera video feed, the ship maneuvered over the hole. At first, the bit entered the center of the cone, but it soon met resistance and did not pass down into the casing and had to be pulled back above the cone. The second attempt was successful, and the bit reentered Hole U1558D at 1505 h on 28 Jun 2022. We lowered the bit to the depth of the existing hole (150 mbsf) and started coring at 1845 h. The existing hole is designated as drilled interval 390C-U1558D-11. Cores 393-U1558D-2R and 3R penetrated from 150 to 166.5 mbsf and recovered 3.27 m (20%) of sediment. The sediment/basement contact was determined to be at 166.8 mbsf based on an abrupt slowing of the rate of penetration at that depth while starting to drill Core 4R. Coring continued, at first alternating between full and half cores based on the rate of penetration and core recovery, and switching exclusively to half-length cores from Core 16R. PFT was run on all cores. Core 39R reached a healthy 203.4 m into volcanic rock, and coring was stopped to enable wireline logging. Basement Cores 4R–39R penetrated from 166.8 to 370.2 mbsf, recovered 97.53 m (~48%) of core, and took 5.0 days to drill.

At 0330 h on 4 July, we set back the top drive and pulled the bit up to 126.3 mbsf, observing 20,000 lb drag. At 0445 h, we deployed the subsea camera to observe the bit release and guide reentry in preparation for downhole logging. We pulled the bit out of the hole to 4317 mbsl, 17 m above seafloor. However, at 0615 h the drill pipe was observed by the subsea camera to be still inside the reentry cone, with the cone much higher up than it should be. The extra weight on the drill string confirmed that the cone and some, perhaps all, casing had been pulled out of the hole by the BHA. From 0730 to 0830 h, we attempted unsuccessfully to free the casing by pushing into the seafloor. We raised the camera back up to the ship, and from 1030 to 1100 h we attempted to free the drill

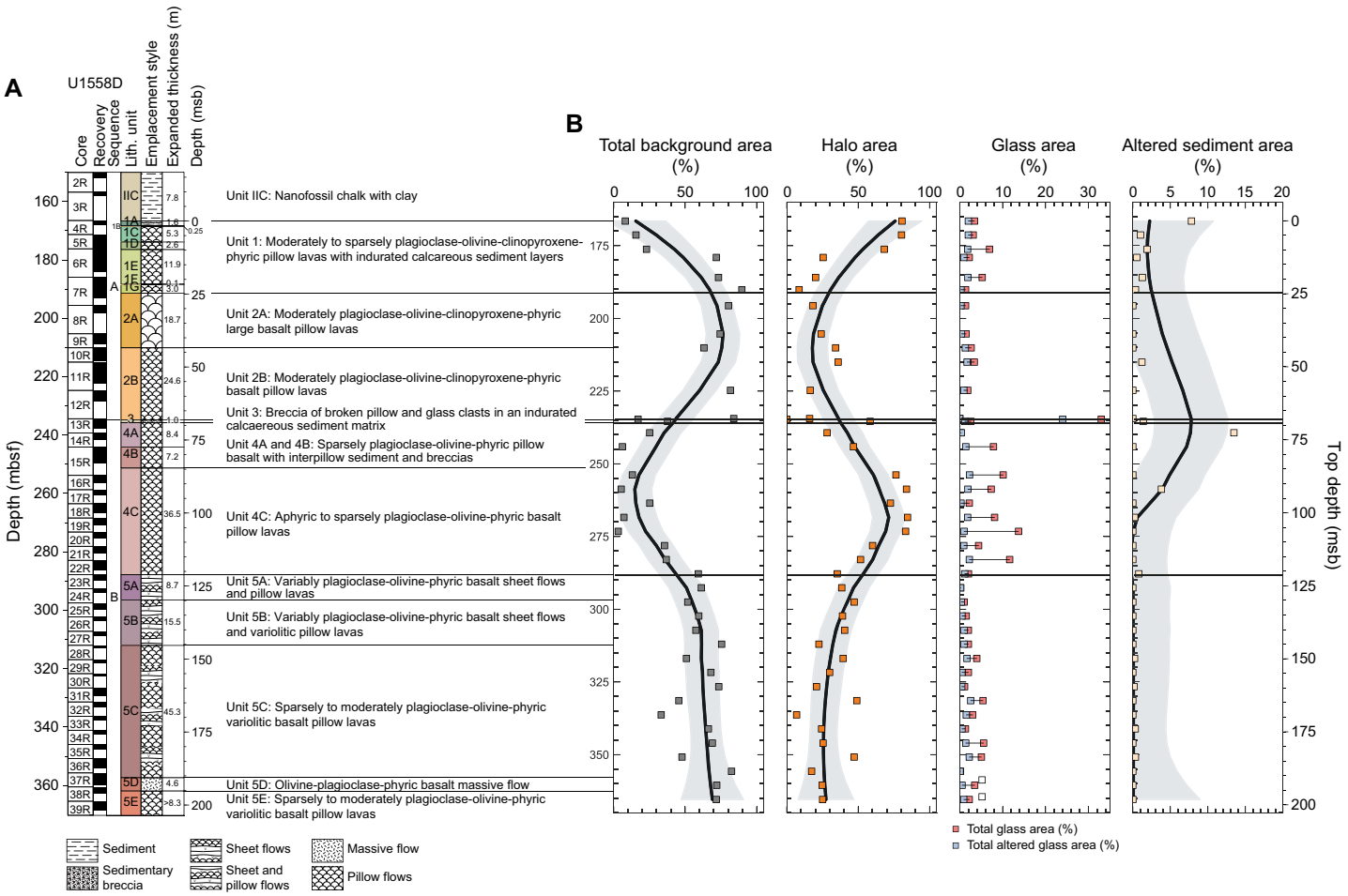

Figure F29. A. Stratigraphic column for igneous basement, Hole U1558D. Unit contact depths and thicknesses are expanded to account for <100% recovery. B. Area abundance of background alteration, alteration halos, fresh and altered glass, and altered sediment. Data are plotted at individual core level. Depths are CSF-A and plotted at top of cored interval. Black trend lines = locally weighted nonparametric regression (LOWESS), gray shading = 2σ of mean.

string from the casing by rotation. During this process, a weight decrease of 30,000 lb was observed on the hook load indicator, showing that at least part of the casing had come free. The subsea camera was deployed again, and at 1345 h we observed that the cone had fallen away and some of the BHA drill collars appeared to be bent; however, the casing hanger and casing crossover were still attached. The decision was made to retrieve the drill string and deal with any casing at the surface. When the drill string reached surface, the casing hanger and casing were no longer attached and must have fallen away while being raised. The bit cleared the rotary on the rig floor at 0215 h on 5 July. We disassembled the BHA and examined it for damage and set aside the bottom three drill collars, one of which was slightly bent. We then secured the rig floor for transit and raised the thrusters, ending operations in Hole U1558D and at Site U1558. The original operations plan had included running three downhole logging tool strings in Hole U1558D, but this could not be undertaken. Unfortunately, Hole U1558D is no longer a legacy hole for potential future operations. At 0530 h on 5 July, we started the 227 nmi transit to Site U1583.

9.4.3. Principal results

Site U1558 targeted 49.2 Ma upper oceanic crust along the SAT. A near-complete sedimentary sequence was recovered from the combination of Holes U1558A and U1558F (Figure **F28**), and uppermost basement rocks were recovered in both holes as well as Hole U1558D. Hole U1558D advanced 203.7 m into basement and recovered a volcanic sequence of moderately altered plagioclase ± olivine ± clinopyroxene phyric pillow lavas and sheet and massive flows with abundant interlava intervals of indurated calcareous sediment (Figure **F29A**).

9.4.3.1. Sediments

9.4.3.1.1. Sedimentology

A near-complete 159–176 m thick sequence of siliciclastic and biogenic sediments was recovered from two sediment holes cored at Site U1558 (Holes U1558A and U1558F), principally comprising brown Early Miocene nannofossil-rich clay overlying pinkish middle Eocene to Early Miocene nannofossil ooze and chalk with clay and foraminifera (Figure **F28**).

Two lithologic units (I and II) are defined at Site U1558. Lithologic Unit I is composed of up to 10.11 m of Pleistocene to Early Miocene brown and reddish brown nannofossil-rich clay containing varying amounts of foraminifera and sponge spicules and subordinate nannofossil ooze with clay and foraminifera. Lithologic Unit II is composed of up to 165.32 m of middle Eocene to Early Miocene biogenic sediments consisting primarily of pink, pinkish white, pinkish gray, and light brown nannofossil ooze and chalk with varying amounts of clay and foraminifera. Unit II is divided into three subunits based on their composition (clay, $CaCO_3$, and foraminifera content) and color. Differences in constituent mineral assemblages between the units and with increasing burial depth are relatively subtle. There is a discernible increase in $CaCO_3$ content with concomitant decrease in clay content downhole. In lower portions of the sediment section, nannofossil ooze is moderately consolidated and is termed chalk. Overall, clay content decreases downhole.

9.4.3.1.2. Biostratigraphy and age-depth model

Calcareous nannofossil and planktic foraminifera biostratigraphy of sediments recovered at Site U1558 were performed primarily on core catcher samples from Holes U1558A and U1558F, examined both on shore and on board *JOIDES Resolution* during Expedition 393.

The mudline sample from Hole U1558A lacks microfossils, preventing an age determination. The mudline sample from Hole U1558F contains Pleistocene planktic foraminifera, whereas calcareous nannofossil assemblages are a predominantly modern assemblage with some Miocene and Paleogene taxa present, indicating some degree of reworking and mixing.

Biostratigraphic analyses indicate that Miocene sediments occur above 22.27 m CSF-B in Hole U1558A and above 13.50 m CSF-B in Hole U1558F. This corresponds to Lithologic Unit I and the uppermost part of Subunit IIA. Oligocene aged sediments occur between 31.85 and 108.90 m CSF-B in Hole U1558A and between 28.83 and 110.40 m CSF-B in Hole U1558F. Thus, most of Lithologic Subunits IIA and IIB are Oligocene.

The Eocene/Oligocene boundary is inferred to occur within the lowermost part of Lithologic Subunit IIB (108.90 m CSF-B in Hole U1558A and 109.45 m CSF-B in Hole U1558F) close to the Subunit IIB–IIC transition. Eocene sediments are approximately 48.41 m thick in Hole U1558A and 50.4 m thick in Hole U1558F, corresponding to Subunit IIC.

The most accurate determination of the age of the sediment/basement interface comes from core catcher samples from Sections 390C-U1558A-18X-CC and 393-U1558F-24X-CC, both of which contained *Reticulofenestra umbilicus*, suggesting that sediments near the sediment/ basement interface are not older than 42.72 Ma. Planktic foraminifera assemblages in Sample 393-U1558F-24X-CC indicate a minimum basement age of 42.6 Ma. These results combined indicate that the first sediments deposited at this site are almost 6.5 My younger than 49.2 Ma, which is the age estimated for ocean crust at Site U1558 (Kardell et al., 2019).

Calcareous nannofossil and planktic foraminifera bioevents in conjunction with paleomagnetic data allowed for comprehensive hole age-depth models and calculation of LSRs. LSRs range 0.38–1.09 m/ky in Hole U1558A and 0.34–1.8 cm/ky in Hole U1558F. Apart from the condensed sedimentation of Unit I, the lowest sedimentation rates occur in the late Oligocene and Early to Middle Miocene, as well as across the EOT. The highest LSRs occur at the base of the holes, in the middle Eocene, and throughout the Oligocene.

9.4.3.1.3. Sedimentary and pore water geochemistry

Samples from Holes U1558A and U1558F were analyzed for IW and sediment geochemistry and, in the case of Hole U1558A, for headspace gas. IW geochemical data from Hole U1558F is consistently higher for sulfate, Na, Mg, and Cl concentrations and lower for Sr than in Hole U1558A. After applying a mudline correction and adjusting Hole U1558A values to expected mudline values, elemental concentrations in Hole U1558A show excellent agreement with data from Hole U1558F. Variations in pore water Ca, Mg, and Sr concentrations and Sr/Ca ratios observed in both holes are consistent with authigenic carbonate formation and recrystallization of a high-Mg calcite phase during sediment diagenesis. Dissolution of biogenic silica, weathering of detrital silicates, and/or ion exchange between sediment and pore waters may explain the sharp increases in fluid B, Li, Si, and K concentrations relative to the mudline in Unit I (nannofossil-rich clay) in both holes (Figure **F30**). The pH of Hole U1558A IW is consistent with local seawater pH, with lower values recorded in Hole U1558F. Alkalinity was conversely higher in Hole U1558F and reached seawater values in Subunit IIC (nannofossil chalk with clay and volcaniclastics). Calcium carbonate contents in clay-rich Lithologic Unit I are lower compared to the underlying nannofossil oozes, as expected. The SO_4 minima in both holes roughly coincide with a spike in Mn concentrations and are likely controlled by organic matter remineralization.

9.4.3.1.4. Paleomagnetism

Paleomagnetic measurements were undertaken to determine the magnetic polarity stratigraphy and constrain the magnetic mineralogy of sedimentary units at Site U1558. Continuous measurements of the remanent magnetization were conducted on sediment cores from Hole U1558F and the sediment/basement interface in Hole U1558D using the SRM at a resolution of 2 cm. Remanent magnetization before and after progressive AF demagnetization of three steps (5, 10, and 20 mT) were measured during this process. Discrete measurements including AMS and AF demagnetization were conducted on a total of 38 cube samples. IRM acquisition experiments were performed on eight selected samples, which is about two per lithologic unit.

The SRM results from Hole U1558F and the sediment/basement interface in Hole U1558D, along with data obtained from Hole U1558A during Expedition 390C, were used to define the magnetostratigraphy for the entire sediment sequence at Site U1558. Viscous overprints are almost completely removed at 20 mT demagnetization to reveal characteristic components. The distribution of inclination values is bimodal in both Holes U1558A and U1558F with peaks near ±56° in Hole U1558A and +60° and −51° in Hole U1558F. These values are steeper than indications expected at 30°S in the GAD (±49.1°). SRM data record clear polarity reversals for most of the sedimentary sequence in both Holes U1558A and U1558F giving confidence in the correlation to the GPTS. Some intervals near the top of each hole reveal indistinct polarities due to core gaps and drilling disturbances. All collected discrete samples were subjected to AF demagnetization up to 100 mT

step to derive the ChRM. A total of 35 of the measured samples revealed well-defined ChRM with maximum angular deviations between 1.9° and 14.8°. The inclination of ChRM components mostly coincide with those shown in the SRM data, providing robustness to the results. The proposed correlation with the current GPTS (Gradstein et al., 2020) has the Chattian/Rupelian boundary (28.1 Ma; Gradstein et al., 2020) in Subunit IIA (~56 m CSF-B in Hole U1558F) and the Oligocene/Eocene boundary at ~110 m CSF-B, near the base of Subunit IIB.

Rock magnetic experiments were conducted on eight samples and reveal the dominance of low-coercivity minerals throughout the cores with no significant variations among different lithologic unit/subunits. AMS measurements mainly reveal a subhorizontal magnetic foliation with neutral to oblate ellipsoidal shapes typical of sedimentary fabric.

9.4.3.1.5. Physical properties

Characterization of the sediment physical properties at Site U1558 was primarily based on cores from Hole U1558F supplemented by measurements from Hole U1558A. Whole-round, section half, and discrete measurements were considered together to characterize the petrophysical signatures for the different lithologic units. All archive halves were imaged using the X-ray image logger. A correlation framework and splice were developed for Site U1558 that consider NGR, GRA, magnetic susceptibility, and magnetic inclination from each hole. The correlation resulted in an almost continuous spliced record to 207 m CCSF, although a cumulative total of ~12 m of core gap still persists in the splice section. Stratigraphic correlation also highlighted ~2 m of lateral thickness variation between Holes U1558A and U1558F, with Hole U1558F having an expanded record relative to Hole U1558A.

Whole-round NGR measurements range 2–50 counts/s through the sedimentary section in Hole U1558F. NGR is highest in the upper 10 m of the section, corresponding to the nannofossil-rich clay and ooze of Lithologic Unit I (mean NGR from Unit I in Hole U1558F is 24 ± 7 [±1σ] counts/s). An additional sharp peak in NGR (between 20 and 29 counts/s) occurs at the Subunit IIB/IIC boundary in Holes U1558A and U1558F. In contrast, intervals dominated by carbonate

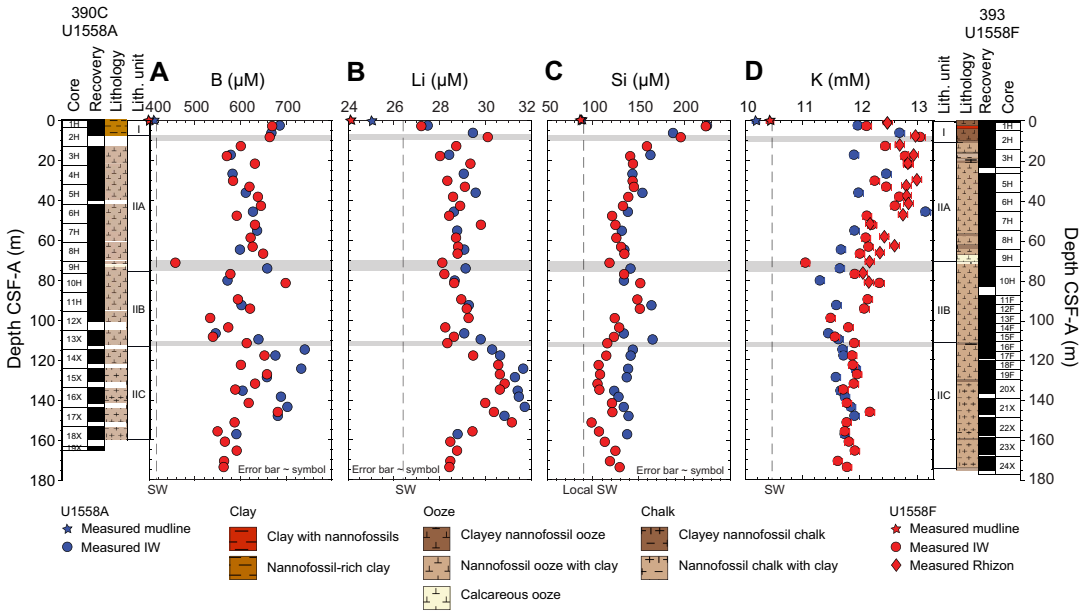

Figure F30. (A) Boron, (B) lithium, (C) silicon, and (D) potassium, Holes U1558A and U1558F. Significant increases in B, Li, Si, and K observed relative to mudline in Unit I (nannofossil-rich clay) in both holes likely result from dissolution of biogenic silica, weathering of detrital silicates, and/or ion exchange between sediment and pore waters. Second increase in B and Li coincides with higher clay contents and lower $CaCO_3$ (weight percent) at Subunit IIB (nannofossil chalk with clay)/IIC (nannofossil chalk with clay and volcaniclastics) boundary. Although Si concentrations show overall decrease with depth in both holes, K values virtually do not change in Subunit IIC. Smectite-to-illite transformation and alteration of underlying oceanic crust may also affect concentration profiles of these elements. Seawater (SW) reference values for B, Li, and K correspond to International Association for the Physical Sciences of the Oceans (IAPSO) standard composition; local Si concentration is sourced from Sarmiento et al. (2007).

ooze generally have low NGR (<15 counts/s). Pass-through magnetic susceptibility follows a similar downhole trend to NGR with an overall range of 0–145 IU (mean = 32 ± 16 IU) in Hole U1558F. The highest values are associated with the clayey nannofossil-rich ooze of Unit I (18–118 IU; average = 70 ± 22 IU). Magnetic susceptibility is relatively low through Unit II, with peaks at ~65 m CSF-A (Subunit IIA), ~112 m CSF-A (Subunit IIB/IIC boundary), and from ~154 to 160 m CSF-A (Subunit IIC). The average GRA bulk density of whole-round cores is lowest in Unit I (mean = 1.6 ± 0.1 g/cm^3) compared to the other three subunits (mean = 1.8 ± 0.1 g/cm^3), and a similar trend is seen in bulk density from discrete samples. Porosity of discrete samples decreases with depth from ~70% at the seafloor to ~50% close to the sediment/basement interface (173 m CSF-A). *P*-wave velocity measured on whole-round cores ranges 1.45–1.74 km/s (mean = 1.56 ± 0.03 km/s) and generally increases with depth. Compressional strength of the sediments increases with depth, whereas shear strength reaches maximum values (~52 kN/m^2) at 30 m CSF-A before decreasing downhole. Thermal conductivity values range 1–1.61 W/(m·K) throughout Hole U1558F (mean = 1.34 ± 0.14 W/[m·K]) and gradually increase downhole. The vertical conductive heat flow for Site U1558 was estimated to be 28–30 mW/m^2, which is lower than modeled heat flow values for ocean crust of this age, requiring significant regional hydrothermal advection of heat to make up the difference (cf. Kardell et al., 2022).

9.4.3.1.6. Microbiology

Microbiological analysis of samples from Hole U1558F will focus on microscopy, culture-based approaches, and culture-independent approaches to characterize microbial activity in the sediments. One microbiology whole-round sample (5–10 cm long) was collected from each 9.5 m core and subdivided for shipboard and shore-based studies. Additional whole-round cores for specialized shore-based analyses were also taken. A number of microbiology analyses on sediment samples from Hole U1558F were initiated shipboard during Expedition 393. To study the extent of viral activity and dynamics between viruses and other microbial life (Bacteria and Archaea), virus-induced microbial mortality and prophage induction experiments were performed on samples taken from six microbiology whole-round cores throughout the sediment column. To study the microbial activity at the sediment/basement interface, ammonium enrichment incubation experiments were started with the deepest sediment cores at Site U1558 along with the uppermost basement samples.

9.4.3.2. Volcanic rocks

9.4.3.2.1. Igneous petrology

Hole U1558D drilled ~203 m of MOR basalts and intersected two distinct volcanic sequences separated by a ~1 m thick layer of indurated calcareous sedimentary breccia with volcanic debris possibly indicating a hiatus in volcanism at this site on the order of tens of thousands of years (Figure **F29A**). The upper Sequence A (166.55–234.64 mbsf) includes volcanic Units 1 and 2, which are moderately to highly plagioclase-olivine-clinopyroxene phyric microcrystalline basaltic lavas mostly emplaced as lava pillows of varying comfort (10–130 cm diameter). Extremely sparse but distinctive green clinopyroxene phenocrysts are a characteristic feature of the Sequence A volcanic rocks. In contrast, the underlying Sequence B (234.65–370.20 mbsf) lacks these green phenocrysts, and its uppermost unit contains abundant interflow sediments and breccias, suggestive of a buried seafloor horizon. This change in phenocryst assemblage indicates that some aspect of the magmatic system changed between eruptive sequences. However, lava geochemistry as assessed by Cr/Ti ratios measured directly on the cores by pXRF is relatively consistent downhole with little evidence for fractionated series apart from Unit 4, which has higher Cr concentrations than the other lava units.

9.4.3.2.2. Alteration petrology

The alteration in Hole U1558D can be divided into four zones. From the top of the volcanic sequence to 179 mbsf in Unit 1, there is a dominance of brown halo alteration associated with pillow lava chilled margins. Between 179 and 234 mbsf (part way through Subunit 1E to the base of Subunit 2B), the second zone is distinguished by a decrease in the abundance of all halo types and gray background alteration and orange speckled background alteration of the pillow lavas dominate (Figure **F29B**). This shift from brown halo dominated to background alteration dominated is interpreted to represent a seafloor weathering overprint and suggests that the pillow lavas

were exposed to open circulation of seawater for some period of time before becoming covered with sediment. The third zone (234–286 mbsf) is broadly associated with Igneous Units 3 and 4 and is marked by the first appearance of orange-reddish yellow alteration within pillow lavas. This color likely represents the strongest alteration in Hole U1558D and is generally associated with alteration fronts developing from the glassy margins of individual pillows (Figure **F29B**). Macroscopically, these orange-reddish yellow alteration fronts transition into the more ubiquitous brown halos seen throughout Hole U1558D. Some of the freshest volcanic glass is preserved where the groundmass alteration of the pillow lavas is strongest. The abundance of breccia and sediment at the top of this interval suggests that these rocks were also exposed to seawater for a significant duration before becoming covered by the overlying lava sequences. The fourth alteration zone is defined by the onset of mixed gray-brown background alteration that has a common but not unique association with variolitic textures. The orange-reddish yellow halos persist through this change in background alteration. Although there are some associations between the igneous units and the different alteration zones, the onset of the key alteration features defining the zones do not generally follow igneous unit boundaries.

9.4.3.2.3. Igneous geochemistry

Representative samples were taken from the freshest portions of each volcanic subunit in Hole U1558D to obtain a downhole record of the primary magmatic conditions, along with one sample near the basalt/sediment contact. Additionally, four samples of breccia were taken to understand the basalt-sediment chemical exchanges that occurred as new lavas erupted and interacted with pelagic sediment. A total of 29 samples were measured for LOI and bulk rock geochemical analysis via ICP-AES. The unoxidized powders of these samples were also characterized for elemental abundances via pXRF to complement the direct core measurements. The Hole U1558D basalts are weakly to strongly altered, with variable MgO and CaO concentrations and elevated abundances of K_2O and Rb. Basaltic protolith compositions change downhole, with TiO_2 contents varying between 1 and 1.2 wt% from 160 to 290 mbsf and increasing to 1.3–1.5 wt% at >290 mbsf. In terms of basaltic rock type, the freshest samples classify as olivine tholeiites per the Yoder and Tilley (1962) normative classification scheme as also displayed in the Zr/Y versus Zr tectonic discrimination plot (Figure **F31**; Pearce and Norry, 1979). K/Zr ratios, a broad measure of alteration extent, vary between 20 and 109 in Site U1558 basalts, averaging 44.5, which is much higher than fresh South Atlantic MORB (average = 7.4). Incompatible element concentrations are consistent with a similar depleted MORB (D-MORB) composition for lavas at Site U1558. The breccia fill materials, which are partly of sedimentary origin, vary widely in composition from very Ca rich to Ca poor, with the most Ca poor samples showing the highest K_2O abundances.

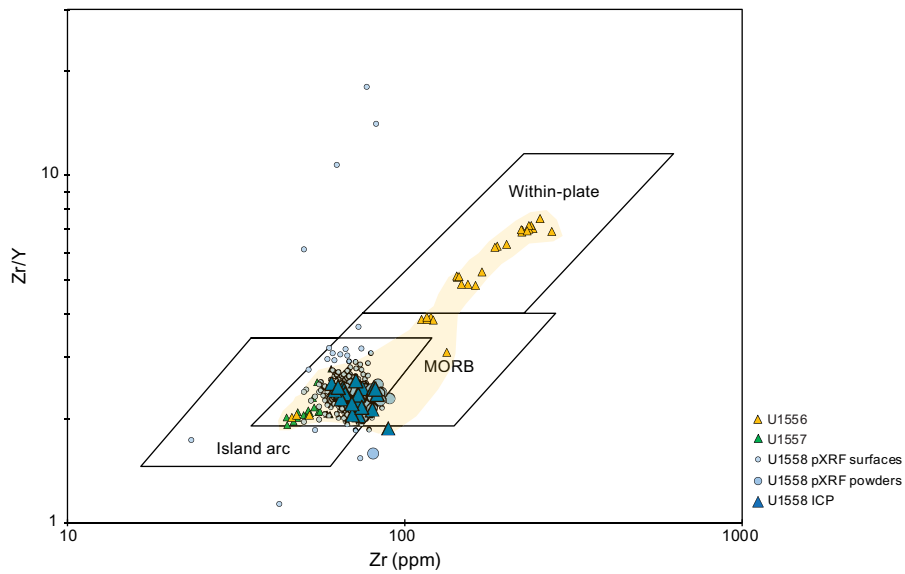

Figure F31. Zr/Y vs. Zr tectonic discrimination diagram from Pearce and Norry (1979) showing combined pXRF and ICP-AES data for Site U1558 basalts compared to data from Sites U1556, U1557, and U1559.

9.4.3.2.4. Paleomagnetism of volcanic rocks

Paleomagnetic measurements were conducted on basement cores from Hole U1558D using the SRM at a resolution of 2 cm. Remanent magnetization before and after progressive AF demagnetization at 5, 10, and 20 mT fields were measured on pieces that are longer than 9 cm. Because the recovery rate varied greatly throughout the hole (11%–90%), there are clear differences in data resolution between cores. Rock magnetic experiments were performed on a total of 36 cube samples, targeting basalts of various degrees of alteration and one sample from the sedimentary breccia.

The SRM results mostly remove all viscous overprints and successfully reveal primary components at the 20 mT demagnetization step. These components mainly show a negative inclination, which indicates a normal polarity, in agreement with the expected polarity for 49.2 Ma (Gradstein et al., 2020; Kardell et al., 2019) ocean crust, although positive inclinations were found in some layers in the lower parts of the hole. The distribution of inclination values is heavily clustered around −55°, which is about 6° steeper than the angle expected in the GAD (±49.1° at 30°S).

A subset of 32 discrete samples were subjected to stepwise AF demagnetization up to 130 mT to derive the ChRM. The remaining six samples were stepwise thermally demagnetized up to 580°C. Discrete sample measurements mostly reveal well-defined ChRM with maximum angular deviation between 0.4° and 5.4°. IRM acquisition experiments were conducted on 24 selected samples, which reveal saturation levels around 150–300 mT, implying that low-coercivity minerals such as titanomagnetite and/or maghemite are the main magnetic carriers (Figure **F32**). Slight variations in remanence intensity and magnetic susceptibility occurred depending on the alteration degree. AMS measurements reveal a well-defined prolate fabric characterized by subhorizontal magnetic foliation.

9.4.3.2.5. Physical properties

Characterization of the basement physical properties at Site U1558 is primarily based on cores from Hole U1558D supplemented by information from Holes U1558A and U1558F where the uppermost basement was also recovered. Whole-round, section half, and discrete measurements were considered together to characterize the petrophysical signatures for the different lithologic units. All whole-round cores were imaged using an X-ray image logger. About 72% of the recovered material was scanned using the DMT core scanner.

NGR in Hole U1558D ranges 0.1–11.6 counts/s with a mean of 4.0 counts/s. The highest NGR in this section is associated with an indurated calcareous sedimentary breccia (Volcanic Unit 3), although basalts in Subunits 4A and 4B also show elevated NGR. Discrete point magnetic susceptibility measurements from section halves range 1–669 IU (mean = 159 ± 88 IU [± 1σ]). Units 1 and 2 have a higher mean magnetic susceptibility than Units 4 and 5, with the lowest magnetic susceptibility observed in volcaniclastic sedimentary breccia Unit 3. A pronounced peak in magnetic susceptibility is seen in Subunit 5D (massive flow).

To integrate petrophysical measurements with the observations of other groups, all discrete MAD samples were also used for paleomagnetic measurements, and with the help of petrologists all samples were classified according to key attributes such as grain size, alteration, or emplacement style. Discrete MAD measurements (bulk and grain densities and porosity) as well as *P*-wave velocity are affected by the alteration level in the 40 samples that were measured. Samples displaying higher levels of alteration such as those with strongly developed brown alteration halos, mixed gray-brown variolitic textures, or orange-reddish yellow colors, generally have lower bulk and grain density, lower *P*-wave velocity, and higher porosity compared to less altered samples. There is no clear relationship between these physical properties and the igneous units. However, basalts emplaced as large pillow flows appear to have higher density and *P*-wave velocity and lower porosity compared to mixed sheet and pillow flows, with smaller pillow flows occupying an intermediate range of values. The average thermal conductivity measured in basement samples is 1.54 ± 0.14 W/(m·K) (n = 39 measurements). Combined with an estimated vertical conductive heat flow in sediments of 28–30 mW/m^2, this suggests a temperature gradient of about 20°C/km in the shallow basement at Site U1558 if the thermal regime is mostly conductive.

9.4.3.2.6. Microbiology

Microbiology sampling in volcanic rocks occurred in Hole U1558D and was focused on exploring evidence for life in the basement, especially at the sediment/basement interface, using microscopy, culture-based approaches, and culture-independent approaches. A total of 21 whole-round samples between 12 and 23 cm long were sampled to characterize the variety of volcanic formations in Hole U1558D. After the contaminated exteriors of whole-round pieces were removed, the remaining material was split into subsamples that were prepared for different microbiology analyses. Experiments were started shipboard to study microbial activity at the sediment/basement interface using ammonium enrichment incubations. These incubations focused on the uppermost basement samples to correspond with the deep sediment column samples described above.

To determine the extent of contamination of microbiology samples, the PFT PFMD was injected into the drilling fluids during coring in Hole U1558F. Microbiologists then collected samples from both the exterior and interior of core intervals selected for microbiology analysis, as well as core catcher rubble, to quantify the presence of PFMD. PFMD was detected from a majority of the exte-

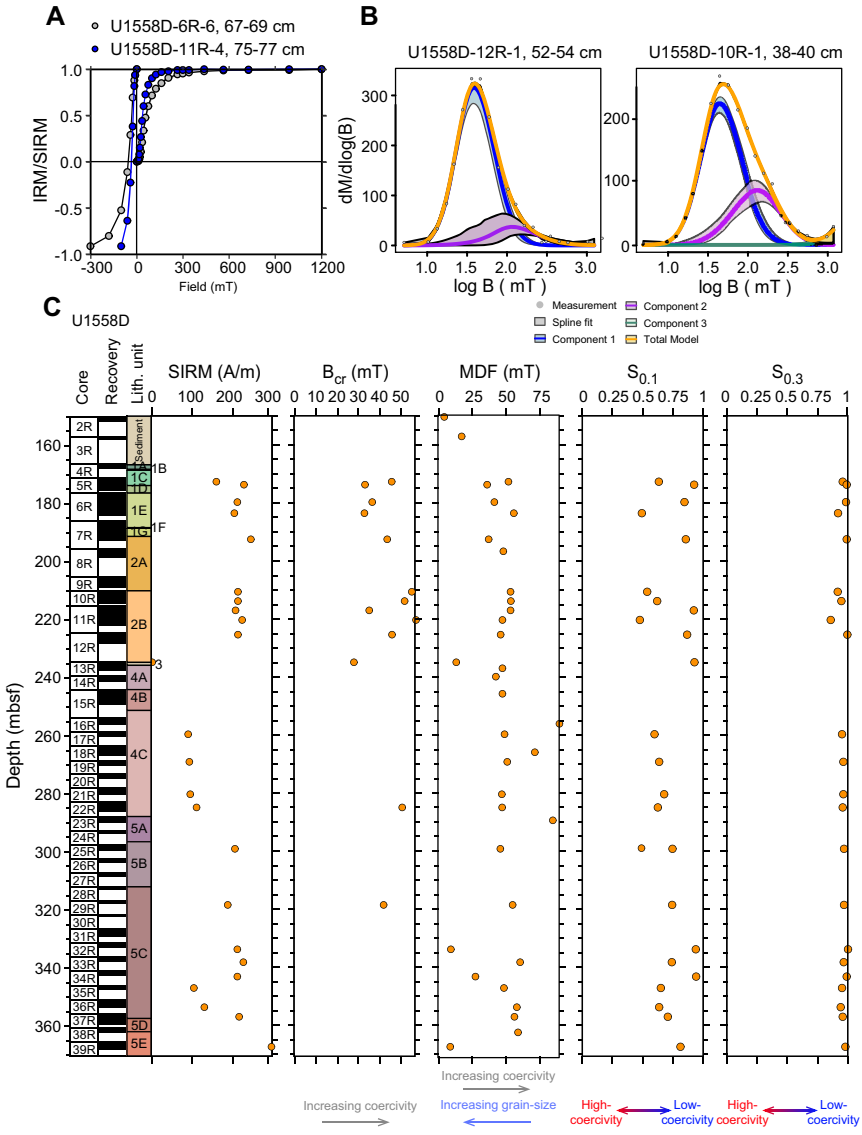

Figure F32. A. Curves of saturation IRM (SIRM) acquisition up to 1200 mT and backfield IRM truncated at −300 mT for two representative samples of basement rock, Hole U1558D (6R-6, 67–69 cm, and 11R-4, 75–77 cm). B. Coercivity distribution and unmixing of IRM acquisition curves (12R-1, 52–54 cm, and 10R-1, 38–40 cm) (Maxbauer et al., 2016). C. IRM acquisition. B_{cr} = coercivity of remanence, MDF = median destructive fields, $S_{0.1}$ = IRM_{100}/SIRM ratios, $S_{0.3}$ = S-ratios.

rior samples, with an average concentration of 18 ppb/g and a median concentration of 10 ppb/g of rock when detected. The tracer was not detected in the interior microbiology samples, suggesting no to minimal drilling contamination of the samples.

10. Preliminary scientific assessment

The primary operational objective of the SAT expeditions was to drill a transect of sites along a crustal flow line at ~31°S across the western flank of the southern Mid-Atlantic Ridge, core the uppermost (~250 m) ocean crust produced between ~7 and 61 Ma at the slow/intermediate-spreading Mid-Atlantic Ridge, and recover complete sections of the overlying sediments. The SAT was designed to target six primary sites on 7, 15, 31, 49, and 61 Ma ocean crust that fill critical gaps in our sampling of intact in situ ocean crust with regards to crustal age, spreading rate, and sediment thickness. After more than three decades focusing on the hydrothermal alteration and basement hydrogeology of well-sedimented intact crust formed by intermediate- to fast-spreading ridges in the Pacific Ocean (e.g., eastern equatorial Pacific Sites 504, 896, and 1256 and Juan de Fuca Ridge flank ODP Sites 1023–1032 and Integrated Ocean Drilling Program Sites U1301, U1362, and U1363), the SAT marks an overdue pivot back to the Atlantic Ocean, and crust formed at slow spreading rates and ridge flanks with abundant basement outcrops out to beyond 60 My (e.g., DSDP Legs 51–53). Drilling at the SAT sites is required to investigate the hydrothermal evolution of the aging ocean crust, the nature and variation of sediment- and basement-hosted microbial communities with increasing substrate age, the paleoceanographic evolution of the South Atlantic Ocean, and the deep-ocean and subtropical gyre responses to changing global climate.

Expedition 393 was the second of two scientific SAT expeditions, following Expedition 390 (Coggon et al., 2022a), that built on the successful engineering operations of Expeditions 390C and 395E (Estes et al., 2021; Williams et al., 2021), which conducted preliminary sediment coring and installed reentry systems cased to basement at five of the six primary SAT sites. The initial operational goals of Expedition 393 were to complete drilling operations across the middle-aged spread of SAT sites on 15 and 49 Ma ocean crust (Sites U1560 and U1558) and establish a new, not previously occupied site (U1583) on 31 Ma ocean crust. Because of the failure of the forward drawworks electromagnetic brake toward the end of Expedition 390, additional basement drilling, coring, and wireline logging operations at Site U1559 were loaded into the Expedition 393 schedule.

10.1. Operational achievements of Expedition 393

Expedition 393 undertook sediment and basement coring and when possible logging operations at four sites to establish a crustal age transect across the western flank of the southern Mid-Atlantic Ridge. Drilling occurred in 12 holes at sites from 6.6 to 49.2 Ma crust (Tables **T2**, **T3**; Figure **F12**). Legacy cased reentry cones remain at Sites U1559 (6.6 Ma) and U1560 (15.2 Ma) to complement Hole U1557D (61.2 Ma) deepened during Expedition 390. A free-fall funnel honoring Dick Kroon (1957–2022) sits on top of the basement drilled in Hole U1583F at the new site on 31 Ma crust, but poor hole conditions suggest further deepening would be challenging. Volcanic rocks of the uppermost ocean crust were cored to 43 (Hole U1559B), 192 (Hole U1560B), 130 (Hole U1583F), and 220 (Hole U1558B) msb in 6.6, 15.2, 30.6, and 49.2 Ma crust, respectively. More than 1150 m of sediment and basement were cored, recovering >775 m of core with an average recovery rate of >67%. Of this coring, 600 m was into hard rocks, recovering 234 m (39%) of core, and more than 550 m of sediment was cored with more than 540 m recovered (>98%). Two holes (U1583F and U1560B) were wireline logged with multiple tool strings (Tables **T2**, **T3**; Figure **F12**).

Microbiological samples were collected from both sediment and basement in all Expedition 393 holes and preserved for postexpedition analyses. Abundant altered glass, hydrothermal veins, complex breccias, and a wide variety of alteration halos in the volcanic sequences of the uppermost SAT ocean crust suggest myriad environments for microbial activity. Sediment pore water chemical profiles of oxygen, manganese, and sulfate concentrations indicate extended redox gradients from both the seafloor and the sediment/basement interface that may support a diversity of microorganisms and metabolisms.

Expedition 393 operations completed the first operational phase of the SAT and leaves open opportunities for future drilling, logging, and geophysical site characterization operations of the legacy and other sites. Detailed postexpedition integration of results across crustal ages and laterally across the ocean basin will establish a benchmark for understanding the aging of the ocean crust and its interactions with life and the oceans above. Below, we document progress made during Expedition 393 toward the primary objectives.

10.2. Objective 1. Quantify the timing, duration, and extent of ridge flank hydrothermal fluid-rock exchange.

Expedition 393 succeeded in drilling basement at a range of ages across the western flank of the southern Mid-Atlantic Ridge (Figure **F33**). The progressive influence of the Tristan da Cunha plume on mantle melting at the Mid-Atlantic Ridge over the past ~50 My at this latitude is preserved by the least altered volcanic rocks recovered during Expedition 393 (Figures **F33**, **F34**). Although detailed mantle source apportioning will require postexpedition radiogenic isotopic analyses and better characterization of magma fractionation, the progressive changes across the western flank of the southern Mid-Atlantic Ridge are already apparent from excellent shipboard ICP-AES data and more than a thousand tightly calibrated pXRF measurements directly measured on the split core surfaces (Figures **F33**, **F34**). Abundant vitreous volcanic glass at all sites and from all volcanic units will provide further opportunities for mantle source definition and description of magmatic processes. Comprehensive postexpedition glass and fresh rock analyses will provide a firm baseline for quantifying the extent of chemical and isotopic hydrothermal exchange through comparison with different styles of more strongly altered materials.

In comparison to the ~61 Ma volcanic rocks recovered during Expedition 390, most volcanic rocks recovered from Sites U1559, U1558, U1560, and U1583 during Expedition 393 are less

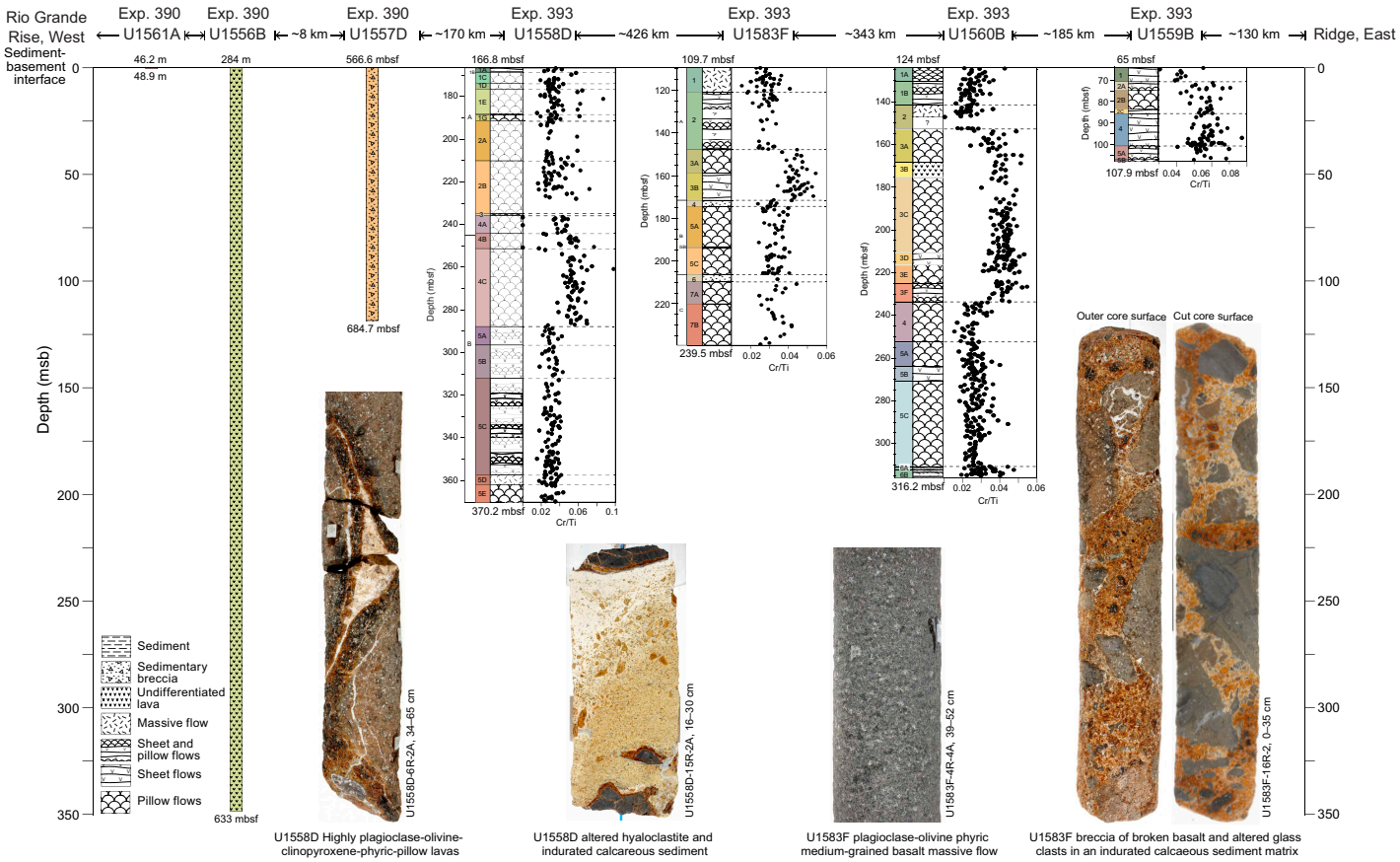

Figure F33. Summary of basement drilling during Expedition 393 across SAT showing examples of basalts, interflow sediments, and breccias. Cr/Ti data were measured directly on split core surfaces by pXRF.

altered. However, clear differences are apparent from the alteration at the ocean crustal reference site Hole 504B (Alt et al., 1986, 1996). High abundance of iron-stained brown to orange halos and mineralogical and geochemical evidence for alteration, such as the formation of relatively refractory clay minerals are present. These result from seafloor weathering due to extended exposure to ocean bottom water for millions to perhaps tens of millions of years.

Our quantitative logging of the variations in the style and extent of alteration of the volcanic rocks recovered at Sites U1558, U1559, U1560, and U1583 (e.g., Figure **F29**) in conjunction with analyses of cores recovered at older crustal ages along the SAT during Expedition 390 will allow us to evaluate hydrothermal contributions to global biogeochemical cycles. Postexpedition analyses will include radiometric dating of different hydrothermal minerals (e.g., clay and carbonate minerals) to determine the timing and hence duration of hydrothermal exchange. High spatial resolution elemental and isotopic mapping will illuminate hydrothermal alteration processes and together with X-ray diffraction and electron beam analyses will allow us to write rigors reactions and mass balances to quantify the evolving seawater-basalt hydrothermal exchanges. These rocks will provide essential well-characterized samples to better constrain the biogeochemical budgets of a whole suite of traditional (such as O, D, C, S, and ^{87}Sr) and boutique (including Li, B, Mg, K, Ca, and Tl) isotopic tracers. Additionally, they will provide insights into low-temperature hydrothermal exchange and the influence of these processes on global biogeochemical processes and the composition of seawater over the Cenozoic. Our quantitative descriptions and mineralogical studies will provide a reference framework for the changing physical properties of the ocean crust in terms of density, seismic velocity, and thermal conductivity.

Expedition 393 benefited from the addition of two nonstandard imaging systems. The DMT CoreScan3 system, loaned by the International Continental Scientific Drilling Program (ICDP), with transfers supported by Natural Environment Research Council (United Kingdom) IODP (to Teagle/Coggon), was used to capture high-resolution images of basement core exteriors prior to cutting. The images collected preserve key information about the orientations of contacts and structures in the core that are lost because of fracturing during core splitting. These presplitting images will be integrated with wireline borehole images to establish a more complete stratigraphy through intervals of low recovery. These data also allow development of novel computer visualization approaches for automated objective quantitative core logging. Samples destroyed as part of the basement microbiological sampling were imaged using the Foldio turntable system prior to breaking them open with a hammer. This system generates a series of 36 images that capture all sides of the core sample and will allow both the microbiologists and other scientists to gain insight into the composition and structure of removed core.

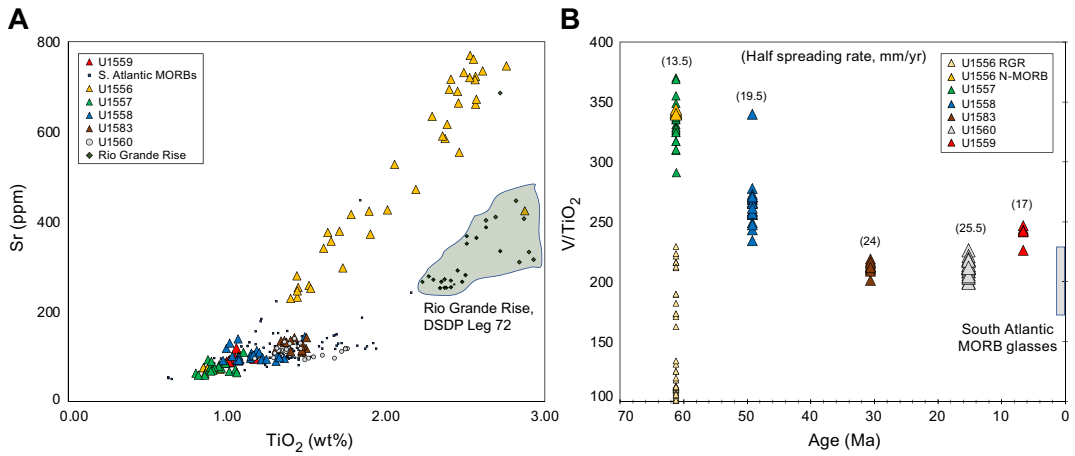

Figure F34. Geochemistry of igneous rocks from across SAT. A. Shipboard analyses of Sr vs. TiO_2 concentrations for basalts showing clustering Expedition 393 analyses (Sites U1558–U1560 and U1583) atop of analysis of fresh glasses from modern South Atlantic Ridge MORB in contrast to analyses from Hole U1556B and Rio Grande Rise. B. Basalt V/TiO_2 ratios vs. age. Geochemistry of lavas with MORB affinities show progressive, albeit irregular, progression from compositions with strong influence from Tristan da Cunha plume to V/TiO_2 values similar to lavas on modern southern Mid-Atlantic Ridge.

10.3. Objective 2. Investigate sediment- and basement-hosted microbial community variation with substrate composition and age.

Samples were collected for postexpedition analysis of cell counts, microbial community composition and function using molecular approaches, and lipid-based microbial composition from throughout the sediment columns in Holes U1558F, U1560C, and U1583C, as well as from basement cores from Holes U1558D, U1559B, U1560B, and U1583F. In addition, microbial enrichment incubation experiments targeting ammonium oxidizers and viral production and prophage induction experiments were begun on the ship and will be analyzed during shore-based research. Altogether, the work initiated during Expedition 393 will allow postexpedition work to analyze changes in microbial community abundance, composition, function, and activity from the seafloor to the deepest basement sampled.

Knowledge of the microbial communities active in both sediment and basalt environments were supplemented by geochemical measurements of sediment pore water and other parameters such as heat flow at all sites. These measurements reveal information on diagenetic reactions, elemental diffusion, and the flow of fluids along the sediment/basement interface at some sites (e.g., Site U1560).

10.4. Objective 3. Investigate the responses of Atlantic Ocean circulation patterns and the Earth's climate system to rapid climate change, including elevated atmospheric CO_2 during the Cenozoic.

The recovery of nannofossil oozes with varying amounts of clay at Sites U1558, U1560, and U1583 indicate shoaling and deepening of CCD at these sites from the Oligocene through the Holocene (Figure F35). Planktic foraminifera and calcareous nannoplankton are poorly preserved in clay-rich intervals, but the abundant well-preserved microfossils in carbonate intervals supported the construction of robust age models in combination with magnetostratigraphic reversals for all

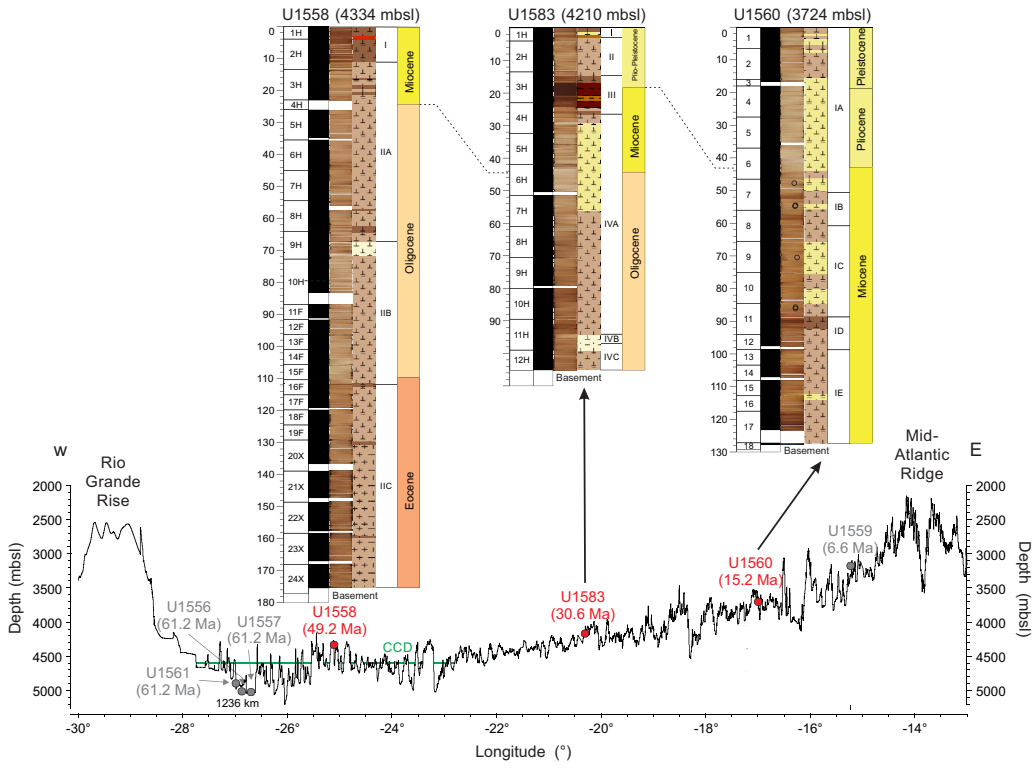

Figure F35. Bathymetric cross section of western flank of southern Mid-Atlantic Ridge at 31°S showing location of sediment coring during Expedition 393 (red) that complete SAT operations initiated during Expeditions 390C, 395E, and 390 (gray). Green line = modern-day CCD.

Expedition 393 sedimentary sites (U1558, U1560, and U1583; Figure **F35**). Carbonate dissolution is indicated by high pore water Ca/Mg relative to seawater in the deepwater Holes U1558A, U1558F, U1560A, U1560C, U1583C, and U1583E.

Together with Expedition 390, we recovered almost the entire Cenozoic across the SAT. Expedition 393 had excellent recovery of the Oligocene, Miocene, and Pliocene. Based on biostratigraphic and paleomagnetic events, we interpreted a ~6 My hiatus at Site U1583 and two hiatuses at Site U1558 (~18 My at the top and ~7 My before the accumulation of the lowermost sediments), suggesting changes in bottom water masses resulting in dissolution, low sedimentation rates, and potentially erosion. Despite these hiatuses, the sedimentologic records can be correlated well with sediments of Paleocene and Eocene age recovered during Expedition 390. High-resolution biostratigraphic and isotope studies postexpedition will help to refine age models and calculations for mass accumulation rates, carbonate accumulation rates, and organic carbon accumulation rates that will allow us to answer questions surrounding ocean productivity and circulation through the Cenozoic.

10.5. Operational considerations

The SAT objectives were ambitious but mostly achieved because of the preliminary engineering operations undertaken during Expeditions 390C and 395E, new developments in drilling capabilities, and the ingenuity of the *JOIDES Resolution* crew, Texas A&M University (USA) team, and Expedition 390/393 science parties. The majority of Expedition 393 operations were successful. More than 600 m of sediments and ~570 m of volcanic rocks were drilled at Sites U1559, U1558, U1583, and U1560 during Expedition 393. Although basement coring at the 7 Ma Site U1559 was challenging and this hole was deepened only ~49 m into basalts, penetrations >130 m were achieved at Sites U1558, U1583, and U1560 and these cores address critical gaps in our sampling of intact in situ ocean crust with regards to crustal age, spreading rate, and sediment thickness.

10.5.1. Casing requirements for basement legacy holes

Reentry cones with casing installed at five of the six primary SAT sites in advance of Expeditions 390 and 393 greatly expedited basement drilling. Most of the basement drilling during Expedition 393 was in holes with reentry cones and casing strings to near the sediment/basement interface. Only the newly occupied Site U1583 did not have legacy infrastructure preinstalled. Unforeseen operational challenges in Hole U1583E resulting in significant time loss precluded the installation of a reentry cone and casing system in the basement of Hole U1583F. Instead, only a free-fall funnel was deployed (the Dick Kroon Cone) to allow the RCB bit to be dropped on the seafloor and the hole reentered for wireline logging. The absence of casing in Hole U1583F caused difficulties drilling with abundant fill accumulating at the bottom of the hole between each wireline core run because of the washing out of both sediment and basement cavities and the incomplete removal of these clastic materials from the hole even with large and regular mud sweeps. Ledges at the bottom of large cavities, particularly at the sediment/basement interface and within the basement, can impede the downward motion of logging tools, although this was only a problem within basement in Hole U1583F.

These experiences emphasize the need for reentry systems with casing installed into basement for legacy holes. However, it should be noted that to install casing into basement the hole either needs to be fully drilled out beforehand or a hydraulic release tool reentry system must be used, which does not allow extension of casing after the initial installation. The preliminary engineering expeditions discovered that the Dril-Quip reentry systems cannot be installed into basement in a single step; when the casing is in basement, weight cannot be removed from the drill string to allow the Dril-Quip release mechanism to operate. This finding from the SAT expeditions will aid planning of future expeditions that are considering such installations.

With the enviable clarity of 20:20 hindsight and knowledge that this phase of the SAT campaign would eventually involve two engineering plus two science expeditions, had the SAT team known that it would have such a generous investment of operational time, SAT operations could have been better optimized. More time could have been dedicated to installing reentry systems cemented into basement, rather than just above basement. Such basement anchored reentry sys-

tems would have improved hole conditions and cleaning, drilling, and wireline logging operations and provided superior legacy sites for future deepening.

10.5.2. TransCo C-4 and C-7 drill bits

Expedition 390 showed that TransCo C-4 RCB drill bits are more durable than drill bits from previous suppliers, and a single C-4 RCB drill bit operated with minimal damage for 65.4 rotational hours to deepen Hole U1558D more than 220 m into basement with reasonable recovery (~46%). Such durability saved a pipe trip and bit change, freeing up time for other operations. However, the C-4 RCB drill bit did not perform well when drilling Hole U1559D into relatively young 6.6 Ma ocean crust on the eastern end of the transect. Basement drilling operations at Site U1559 were slow (< 0.5 m/h) with recovery decreasing to 9% and returning undergauge core that showed elephant-foot flares on the bottom of some cored pieces. On its return to the ship, the C-4 RCB bit was catastrophically damaged in ways also endured during recent operations drilling young basalts during Expedition 395C in Holes U1562B and U1554F. For future drilling operations in young, less altered ocean crust, a C-7 RCB drill bit should be more suitable than C-4 drill bits in these challenging formations. Any return to deepen Hole U1559B should start with a short duration C-7 RCB bit run. Sites such as Site U1559 with only thin sediment cover (≪100 m) would benefit from shorter, denser drilling collars and bottom-hole assemblage to provide more substantial weight on bit to facilitate making hole. The TransCo C-7 drill bits used in Holes U1560B and U1583F achieved between 1.8 and 2.8 m of ocean crust penetration per hour on the drill bit, which is just less than the 3.0 m/h achieved in the deep Hole U1556B during Expedition 390. These TransCo C-7 bits also showed admirable durability (Hole U1583F = ~73 h) that resulted in fewer bit changes and increased science operations.

10.5.3. APC/XCB PDC bit and XCB PDC cutting shoe

As observed during previous SAT expeditions, the XCB PDC cutting shoe provided good recovery of the sediments and basalts during Expedition 393 although a continuous well-preserved sediment/basalt boundary was not achieved at any site on Expedition 393. In addition, an APC/XCB PDC bit allowed us to adapt the operations plan for Site U1560 in response to weather conditions without losing time. Wireline logging was performed in Hole U1560B through the APC/XCB PDC bit, followed by APC/XCB coring of sediments and the critical sediment/basement interface in Hole U1560C without an extra pipe trip.

11. Outreach

Expedition 393 had one Onboard Outreach Officer: Tessa Peixoto, an adult education science instructor for the nonprofit organization JVS Boston in Boston, Massachusetts (USA). The officer shared the science of the expedition with audiences through ship-to-shore broadcasts, posting on the *JOIDES Resolution* social media channels, authoring entries for the expedition blog, and generating additional education and outreach materials. Because of occasional backlogs in the core flow, the Onboard Outreach Officer also assisted in the core laboratory when available. Tasks included entering structural vein measurements into the database, collecting Rhizon samples, and running hard rock cores through the Section Half Multisensor Logger (SHMSL).

Additional outreach activities were performed by the Onshore Outreach Officer, Marlo Garnsworthy, who sailed as one of the two Onboard Outreach Officers for Expedition 390 and remained involved in the SAT program through remote work. The Onshore Outreach Officer continued producing short videos about the missions of Expeditions 390 and 393 and the transition between them. These included six short social media–friendly videos about Expedition 393's goals, motivations, and processes using footage captured by the Onboard Outreach Officer and shared on the *JOIDES Resolution* social media platforms, expedition blog, and YouTube channel.

11.1. Live broadcasts

With a direct satellite link, an iPad, and Zoom videoconferencing software, the Onboard Outreach Officer connected with schools (K–12 and adult education), summer programs, professional development for teachers, elderly homes, Meetup groups, museums, and groups of interested

adults. The broadcasts connected with audiences in 15 countries and were presented in 3 different languages to share the scientific mission of Expedition 393. These broadcasts generally included a brief introduction to the expedition, a tour of the ship and scientific facilities, conversations with scientists in the core laboratory and/or geochemistry laboratory, and a question-and-answer period. Participating countries were Brazil, Japan, Ghana, South Africa, India, Portugal, Mexico, France, Basque, Canada, Norway, New Zealand, Trinidad, the United Kingdom, and the United States (at least nine different states). The school groups ranged from 5 y old kindergarten classes through graduate school and up to adult education. Group sizes ranged 1–187 individuals. Examples of broadcasts include those held for museums (Harvard Museum of Natural History [USA], Kochi Miraikan Science Museum [Japan], and Sternberg Museum of Natural History [USA]), Two Oceans Aquarium (South Africa), and Northeastern University outreach program (USA). A total of 63 sessions were held for over 1100 individuals (Table **T4**).

Participants were provided links to the research goals discussed on the *JOIDES Resolution* blog post for the South Atlantic Transect 2 expedition (**https://joidesresolution.org/expedition/south-atlantic-transit-2**). Additionally, if the participants were from education institutions, they were provided links to education materials that were generated from Expedition 390 resources (**https://joidesresolution.org/educator-resources-exp-390**).

During the broadcast, a short introduction and background to scientific concepts (plate tectonics, ocean crust age, and seafloor spreading) were provided through a PowerPoint presentation shared on the screen. It had the purpose of making sure those attending started the broadcast with enough background knowledge to understand the general objectives of the activities done on board the ship.

One unique collaboration for the broadcasts was between *JOIDES Resolution* and Reach the World out of New York (USA). Reach the World partnered with teachers during the summer school session to follow the journey of Stephen Pekar and scheduled two ship-to-shore sessions for Grade 6 classes. The broadcasts were facilitated by Tim Jacobs (Reach the World contact) and the Onboard Outreach Officer. The two ship-to-shore sessions were hosted for the MS 577 School Settlement Association (Brooklyn, New York [USA]; 14 students) and the Greenpoint Beacon MS 126 St. Nicks Alliance (Brooklyn, New York [USA]; 12 students).

It was expected that there would not be big groups because of the timing of the expedition overlapping with the summer months. Please note that the Reach the World articles and video recordings will be transformed into on-demand itineraries that any K–12 classroom can follow during the coming academic year at no cost, reliving the journey. Those itineraries will be available in the coming weeks (**https://about.reachtheworld.org/explore**).

The Onboard Outreach Officer experimented by creating two events on the Meetup social networking platform for people to sign up to join a ship-to-shore broadcast. The first event had more lead time and resulted in 13 people joining. The second event had less lead time, and only 6 people joined. Both events engaged groups of inquisitive adults extremely curious about the expedition.

Table T4. Number of broadcasts held weekly, Expedition 393. Some broadcasts were provided for groups of friends and family and were not counted as a group from an institution. Prerecorded events were not done live because of time zone differences making it difficult to have a live audience.

Date (2022)	Week	Events	Institutions	Participants
3–10 Jun	1	1	1	No participants (prerecorded)
11–17 Jun	2	1	1	No participants (prerecorded)
18–24 Jun	3	7	7	163
25 Jun–1 Jul	4	9	3	265
2–8 Jul	5	7	5	116
9–15 Jul	6	9	5	81
16–22 Jul	7	10	8	241
23–29 Jul	8	10	5	136
30 Jul–7 Aug	9	10	9	169
	Total:	63	44	1171

The Onboard Outreach Officer experimented with providing broadcasts to elderly homes in New York (USA). The feedback provided has been that the residents have enjoyed it, and one director of activities from San Simeon by the Sound mentioned that having the broadcast be virtual was really important to them because they cannot provide too many in person events because of COVID-19 risk. Four of the broadcasts were given to elderly homes to roughly 66 participants.

11.2. Social media

The Onboard Outreach Officer maintained the ship's Twitter, Instagram, and Facebook accounts from 3 June 2022 until the Onboard Outreach Officer departed the ship on 7 August. Three to four posts were published on Twitter, Facebook, and Instagram daily to update the audience about life at sea and research activities. Because of the Onboard Outreach Officer's shift partially overlapping various time zones, posts were published throughout the day to hit various social media viewing times.

Throughout the 2 months, social media statistics including the number of followers, engagements, and reach were tracked. Reach is defined by how many times the content was displayed or seen by someone, whereas an engagement is any action on a post that includes reactions, comments, shares, saves, video views, or bookmarking (Table **T5**). Between 3 June and 4 August, Twitter had a total of 438,435 impressions. Instagram and Facebook reach values are estimates calculated by the respective platforms using computer modeling. Instagram was estimated to have reached more than 9,300 people, and Facebook estimated to have reached more than 33,000 people.

11.3. Expedition blog

A total of 21 blog posts were written for the *JOIDES Resolution* Expedition 393 web page: 10 by the Outreach Officer and 11 by members of the science party. Examples of the topics for the blog posts include a poem about rocks, how weather affects transit time, and unexpected drilling delays. There were over 10,000 page sessions, which indicates how many single users browsed the website.

The Onboard Outreach Officer collaborated with Deana Schwarz at APGO Education Foundation to write a blog about the South Atlantic Transect 2 expedition for their GeoscienceINFO Beneath Your Feet blog (**https://geoscienceinfo.com/scientific-ocean-drilling-with-the-joides-resolution-a-summary**). This blog linked back to the *JOIDES Resolution* website to bring more foot traffic to the expedition page.

The Onboard Outreach Officer collaborated with Adriane Lam to publish blog posts written by the science party on Lam's website Time Scavengers, which is also recognized as a nonprofit organization. The blog posts are called Meet the Scientist, and they showcase not only scientists' science interests but also other parts of their lives. Two scientists and the Onboard Outreach Officer each wrote a blog post that was published on Time Scavengers.

Table T5. Total weekly reach and engagement for each social media platform including precruise hotel quarantine, Expedition 393. * = weekly Facebook reach and engagement is calculated as individual post reach and engagement totaled together.

		Twitter				Instagram				Facebook			
Date (2022)	Week	Posts	New followers	Impressions	Engagement	Posts	New followers	Reach	Engagement	Posts	New followers	Reach*	Engagement*
3–10 Jun	1	8	9	16,382	553	9	77	2,066	285	7	10	20,730	1,008
11–17 Jun	2	24	32	45,158	1,846	21	35	2,670	365	23	24	38,786	1,844
18–24 Jun	3	33	36	70,248	2,808	28	18	2,577	411	30	8	51,890	2,088
25 Jun–1 Jul	4	33	45	61,003	2,506	30	20	2,559	408	34	10	49,257	1,895
2–8 Jul	5	32	33	84,761	2,956	31	20	2,929	389	31	20	46,668	2,036
9–15 Jul	6	33	63	50,309	1,963	34	21	1,857	298	33	6	38,349	1,653
16–22 Jul	7	30	32	43,313	1,842	31	11	2,175	328	31	6	36,503	1,879
23–29 Jul	8	33	0	38,885	1,630	31	9	2,363	295	33	0	36,125	1,478
30 Jul–7 Aug	9	25	24	28,376	1,034	25	5	2,121	261	25	5	26,385	1,092
	Total:	193	274	438,435	17,138	240	216	21,317	3,040	247	89	344,693	14,973

11.4. Educational materials

Three classroom lesson plans were generated for a target audience of adults seeking their high school diploma or high school equivalency. The Onboard Outreach Officer has a background in adult education and created new materials that catered to science teachers needing more science material for their specific standards.

The first lesson plan focuses on the skill of using rulers and discusses how measurements show up in various fields including many of those in science. The lesson was inspired by the fact that at the Onboard Outreach Officer's job on shore, her students didn't always competently use a ruler or communicate what the ruler was showing them. This train of thought is reflected in a blog to which the lesson plan is linked.

The second lesson plan focuses on the skill of reading diagrams. The students are then asked to practice reading comprehension of an article that discusses the concept of tectonic plates and Earth's layers, including three diagrams they could practice analyzing.

The third lesson plan is about learning the skill of reading coordinates and then using earthquake data to observe tectonic plate boundaries. All three lesson plans focus on learning a skill and then applying it to a scientific concept. The lesson plans had an in-person teaching setting in mind, but the digital nature of all materials means it can be modified for virtual teaching.

11.5. Media coverage

Stephen Pekar was interviewed by anchors Shannan Ferry and Rocco Vertuccio on NY1 Spectrum News on June 5th for a special on climate change (**https://www.ny1.com/nyc/all-boroughs/CTV/2022/06/06/ny1-presents--climate-in-crisis**).

Alexandra Villa was interviewed by a journalist at Madison Media Partners, and her interview was featured on July 12, 2022 (**https://madison.com/news/local/environment/uw-student-studying-rocks-on-ocean-floor-to-help-with-climate-change-solution/article_ccda841f-3814-5c72-adf7-3578875c9e56.html**). It discusses the importance of the science done on board the ship and her personal research interests.

References

Alt, J.C., 2004. Alteration of the upper oceanic crust: mineralogy, chemistry, and processes. In Davis, E., and Elderfield, H. (Eds.), Hydrogeology of the Oceanic Lithosphere. Cambridge, England (Cambridge University Press), 456–488.

Alt, J.C., Honnorez, J., Laverne, C., and Emmermann, R., 1986. Hydrothermal alteration of a 1 km section through the upper oceanic crust, Deep Sea Drilling Project Hole 504B: mineralogy, chemistry and evolution of seawater-basalt interactions. Journal of Geophysical Research: Solid Earth, 91(B10):10309–10335. **https://doi.org/10.1029/JB091iB10p10309**

Alt, J.C., and Teagle, D.A.H., 1999. The uptake of carbon during alteration of ocean crust. Geochimica et Cosmochimica Acta, 63(10):1527–1535. **https://doi.org/10.1016/S0016-7037(99)00123-4**

Alt, J.C., Teagle, D.A.H., Laverne, C., Vanko, D.A., Bach, W., Honnorez, J., Becker, K., Ayadi, M., and Pezard, P.A., 1996. Ridge flank alteration of upper ocean crust in the eastern Pacific: synthesis of results for volcanic rocks of holes 504B and 896A. In Alt, J.C., Kinoshita, H., Stokking, L.B., and Michael, P.J. (Eds.), Proceedings of the Ocean Drilling Program, Scientific Results. 148: College Station, TX (Ocean Drilling Program), 435–450. **https://doi.org/10.2973/odp.proc.sr.148.150.1996**

Andrén, T., Jørgensen, B.B., Cotterill, C., Green, S., Andrén, E., Ash, J., Bauersachs, T., Cragg, B., Fanget, A.-S., Fehr, A., Granoszewski, W., Groeneveld, J., Hardisty, D., Herrero-Bervera, E., Hyttinen, O., Jensen, J.B., Johnson, S., Kenzler, M., Kotilainen, A., Kotthoff, U., Marshall, I.P.G., Martin, E., Obrochta, S., Passchier, S., Quintana Krupinski, N., Riedinger, N., Slomp, C., Snowball, I., Stepanova, A., Strano, S., Torti, A., Warnock, J., Xiao, N., and Zhang, R., 2015. Expedition 347 summary. In Andrén, T., Jørgensen, B.B., Cotterill, C., Green, S., and the Expedition 347 Scientists, Proceedings of the Integrated Ocean Drilling Program. 347: College Station, TX (Integrated Ocean Drilling Program). **https://doi.org/10.2204/iodp.proc.347.101.2015**

Antonelli, M.A., Pester, N.J., Brown, S.T., and DePaolo, D.J., 2017. Effect of paleoseawater composition on hydrothermal exchange in midocean ridges. Proceedings of the National Academy of Sciences of the United States of America, 114(47):12413–12418. **https://doi.org/10.1073/pnas.1709145114**

Bach, W., and Edwards, K.J., 2003. Iron and sulfide oxidation within the basaltic ocean crust; implications for chemolithoautotrophic microbial biomass production. Geochimica et Cosmochimica Acta, 67(20):3871–3887. **https://doi.org/10.1016/S0016-7037(03)00304-1**

Barker, P.F., and Thomas, E., 2004. Origin, signature and palaeoclimatic influence of the Antarctic Circumpolar Current. Earth-Science Reviews, 66(1–2):143–162. **https://doi.org/10.1016/j.earscirev.2003.10.003**

Barrera, E., Savin, S.M., Thomas, E., and Jones, C.E., 1997. Evidence for thermohaline-circulation reversals controlled by sea-level change in the latest Cretaceous. Geology, 25(8):715–718. **https://doi.org/10.1130/0091-7613(1997)025<0715:EFTCRC>2.3.CO;2**

Becker, K., Fisher, A.T., and Tsuji, T., 2013. New packer experiments and borehole logs in upper oceanic crust: evidence for ridge-parallel consistency in crustal hydrogeological properties. Geochemistry, Geophysics, Geosystems, 14(8):2900–2915. **https://doi.org/10.1002/ggge.20201**

Berner, R.A., Lasaga, A.C., and Garrels, R.M., 1983. The carbonate-silicate geochemical cycle and its effect on atmospheric carbon dioxide over the past 100 million years. American Journal of Science, 283(7):641–683. **https://doi.org/10.2475/ajs.283.7.641**

Billups, K., 2002. Late Miocene through early Pliocene deep water circulation and climate change viewed from the sub-Antarctic South Atlantic. Palaeogeography, Palaeoclimatology, Palaeoecology, 185(3–4):287–307. **https://doi.org/10.1016/S0031-0182(02)00340-1**

Bohaty, S.M., Zachos, J.C., Florindo, F., and Delaney, M.L., 2009. Coupled greenhouse warming and deep-sea acidification in the middle Eocene. Paleoceanography and Paleoclimatology, 24(2):PA2207. **https://doi.org/10.1029/2008PA001676**

Borrelli, C., Cramer, B.S., and Katz, M.E., 2014. Bipolar Atlantic deepwater circulation in the middle-late Eocene: effects of Southern Ocean gateway openings. Paleoceanography and Paleoclimatology, 29(4):308–327. **https://doi.org/10.1002/2012PA002444**

Broecker, W.S., 1991. The great ocean conveyor. Oceanography, 4(2):79–89. **http://www.jstor.org/stable/43924572**

Christeson, G., and Reece, R., 2020. Bathymetric site survey gridded data in support of IODP Expeditions 390 and 393, South Atlantic Transect (MGL1601, CREST). Interdisciplinary Earth Data Alliance (IEDA). **https://doi.org/10.26022/IEDA/327528**

Christeson, G.L., Reece, R.S., Kardell, D.A., Estep, J.D., Fedotova, A., and Goff, J.A., 2020. South Atlantic transect: variations in oceanic crustal structure at 31°S. Geochemistry, Geophysics, Geosystems, 21(7):e2020GC009017. **https://doi.org/10.1029/2020GC009017**

Coggon, R.M., Christeson, G.L., Sylvan, J.B., Teagle, D.A.H., Estes, E., Williams, T., and Alvarez Zarikian, C.A., 2020. Expedition 390/393 Scientific Prospectus: The South Atlantic Transect. International Ocean Discovery Program. **https://doi.org/10.14379/iodp.sp.390393.2020**

Coggon, R.M., Sylvan, J.B., Teagle, D.A.H., Reece J., Christeson, G.L., Estes, E.R., Williams, T.J., and the Expedition 390 Scientists, 2022a. Expedition 390 Preliminary Report: South Atlantic Transect 1. International Ocean Discovery Program. **https://doi.org/10.14379/iodp.pr.390.2022**

Coggon, R.M., Sylvan, J.B., Teagle, D.A.H., Reece, J.S., Christeson, G.L., Estes, E.R., and Williams, T., 2022b. Expedition 390/393 Scientific Prospectus Addendum: South Atlantic Transect. International Ocean Discovery Program. **https://doi.org/10.14379/iodp.sp.390393add.2022**

Coggon, R.M., and Teagle, D.A.H., 2011. Hydrothermal calcium-carbonate veins reveal past ocean chemistry. TrAC Trends in Analytical Chemistry, 30(8):1252–1268. **https://doi.org/10.1016/j.trac.2011.02.011**

Coggon, R.M., Teagle, D.A.H., Cooper, M.J., and Vanko, D.A., 2004. Linking basement carbonate vein compositions to porewater geochemistry across the eastern flank of the Juan de Fuca Ridge, ODP Leg 168. Earth and Planetary Science Letters, 219(1–2):111–128. **https://doi.org/10.1016/S0012-821X(03)00697-6**

Coggon, R.M., Teagle, D.A.H., Smith-Duque, C.E., Alt, J.C., and Cooper, M.J., 2010. Reconstructing past seawater Mg/Ca and Sr/Ca from mid-ocean ridge flank calcium carbonate veins. Science, 327(5969):1114–1117. **https://doi.org/10.1126/science.1182252**

Coogan, L.A., Parrish, R.R., and Roberts, N.M.W., 2016. Early hydrothermal carbon uptake by the upper oceanic crust: insight from in situ U-Pb dating. Geology, 44(2):147–150. **https://doi.org/10.1130/G37212.1**

Cramer, B.S., Toggweiler, J.R., Wright, J.D., Katz, M.E., and Miller, K.G., 2009. Ocean overturning since the Late Cretaceous: inferences from a new benthic foraminiferal isotope compilation. Paleoceanography and Paleoclimatology, 24(4):PA4216. **https://doi.org/10.1029/2008PA001683**

Davis, A.C., Bickle, M.J., and Teagle, D.A.H., 2003. Imbalance in the oceanic strontium budget. Earth and Planetary Science Letters, 211(1–2):173–187. **https://doi.org/10.1016/S0012-821X(03)00191-2**

Devey, C., 2014. SoMARTherm: the Mid-Atlantic Ridge 13–33°S – Cruise No. MSM25 – January 24–March 5, 2013 – Cape Town (South Africa) – Mindelo (Cape Verde). MARIA S. MERIAN-Berichte, MSM25(80). **https://doi.org/10.2312/cr_msm25**

D'Hondt, S., Pockalny, R., Fulfer, V.M., and Spivack, A.J., 2019. Subseafloor life and its biogeochemical impacts. Nature Communications, 10(1):3519. **https://doi.org/10.1038/s41467-019-11450-z**

D'Hondt, S., Inagaki, F., Alvarez Zarikian, C., Abrams, L.J., Dubois, N., Engelhardt, T., Evans, H., Ferdelman, T., Gribsholt, B., Harris, R.N., Hoppie, B.W., Hyun, J.-H., Kallmeyer, J., Kim, J., Lynch, J.E., McKinley, C.C., Mitsunobu, S., Morono, Y., Murray, R.W., Pockalny, R., Sauvage, J., Shimono, T., Shiraishi, F., Smith, D.C., Smith-Duque, C.E., Spivack, A.J., Steinsbu, B.O., Suzuki, Y., Szpak, M., Toffin, L., Uramoto, G., Yamaguchi, Y.T., Zhang, G.-l., Zhang, X.-H., and Ziebis, W., 2015. Presence of oxygen and aerobic communities from sea floor to basement in deep-sea sediments. Nature Geoscience, 8(4):299–304. **https://doi.org/10.1038/NGEO2387**

Dickens, G.R., Castillo, M.M., and Walker, J.C.G., 1997. A blast of gas in the latest Paleocene: simulating first-order effects of massive dissociation of oceanic methane hydrate. Geology, 25(3):259–262. **https://doi.org/10.1130/0091-7613(1997)025%3C0259:ABOGIT%3E2.3.CO;2**

Engelen, B., Ziegelmüller, K., Wolf, L., Köpke, B., Gittel, A., Cypionka, H., Treude, T., Nakagawa, S., Inagaki, F., Lever, M.A., and Steinsbu, B.O., 2008. Fluids from the oceanic crust support microbial activities within the deep biosphere. Geomicrobiology Journal, 25(1):56–66. **https://doi.org/10.1080/01490450701829006**

Estep, J., Reece, R., Kardell, D.A., Christeson, G.L., and Carlson, R.L., 2019. Seismic Layer 2A: evolution and thickness from 0- to 70-Ma crust in the slow-intermediate spreading South Atlantic. Journal of Geophysical Research: Solid Earth, 124(8):7633–7651. **https://doi.org/10.1029/2019JB017302**

Estes, E.R., Williams, T., Midgley, S., Coggon, R.M., Sylvan, J.B.,Christeson, G.L., Teagle, D.A.H., and the Expedition 390C Scientists, 2021. Expedition 390C Preliminary Report: South Atlantic Transect Reentry Systems. International Ocean Discovery Program. **https://doi.org/10.14379/iodp.pr.390C.2021**

Expedition 301 Scientists, 2005. Expedition 301 summary. In Fisher, A.T., Urabe, T., Klaus, A., and the Expedition 301 Scientists, Proceedings of the Integrated Ocean Drilling Program. 301: College Station, TX (Integrated Ocean Drilling Program Management International, Inc.). **https://doi.org/10.2204/iodp.proc.301.101.2005**

Expedition 308 Scientists, 2006. Expedition 308 summary. In Flemings, P.B., Behrmann, J.H., John, C.M., and the Expedition 308 Scientists, Proceedings of the Integrated Ocean Drilling Program. 308: College Station, TX (Integrated Ocean Drilling Program Management International, Inc.). **https://doi.org/10.2204/iodp.proc.308.101.2006**

Expedition 309/312 Scientists, 2006. Expedition 309/312 summary. In Teagle, D.A.H., Alt, J.C., Umino, S., Miyashita, S., Banerjee, N.R., Wilson, D.S., and the Expedition 309/312 Scientists, Proceedings of the Integrated Ocean Drilling Program. 309/312: Washington, DC (Integrated Ocean Drilling Program Management International, Inc.). **https://doi.org/10.2204/iodp.proc.309312.101.2006**

Expedition 313 Scientists, 2010. Expedition 313 summary. In Mountain, G., Proust, J.-N., McInroy, D., Cotterill, C., and the Expedition 313 Scientists, Proceedings of the Integrated Ocean Drilling Program. 313: Tokyo (Integrated Ocean Drilling Program Management International, Inc.). **https://doi.org/10.2204/iodp.proc.313.101.2010**

Expedition 325 Scientists, 2011. Expedition 325 summary. In Webster, J.M., Yokoyama, Y., Cotterill, C., and the Expedition 325 Scientists, Proceedings of the Integrated Ocean Drilling Program. 325: Tokyo (Integrated Ocean Drilling Program Management International, Inc.). **https://doi.org/10.2204/iodp.proc.325.101.2011**

Expedition 327 Scientists, 2011. Expedition 327 summary. In Fisher, A.T., Tsuji, T., Petronotis, K., and the Expedition 327 Scientists, Proceedings of the Integrated Ocean Drilling Program. 327: Tokyo (Integrated Ocean Drilling Program Management International, Inc.). **https://doi.org/10.2204/iodp.proc.327.101.2011**

Expedition 329 Scientists, 2011. Expedition 329 summary. In D'Hondt, S., Inagaki, F., Alvarez Zarikian, C.A., and the Expedition 329 Scientists, Proceedings of the Integrated Ocean Drilling Program. 329: Tokyo (Integrated Ocean Drilling Program Management International, Inc.). **https://doi.org/10.2204/iodp.proc.329.101.2011**

Expedition 330 Scientists, 2012. Expedition 330 summary. In Koppers, A.A.P., Yamazaki, T., Geldmacher, J., and the Expedition 330 Scientists, Proceedings of the Integrated Ocean Drilling Program. 330: Tokyo (Integrated Ocean Drilling Program Management International, Inc.). **https://doi.org/10.2204/iodp.proc.330.101.2012**

Expedition 335 Scientists, 2012. Expedition 335 summary. In Teagle, D.A.H., Ildefonse, B., Blum, P., and the Expedition 335 Scientists, Proceedings of the Integrated Ocean Drilling Program. 335: Tokyo (Integrated Ocean Drilling Program Management International, Inc.). **https://doi.org/10.2204/iodp.proc.335.101.2012**

Expedition 336 Scientists, 2012. Expedition 336 summary. In Edwards, K.J., Bach, W, Klaus, A., and the Expedition 336 Scientists, Proceedings of the Integrated Ocean Drilling Program. 336: Tokyo (Integrated Ocean Drilling Program Management International, Inc.). **https://doi.org/10.2204/iodp.proc.336.101.2012**

Fisher, A.T., and Harris, R.N., 2010. Using seafloor heat flow as a tracer to map subseafloor fluid flow in the ocean crust. Geofluids, 10(1–2):142–160. **https://doi.org/10.1111/j.1468-8123.2009.00274.x**

Frank, T.D., and Arthur, M.A., 1999. Tectonic forcings of Maastrichtian ocean-climate evolution. Paleoceanography and Paleoclimatology, 14(2):103–117. **https://doi.org/10.1029/1998PA900017**

Fryer, P., Wheat, C.G., Williams, T., Albers, E., Bekins, B., Debret, B.P.R., Jianghong, D., Yanhui, D., Eickenbusch, P., Frery, E.A., Ichiyama, Y., Johnson, K., Johnston, R.M., Kevorkian, R.T., Kurz, W., Magalhaes, V., Mantovanelli, S.S., Menapace, W., Menzies, C.D., Michibayashi, K., Moyer, C.L., Mullane, K.K., Park, J.-W., Price, R.E., Ryan, J.G., Shervais, J.W., Sissmann, O.J., Suzuki, S., Takai, K., Walter, B., and Rui, Z., 2018. Expedition 366 summary. In Fryer, P., Wheat, C.G., Williams, T., and the Expedition 366 Scientists, Mariana Convergent Margin and South Chamorro Seamount. Proceedings of the International Ocean Discovery Program, 366: College Station, TX (International Ocean Discovery Program). **https://doi.org/10.14379/iodp.proc.366.101.2018**

Gillis, K.M., and Coogan, L.A., 2011. Secular variation in carbon uptake into the ocean crust. Earth and Planetary Science Letters, 302(3–4):385–392. **https://doi.org/10.1016/j.epsl.2010.12.030**

Goldberg, D.S., Takahashi, T., and Slagle, A.L., 2008. Carbon dioxide sequestration in deep-sea basalt. Proceedings of the National Academy of Sciences of the United States of America, 105(29):9920–9925. **https://doi.org/10.1073/pnas.0804397105**

Gradstein, F.M., Ogg, J.G., Schmitz, M.D., and Ogg, G.M. (Eds.), 2020. The Geologic Time Scale 2020: Amsterdam (Elsevier BV). **https://doi.org/10.1016/C2020-1-02369-3**

Harris, M., Coggon, R.M., Smith-Duque, C.E., Cooper, M.J., Milton, J.A., and Teagle, D.A.H., 2015. Channelling of hydrothermal fluids during the accretion and evolution of the upper oceanic crust: Sr isotope evidence from ODP Hole 1256D. Earth and Planetary Science Letters, 416:56–66. **https://doi.org/10.1016/j.epsl.2015.01.042**

Harris, M., Coggon, R.M., Teagle, D.A.H., Roberts, N.M.W., and Parrish, R.R., 2014. Laser ablation MC-ICP-MS U/Pb geochronology of ocean basement calcium carbonate veins. Presented at the 2014 American Geophysical Union Fall Meeting, San Francisco, CA, 15–19 December 2014. **https://agu.confex.com/agu/fm14/meetingapp.cgi/Paper/12488**

Houtz, R., and Ewing, J., 1976. Upper crustal structure as a function of plate age. Journal of Geophysical Research, 81(14):2490–2498. **https://doi.org/10.1029/JB081i014p02490**

Hutnak, M., and Fisher, A.T., 2007. Influence of sedimentation, local and regional hydrothermal circulation, and thermal rebound on measurements of seafloor heat flux. Journal of Geophysical Research Solid Earth, 112(B12):B12101. **https://doi.org/10.1029/2007JB005022**

Hutnak, M., Fisher, A.T., Harris, R., Stein, C., Wang, K., Spinelli, G., Schindler, M., Villinger, H., and Silver, E., 2008. Large heat and fluid fluxes driven through mid-plate outcrops on ocean crust. Nature Geoscience, 1(9):611-614. **https://doi.org/10.1038/ngeo264**

Inagaki, F., Nunoura, T., Nakagawa, S., Teske, A., Lever, M., Lauer, A., Suzuki, M., Takai, K., Delwiche, M., Colwell, F.S., Nealson, K.H., Horikoshi, K., D'Hondt, S., and Jørgensen, B.B., 2006. Biogeographical distribution and diversity of microbes in methane hydrate-bearing deep marine sediments on the Pacific Ocean margin. Proceedings of the National Academy of Sciences of the United States of America, 103(8):2815–2820. **https://doi.org/10.1073/pnas.0511033103**

Inagaki, F., and Orphan, V., 2014. Exploration of subseafloor life and the biosphere through IODP (2003–2013). In Stein, R., Blackman, Donna K., Inagaki, Fumio, and Larsen, Hans-Christian (Eds.), A Decade of Science Achieved by the Integrated Ocean Drilling Program (IODP). Developments in Marine Geology. R. Stein (Series Ed.), 7: 39–63. **https://doi.org/10.1016/B978-0-444-62617-2.00002-5**

Jungbluth, S.P., Grote, J., Lin, H.-T., Cowen, J.P., and Rappé, M.S., 2013. Microbial diversity within basement fluids of the sediment-buried Juan de Fuca Ridge flank. The ISME Journal, 7(1):161–172. **https://doi.org/10.1038/ismej.2012.73**

Kallmeyer, J., Pockalny, R., Adhikari, R.R., Smith, D.C., and D'Hondt, S., 2012. Global distribution of microbial abundance and biomass in subseafloor sediment. Proceedings of the National Academy of Sciences of the United States of America, 109(40):16213–16216. **https://doi.org/10.1073/pnas.1203849109**

Kardell, D.A., Christeson, G.L., Estep, J.D., Reece, R.S., and Carlson, R.L., 2019. Long-lasting evolution of Layer 2A in the western South Atlantic: evidence for low-temperature hydrothermal circulation in old oceanic crust. Journal of Geophysical Research: Solid Earth, 124(3):2252–2273. **https://doi.org/10.1029/2018JB016925**

Kardell, D.A., Zhao, Z., Ramos, E.J., Estep, J., Christeson, G.L., Reece, R.S., and Hesse, M.A., 2021. Hydrothermal models constrained by fine-scale seismic velocities confirm hydrothermal cooling of 7–63 Ma South Atlantic crust. Journal of Geophysical Research: Solid Earth, 126(6):e2020JB021612. **https://doi.org/10.1029/2020JB021612**

Katz, M.E., Cramer, B.S., Toggweiler, J.R., Esmay, G., Liu, C., Miller, K.G., Rosenthal, Y., Wade, B.S., and Wright, J.D., 2011. Impact of Antarctic Circumpolar Current development on late Paleogene ocean structure. Science, 332(6033):1076–1079. **https://doi.org/10.1126/science.1202122**

Kennett, J.P., and Stott, L.D., 1990. Proteus and proto-oceanus: ancestral Paleogene oceans as revealed from Antarctic stable isotopic results; ODP Leg 113. In Barker, P.F., Kennett, J. P., et al., Proceedings of the Ocean Drilling Program, Scientific Results. 113: College Station, TX (Ocean Drilling Program), 865–880. **https://doi.org/10.2973/odp.proc.sr.113.188.1990**

Kennett, J.P., and Stott, L.D., 1991. Abrupt deep-sea warming, palaeoceanographic changes and benthic extinctions at the end of the Palaeocene. Nature, 353(6341):225–229. **https://doi.org/10.1038/353225a0**

Koppers, A., and Coggon, R. (Eds.), 2020. Exploring Earth by Scientific Ocean Drilling: 2050 Science Framework: San Diego, CA (UC San Diego Library). **https://doi.org/10.6075/J0W66J9H**

Langseth, M.G., Cann, J.R., Natland, J.H., and Hobart, M., 1983. Geothermal phenomena at the Costa Rica Rift; background and objectives for drilling at Deep Sea Drilling Project Sites 501, 504, and 505. In Cann, J.R., Langseth, M. G., Honnorez, J., Von Herzen, R. P., White, S. M., et al., Initial Reports of the Deep Sea Drilling Project. 69: Washington, DC (US Government Printing Office), 5–29. **https://doi.org/10.2973/dsdp.proc.69.101.1983**

Langseth, M.G., Mottl, M.J., Hobart, M.A., and Fisher, A., 1988. The distribution of geothermal and geochemical gradients near site 501/504: implications for hydrothermal circulation in the oceanic crust. In Becker, K., Sakai, H., et al., Proceedings of the Ocean Drilling Program, Initial Reports (Part A). 111: College Station, TX (Ocean Drilling Program), 23–32. **https://doi.org/10.2973/odp.proc.ir.111.102.1988**

Lee, M.D., Walworth, N.G., Sylvan, J.B., Edwards, K.J., and Orcutt, B.N., 2015. Microbial communities on seafloor basalts at Dorado Outcrop reflect level of alteration and highlight global lithic clades. Frontiers in Microbiology, 6:1470. **https://doi.org/10.3389/fmicb.2015.01470**

Lever, M.A., Rouxel, O., Alt, J.C., Shimizu, N., Ono, S., Coggon, R.M., Shanks, W.C., III, Lapham, L., Elvert, M., Prieto-Mollar, X., Hinrichs, K.-U., Inagaki, F., and Teske, A., 2013. Evidence for microbial carbon and sulfur cycling in deeply buried ridge flank basalt. Science, 339(6125):1305–1308. **https://doi.org/10.1126/science.1229240**

Lever, M.A., Rogers, K.L., Lloyd, K.G., Overmann, J., Schink, B., Thauer, R.K., Hoehler, T.M., and Jørgensen, B.B., 2015. Life under extreme energy limitation: a synthesis of laboratory- and field-based investigations. FEMS Microbiology Ecology, 39(5):688–728. **https://doi.org/10.1093/femsre/fuv020**

Lister, C.R.B., 1972. On the thermal balance of a mid-ocean ridge. Geophysical Journal International, 26(5):515–535. **https://doi.org/10.1111/j.1365-246X.1972.tb05766.x**

Lomstein, B.A., Langerhuus, A.T., D'Hondt, S., Jørgensen, B.B., and Spivack, A.J., 2012. Endospore abundance, microbial growth and necromass turnover in deep sub-seafloor sediment. Nature, 484(7392):101–104. **https://doi.org/10.1038/nature10905**

Mallows, C., and Searle, R.C., 2012. A geophysical study of oceanic core complexes and surrounding terrain, Mid-Atlantic Ridge 13°N–14°N. Geochemistry, Geophysics, Geosystems, 13(6):Q0AG08. **https://doi.org/10.1029/2012GC004075**

Marieni, C., Henstock, T.J., and Teagle, D.A.H., 2013. Geological storage of CO_2 within the oceanic crust by gravitational trapping. Geophysical Research Letters, 40(23):6219–6224. **https://doi.org/10.1002/2013GL058220**

Mason, O.U., Nakagawa, T., Rosner, M., Van Nostrand, J.D., Zhou, J., Maruyama, A., Fisk, M.R., and Giovannoni, S.J., 2010. First investigation of the microbiology of the deepest layer of ocean crust. PloS One, 5(11):e15399. **https://doi.org/10.1371/journal.pone.0015399**

Matter, J.M., Stute, M., Snæbjörnsdottir, S.Ó., Oelkers, E.H., Gislason, S.R., Aradottir, E.S., Sigfusson, B., Gunnarsson, I., Sigurdardottir, H., Gunnlaugsson, E., Axelsson, H.A., Woff-Boenisch, D., Mesfin, K., de la Reguera Taaya, D.F.,

Hall, J., Diderikson, K., and Broecker, W.S., 2016. Rapid carbon mineralization for permanent disposal of anthropogenic carbon dioxide emissions. Science, 352(6291):1312–1314. **https://doi.org/10.1126/science.aad8132**

Maxbauer, D.P., Feinberg, J.M., and Fox, D.L., 2016. MAX UnMix: a web application for unmixing magnetic coercivity distributions. Computers & Geosciences, 95:140–145. **https://doi.org/10.1016/j.cageo.2016.07.009**

Meyer, B., Saltus, R., and Chulliat, A., 2017. EMAG2v3: Earth Magnetic Anomaly Grid (2-arc-minute resolution). Version 3. NOAA National Centers for Environmental Information. **https://doi.org/10.7289/V5H70CVX**

Michibayashi, K., Tominaga, M., Ildefonse, B., and Teagle, D.A.H., 2019. What lies beneath: the formation and evolution of oceanic lithosphere. Oceanography, 32(1):138–149. **https://doi.org/10.5670/oceanog.2019.136**

Mottl, M.J., 1989. Hydrothermal convection, reaction, and diffusion in sediments on the Costa Rica Rift flank: porewater evidence from ODP Sites 677 and 678. In Becker, K., Sakai, H., et al., Proceedings of the Ocean Drilling Program, Scientific Results. 111: College Station, TX (Ocean Drilling Program), 195–213. **https://doi.org/10.2973/odp.proc.sr.111.125.1989**

Mottl, M.J., 2003. Partitioning of energy and mass fluxes between mid-ocean ridge axes and flanks at high and low temperature. In Halbach, P.E., Tunnicliffe, V., and Hein, J.R. (Eds.), Energy and mass transfer in marine hydrothermal systems. Berlin (Dahlem University Press), 271–286.

Mottl, M.J., Anderson, R.N., Jenkins, W.J., and Lawrence, J.R., 1983. Chemistry of waters sampled from basaltic basement in Deep Sea Drilling Project Holes 501, 504B, and 505B. In Cann, J.R., Langseth, M.G., Honnorez, J., Von Herzen, R.P., White, S.M., et al., Initial Reports of the Deep Sea Drilling Project. 69: Washington, DC (US Government Printing Office), 475–483. **https://doi.org/10.2973/dsdp.proc.69.122.1983**

Mottl, M.J., Druffel, E.R.M., Hart, S.R., Lawrence, J.R., and Saltzman, E.S., 1985. Chemistry of hot waters sampled from basaltic basement in Hole 504B, Deep Sea Drilling Project Leg 83, Costa Rica Rift. In Anderson, R.N., Honnorez, J., Becker, K., et al., Initial Reports of the Deep Sea Drilling Project. 83: 315–318. **https://doi.org/10.2973/dsdp.proc.83.115.1985**

Mottl, M.J., and Gieskes, J.M., 1990. Chemistry of waters sampled from oceanic basement boreholes, 1979–1988. Journal of Geophysical Research: Solid Earth, 95(B6):9327–9342. **https://doi.org/10.1029/JB095iB06p09327**

Mottl, M.J., Lawrence, J.R., and Keigwin, L.D., 1983. Elemental and stable-isotope composition of pore waters and carbonate sediments from Deep Sea Drilling Project Sites 501/504 and 505. In Cann, J.R., Langseth, M.G., Honnorez, J., Von Herzen, R.P., White, S.M., et al., Initial Reports of the Deep Sea Drilling Project. 69: Washington, DC (US Government Printing Office), 461–473. **https://doi.org/10.2973/dsdp.proc.69.121.1983**

Müller, R.D., Sdrolias, M., Gaina, C., Steinberger, B., and Heine, C., 2008. Long-term sea-level fluctuations driven by ocean basin dynamics. Science, 319(5868):1357–1362. **https://doi.org/10.1126/science.1151540**

Neira, N.M., Clark, J.F., Fisher, A.T., Wheat, C.G., Haymon, R.M., and Becker, K., 2016. Cross-hole tracer experiment reveals rapid fluid flow and low effective porosity in the upper oceanic crust. Earth and Planetary Science Letters, 450:355–365. **https://doi.org/10.1016/j.epsl.2016.06.048**

Norris, R.D., Wilson, P.A., Blum, P., Fehr, A., Agnini, C., Bornemann, A., Boulila, S., Bown, P.R., Cournede, C., Friedrich, O., Ghosh, A.K., Hollis, C.J., Hull, P.M., Jo, K., Junium, C.K., Kaneko, M., Liebrand, D., Lippert, P.C., Liu, Z., Matsui, H., Moriya, K., Nishi, H., Opdyke, B.N., Penman, D., Romans, B., Scher, H.D., Sexton, P., Takagi, H., Turner, S.K., Whiteside, J.H., Yamaguchi, T., and Yamamoto, Y., 2014. Expedition 342 summary. In Norris, R.D., Wilson, P.A., Blum, P., and the Expedition 342 Scientists, Proceedings of the Integrated Ocean Drilling Program. 342: College Station, TX (Integrated Ocean Drilling Program). **https://doi.org/10.2204/iodp.proc.342.101.2014**

Olson, P., Reynolds, E., Hinnov, L., and Goswami, A., 2016. Variation of ocean sediment thickness with crustal age. Geochemistry, Geophysics, Geosystems, 17(4):1349–1369. **https://doi.org/10.1002/2015GC006143**

Orcutt, B.N., Bach, W., Becker, K., Fisher, A.T., Hentscher, M., Toner, B.M., Wheat, C.G., and Edwards, K.J., 2011. Colonization of subsurface microbial observatories deployed in young ocean crust. The ISME Journal, 5(4):692–703. **https://doi.org/10.1038/ismej.2010.157**

Orcutt, B.N., LaRowe, D.E., Lloyd, K.G., Mills, H., Orsi, W., Reese, B.K., Sauvage, J., Huber, J.A., and Amend, J., 2014. IODP Deep Biosphere Research Workshop report – a synthesis of recent investigations, and discussion of new research questions and drilling targets. Scientific Drilling, 17:61–66. **https://doi.org/10.5194/sd-17-61-2014**

Orcutt, B.N., Wheat, C.G., Rouxel, O., Hulme, S., Edwards, K.J., and Bach, W., 2013. Oxygen consumption rates in subseafloor basaltic crust derived from a reaction transport model. Nature Communications, 4:2539. **https://doi.org/10.1038/ncomms3539**

Pälike, H., Lyle, M.W., Nishi, H., Raffi, I., Ridgwell, A., Gamage, K., Klaus, A., Acton, G., Anderson, L., Backman, J., Baldauf, J., Beltran, C., Bohaty, S.M., Bown, P., Busch, W., Channell, J.E.T., Chun, C.O.J., Delaney, M., Dewangan, P., Dunkley Jones, T., Edgar, K.M., Evans, H., Fitch, P., Foster, G.L., Gussone, N., Hasegawa, H., Hathorne, E.C., Hayashi, H., Herrle, J.O., Holbourn, A., Hovan, S., Hyeong, K., Iijima, K., Ito, T., Kamikuri, S.-i., Kimoto, K., Kuroda, J., Leon-Rodriguez, L., Malinverno, A., Moore Jr, T.C., Murphy, B.H., Murphy, D.P., Nakamura, H., Ogane, K., Ohneiser, C., Richter, C., Robinson, R., Rohling, E.J., Romero, O., Sawada, K., Scher, H., Schneider, L., Sluijs, A., Takata, H., Tian, J., Tsujimoto, A., Wade, B.S., Westerhold, T., Wilkens, R., Williams, T., Wilson, P.A., Yamamoto, Y., Yamamoto, S., Yamazaki, T., and Zeebe, R.E., 2012. A Cenozoic record of the equatorial Pacific carbonate compensation depth. Nature, 488(7413):609–614. **https://doi.org/10.1038/nature11360**

Palmer, M.R., and Edmond, J.M., 1989. The strontium isotope budget of the modern ocean. Earth and Planetary Science Letters, 92(1):11–26. **https://doi.org/10.1016/0012-821X(89)90017-4**

Pearce, J.A., and Norry, M.J., 1979. Petrogenetic implications of Ti, Zr, Y, and Nb variations in volcanic rocks. Contributions to Mineralogy and Petrology, 69(1):33–47. **https://doi.org/10.1007/BF00375192**

Penrose Conference Participants, 1972. Report of the Penrose field conference on ophiolites. Geotimes, 17:24–25.

Pérez-Díaz, L., and Eagles, G., 2017a. A new high-resolution seafloor age grid for the South Atlantic. Geochemistry, Geophysics, Geosystems, 18(1):457–470. **https://doi.org/10.1002/2016GC006750**

Pérez-Díaz, L., and Eagles, G., 2017b. South Atlantic paleobathymetry since Early Cretaceous. Scientific Reports, 7(1):11819. **https://doi.org/10.1038/s41598-017-11959-7**

Perfit, M.R., and Chadwick, W.W., Jr., 1998. Magmatism at mid-ocean ridges: constraints from volcanological and geochemical investigations. In Buck, W.R., Delaney, J.A., Karson, J.A. and Lagabrielle, Y., Faulting and Magmatism at Mid-Ocean Ridges. Geophysical Monograph, 106: 59–115. **https://doi.org/10.1029/GM106p0059**

Rausch, S., Böhm, F., Bach, W., Klügel, A., and Eisenhauer, A., 2013. Calcium carbonate veins in ocean crust record a threefold increase of seawater Mg/Ca in the past 30 million years. Earth and Planetary Science Letters, 362:215–224. **https://doi.org/10.1016/j.epsl.2012.12.005**

Reece, R., Christeson, G., Amara, A., Estep, J., Greene, J., Koch, C., Henning, L., Worman, W., and Wright, A., 2016. CREST: Crustal Reflectivity Experiment southern transect South Atlantic multichannel seismic and ocean bottom seismometer experiment, 4 Jan–25 Feb 2016 Cruise Report. **http://www.iris.washington.edu/data/reports/2016/16-003/CREST_2016-01-04-2016-02-25_MGL1601_CruiseReport.pdf**

Reece, R., and Estep, J., 2019. Processed MCS (PSTM) data from the Mid-Atlantic Ridge (MAR) to the Rio Grande Rise, South Atlantic Ocean, acquired by the R/V *Marcus G. Langseth* in 2016 (MGL1601) **https://doi.org/10.1594/IEDA/500255**

Reese, B.K., Zinke, L.A., Sobol, M.S., LaRowe, D.E., Orcutt, B.N., Zhang, X., Jaekel, U., Wang, F., Dittmar, T., Defforey, D., Tully, B., Paytan, A., Sylvan, J.B., Amend, J.P., Edwards, K.J., and Girguis, P., 2018. Nitrogen cycling of active bacteria within oligotrophic sediment of the Mid-Atlantic Ridge flank. Geomicrobiology Journal, 35(6):468–483. **https://doi.org/10.1080/01490451.2017.1392649**

Ryan, W.B.F., Carbotte, S.M., Coplan, J.O., O'Hara, S., Melkonian, A., Arko, R., Weissel, R.A., Ferrini, V., Goodwillie, A., Nitsche, F., Bonczkowski, J., and Zemsky, R., 2009. Global multi-resolution topography synthesis. Geochemistry, Geophysics, Geosystems, 10(3):Q03014. **https://doi.org/10.1029/2008GC002332**

Santelli, C.M., Edgcomb, V.P., Bach, W., and Edwards, K.J., 2009. The diversity and abundance of bacteria inhabiting seafloor lavas positively correlate with rock alteration. Environmental Microbiology, 11(1):86–98. **https://doi.org/10.1111/j.1462-2920.2008.01743.x**

Sarmiento, J.L., Simeon, J., Gnanadesikan, A., Gruber, N., Key, R.M., and Schlitzer, R., 2007. Deep ocean biogeochemistry of silicic acid and nitrate. Global Biogeochemical Cycles, 21(1). **https://doi.org/10.1029/2006GB002720**

Scher, H.D., and Martin, E.E., 2006. Timing and climatic consequences of the opening of Drake Passage. Science, 312(5772):428–430. **https://doi.org/10.1126/science.1120044**

Shipboard Scientific Party, 1970. Introduction. In Maxwell, A.E., et al., Initial Reports of the Deep Sea Drilling Project. 83: Washington, DC (US Government Printing Office), 7–9. **https://doi.org/10.2973/dsdp.proc.3.101.1970**

Shipboard Scientific Party, 1983. Site 505: sediments and ocean crust in an area of low heat flow south of the Costa Rica Rift. In Cann, J.R., Langseth, M. G., Honnorez, J., Von Herzen, R. P., White, S. M., et al., Initial Reports of the Deep Sea Drilling Project. 69: Washington, DC (US Government Printing Office), 175–214. **https://doi.org/10.2973/dsdp.proc.69.103.1983**

Shipboard Scientific Party, 1985. Explanatory notes. In Anderson, R.N., Honnorez, J., Becker, K., et al., Initial Reports of the Deep Sea Drilling Project. 83: Washington, DC (US Government Printing Office), 5–11. **https://doi.org/10.2973/dsdp.proc.83.101.1985**

Shipboard Scientific Party, 1993a. Explanatory notes. In Alt, J.C., Kinoshita, H., Stokking, L.B., et al., Proceedings of the Ocean Drilling Program, Initial Reports. 148: College Station, TX (Ocean Drilling Program). **https://doi.org/10.2973/odp.proc.ir.148.101.1993**

Shipboard Scientific Party, 1993b. Site 896. In Alt, J.C., Kinoshita, H., Stokking, L.B., et al., Proceedings of the Ocean Drilling Program, Initial Reports, 148. College Station, TX (Ocean Drilling Program), 123–192. **https://doi.org/10.2973/odp.proc.ir.148.103.1993**

Shipboard Scientific Party, 1997. Introduction and summary: hydrothermal circulation in the oceanic crust and its consequences on the eastern flank of the Juan de Fuca Ridge. In Davies, E.E., Fisher, A.T., Firth, J.V., et al., Proceedings of the Ocean Drilling Program, Initial Reports. 168: College Station, TX (Ocean Drilling Program), 7–21. **https://doi.org/10.2973/odp.proc.ir.168.101.1997**

Shipboard Scientific Party, 2002. Leg 199 summary. In Lyle, M., Wilson, P.A., Janecek, T.R., et al., Proceedings of the Ocean Drilling Program, Initial Reports. 199: College Station, TX (Ocean Drilling Program). **https://doi.org/10.2973/odp.proc.ir.199.101.2002**

Shipboard Scientific Party, 2003a. Leg 201 summary. In D'Hondt, S.L., Jørgensen, B.B., Miller, D.J., et al., Proceedings of the Ocean Drilling Program, Initial Reports, 201. College Station, TX (Ocean Drilling Program), 1–81. **https://doi.org/10.2973/odp.proc.ir.201.101.2003**

Shipboard Scientific Party, 2003b. Leg 206 summary. In Wilson, D.S., Teagle, D.A.H., Acton, G.D., et al., Proceedings of the Ocean Drilling Program, Initial Reports. 206: College Station, TX (Ocean Drilling Program). **https://doi.org/10.2973/odp.proc.ir.206.101.2003**

Shipboard Scientific Party, 2004. Leg 208 summary. In Zachos, J.C., Kroon, D., Blum, P., et al., Proceedings of the Ocean Drilling Program, Initial Reports. 208: College Station, TX (Ocean Drilling Program). **https://doi.org/10.2973/odp.proc.ir.208.101.2004**

Spinelli, G.A., Giambalvo, E.R., and Fisher, A.T., 2004. Sediment permeability, distribution, and influence on fluxes in oceanic basement. In Davis, E.E., and Elderfield, H. (Eds.), Hydrogeology of the Oceanic Lithosphere. Cambridge, UK (Cambridge University Press), 151–188.

Staudigel, H., Hart, S.R., Schmincke, H.-U., and Smith, B.M., 1989. Cretaceous ocean crust at DSDP Sites 417 and 418: carbon uptake from weathering versus loss by magmatic outgassing. Geochimica et Cosmochimica Acta, 53(11):3091–3094. **https://doi.org/10.1016/0016-7037(89)90189-0**

Stein, C.A., and Stein, S., 1994. Constraints on hydrothermal heat flux through the oceanic lithosphere from global heat flow. Journal of Geophysical Research: Solid Earth, 99(B2):3081–3095. **https://doi.org/10.1029/93JB02222**

Stommel, H., 1961. Thermohaline convection with two stable regimes of flow. Tellus, 13(2):224–230. **https://doi.org/10.1111/j.2153-3490.1961.tb00079.x**

Straume, E.O., Gaina, C., Medvedev, S., Hochmuth, K., Gohl, K., Whittaker, J.M., Abdul Fattah, R., Doornenbal, J.C., and Hopper, J.R., 2019. GlobSed: updated total sediment thickness in the world's oceans. Geochemistry, Geophysics, Geosystems, 20(4):1756–1772. **https://doi.org/10.1029/2018GC008115**

Sylvan, J.B., Hoffman, C.L., Momper, L.M., Toner, B.M., Amend, J.P., and Edwards, K.J., 2015. Bacillus rigiliprofundi sp. nov., an endospore-forming, Mn-oxidizing, moderately halophilic bacterium isolated from deep subseafloor basaltic crust. International Journal of Systematic and Evolutionary Microbiology, 65(6):1992–1998. **https://doi.org/10.1099/ijs.0.000211**

The Shipboard Scientific Party, 1970. Summary and conclusions. In Maxwell, A.E., et al., Initial Reports of the Deep Sea Drilling Project. 3: Washington, DC (US Government Publishing Company), 441–471. **https://doi.org/10.2973/dsdp.proc.3.113.1970**

Thomas, D.J., Bralower, T.J., and Jones, C.E., 2003. Neodymium isotopic reconstruction of late Paleocene–early Eocene thermohaline circulation. Earth and Planetary Science Letters, 209(3–4):309–322. **https://doi.org/10.1016/S0012-821X(03)00096-7**

Tobin, H.J., Kinoshita, M., Ashi, J., Lallemant, S., Kimura, G., Screaton, E.J., Thu, M.K., Masago, H., and Curewitz, D., 2009. NanTroSEIZE Stage 1 expeditions: introduction and synthesis of key results. In Kinoshita, M., Tobin, H., Ashi, J., Kimura, G., Lallemant, S., Screaton, E.J., Curewitz, D., Masago, H., Moe, K.T., and the Expedition 314/315/316 Scientists, Proceedings of the Integrated Ocean Drilling Program. 314/315/316: Washington, DC (Integrated Ocean Drilling Program Management, Inc.). **https://doi.org/10.2204/iodp.proc.314315316.101.2009**

Tripati, A., Backman, J., Elderfield, H., and Ferretti, P., 2005. Eocene bipolar glaciation associated with global carbon cycle changes. Nature, 436(7049):341–346. **https://doi.org/10.1038/nature03874**

Vance, D., Teagle, D.A.H., and Foster, G.L., 2009. Variable Quaternary chemical weathering fluxes and imbalances in marine geochemical budgets. Nature, 458(7237):493–496. **https://doi.org/10.1038/nature07828**

Von Herzen, R., 1959. Heat-flow values from the South-Eastern Pacific. Nature, 183(4665):882–883. **https://doi.org/10.1038/183882a0**

Westerhold, T., Marwan, N., Drury, A.J., Liebrand, D., Agnini, C., Anagnostou, E., Barnet, J.S.K., Bohaty, S.M., De Vleeschouwer, D., Florindo, F., Frederichs, T., Hodell, D.A., Holbourn, A.E., Kroon, D., Lauretano, V., Littler, K., Lourens, L.J., Lyle, M., Pälike, H., Röhl, U., Tian, J., Wilkens, R.H., Wilson, P.A., and Zachos, J.C., 2020. An astronomically dated record of Earth's climate and its predictability over the last 66 million years. Science, 369(6509):1383–1387. **https://doi.org/10.1126/science.aba6853**

Wheat, C.G., and Fisher, A.T., 2008. Massive, low-temperature hydrothermal flow from a basaltic outcrop on 23 Ma seafloor of the Cocos plate: chemical constraints and implications. Geochemistry, Geophysics, Geosystems, 9(12):Q12O14. **https://doi.org/10.1029/2008GC002136**

Williams, T., Estes, E.R., Rhinehart, B., Coggon, R.M., Sylvan, J.B., Christeson, G.L., and Teagle, D.A.H., 2021. Expedition 395E Preliminary Report: Complete South Atlantic Transect Reentry Systems. International Ocean Discovery Program. **https://doi.org/10.14379/iodp.pr.395E.2021**

Wilson, D.S., Teagle, D.A.H., Alt, J.C., Banerjee, N.R., Umino, S., Miyashita, S., Acton, G.D., Anma, R., Barr, S.R., Belghoul, A., Carlut, J., Christie, D.M., Coggon, R.M., Cooper, K.M., Cordier, C., Crispini, L., Durand, S.R., Einaudi, F., Galli, L., Gao, Y., Geldmacher, J., Gilbert, L.A., Hayman, N.W., Herrero-Bervera, E., Hirano, N., Holter, S., Ingle, S., Jiang, S., Kalberkamp, U., Kerneklian, M., Koepke, J., Laverne, C., Vasquez, H.L.L., Maclennan, J., Morgan, S., Neo, N., Nichols, H.J., Park, S.-H., Reichow, M.K., Sakuyama, T., Sano, T., Sandwell, R., Scheibner, B., Smith-Duque, C.E., Swift, S.A., Tartarotti, P., Tikku, A.A., Tominaga, M., Veloso, E.A., Yamasaki, T., Yamazaki, S., and Ziegler, C., 2006. Drilling to gabbro in intact ocean crust. Science, 312(5776):1016–1020. **https://doi.org/10.1126/science.1126090**

Wright, J.D., Miller, K.G., and Fairbanks, R.G., 1991. Evolution of modern deepwater circulation: evidence from the Late Miocene Southern Ocean. Paleoceanography and Paleoclimatology, 6(2):275–290. **https://doi.org/10.1029/90PA02498**

Wunsch, C., 2002. What is the thermohaline circulation? Science, 298(5596):1179–1181. **https://doi.org/10.1126/science.1079329**

Yoder, H.S., Jr., and Tilley, C.E., 1962. Origin of basalt magmas: an experimental study of natural and synthetic rock xystems. Journal of Petrology, 3(3):342–532. **https://doi.org/10.1093/petrology/3.3.342**

Zachos, J., Pagani, M., Sloan, L., Thomas, E., and Billups, K., 2001. Trends, rhythms, and aberrations in global climate 65 Ma to Present. Science, 292(5517):686–693. **https://doi.org/10.1126/science.1059412**

Zachos, J.C., Dickens, G.R., and Zeebe, R.E., 2008. An early Cenozoic perspective on greenhouse warming and carbon-cycle dynamics. Nature, 451(7176):279–283. **https://doi.org/10.1038/nature06588**

Zachos, J.C., Röhl, U., Schellenberg, S.A., Sluijs, A., Hodell, D.A., Kelly, D.C., Thomas, E., Nicolo, M., Raffi, I., Lourens, L.J., McCarren, H., and Kroon, D., 2005. Rapid acidification of the ocean during the Paleocene-Eocene Thermal Maximum. Science, 308(5728):1611–1615. **https://doi.org/10.1126/science.1109004**

Zeebe, R.E., Zachos, J.C., Caldeira, K., and Tyrrell, T., 2008. Oceans: carbon emissions and acidification. Science, 321(5885):51–52. **https://doi.org/10.1126/science.1159124**